UNIVERSITY OF CALIFORNIA SAN DIEGO

Co-opting Rolling Circle Amplification to Create Lower Cost DNA Nanostructures

A dissertation submitted in partial satisfaction of the
requirements for the degree Doctor of Philosophy

in

Nanoengineering

by

Chava Angell

Committee in Charge:

Professor Yi Chen, Chair
Professor Stephen Howell
Professor Michael Kalichman
Professor Michael Sailor
Professor Joseph Wang
Professor Lianfang Zhang

2020

The Dissertation of Chava Angell is approved, and is acceptable in quality and form for publication on microfilm and electronically:

_____

_____

_____

_____

_____

_____

Chair

University of California San Diego

2020

DEDICATION

This thesis is dedicated to all the graduate students who are persevering and have persevered despite struggling with mental health issues that may not be inherently visible. You are seen, you are worthy, and you are loved.

EPIGRAPH

“Hello babies. Welcome to Earth. It's hot in the summer and cold in the winter. It's round and wet and crowded. On the outside, babies, you've got a hundred years here. There's only one rule that I know of, babies-"God damn it, you've got to be kind.”

— Kurt Vonnegut

TABLE OF CONTENTS

LIST OF SUPPLEMENTAL FILES

File 1: Supporting Video 1, nn6b01415_si_002 (2).avi

File 2: Supporting Video 2, nn6b01415_si_003 (1).avi

File 3: Supporting Video 3, nn6b01415_si_004 (1).avi

LIST OF FIGURES AND TABLES

ACKNOWLEDGEMENTS

I would like to acknowledge Professor Yi Chen for his support and patience as my advisor and my committee chair.

I would also like to acknowledge my lab mates, whose research support and emotional support got me through many tough situations during my doctorate.

I would also like to acknowledge my incredible family who have gotten me through the last five and a half years and have always supported me unconditionally. I love you all so much.

Chapter 1, in full, is a reprint of the material as it appears in Small 2016. Angell, Chava; Smith, Sibai X; Liangfang Z; Yi C.. The dissertation author was co-first author with Sibai Xie.

Chapter 2, is a partial reprint of the material as it appears in Advanced Healthcare Materials, 2018, Angell, Chava; Sibai X;.Mingxuan K; Xiangyi D;Yi C. The dissertation author was the primary author of this paper.

Chapter 3, in full, is a reprint of the material as it appears in ACS Nano, 2016. Esteban-Fernández de Ávila, Berta; Chava A; Fernando S; Miguel ALR; Daniela B; Sibai X; Joseph W; Yi C. The dissertation author was the co-first author and investigator of this material.

Chapter 4, in full is currently being prepared for submission for publication of the material. Angell, Chava; Marta J; Berta E; Doris R; Joseph W; Yi C. The dissertation author was the primary investigator and author of this material.

Chapter 5 in full has been submitted for publication of the material. Angell, Chava; Sibai X; Yi C. The dissertation author was the primary investigator and author of this material.

VITA

2014	Bachelors of Science, Carnegie Mellon University
2015-2020	Teaching Assistant, University of California, San Diego
2016	Master of Science, University of California San Diego
2014-2020	Research Assistant, University of California San Diego
2020	Doctor of Philosophy, University of California San Diego

PUBLICATIONS

People Prop. http://www.bme.cmu.edu/ugprog/design/2014PeopleProp.pdf To view further information about the fate of this project, please visit http://www.abililife.com/

Angell, Chava, Sibai Xie, Liangfang Zhang, and Yi Chen. "DNA nanotechnology for precise control over drug delivery and gene therapy." Small 12, no. 9 (2016): 1117-1132.

Esteban-Fernández de Ávila, Berta, Chava Angell, Fernando Soto, Miguel Angel Lopez-Ramirez, Daniela F. Báez, Sibai Xie, Joseph Wang, and Yi Chen. "Acoustically propelled nanomotors for intracellular siRNA delivery." ACS nano 10, no. 5 (2016): 4997-5005.

Soto, Fernando, Gregory L. Wagner, Victor Garcia-Gradilla, Kyle T. Gillespie, Deepak R. Lakshmipathy, Emil Karshalev, Chava Angell, Yi Chen, and Joseph Wang. "Acoustically propelled nanoshells." Nanoscale 8 , no. 41 (2016): 17788-17793.

Angell, Chava, Mingxuan Kai, Sibai Xie, Xiangyi Dong , and Yi Chen.“Bioderived DNA Nanomachines for Potential Uses in Biosensing, Diagnostics, and Therapeutic Applications.” Advanced healthcare materials. (2018)

Angell, Chava., Marta Jarczewska, Berta Esteban-Fernández de Ávila, Doris Ramirez, Joseph Wang, and Yi Chen. 2020. An Investigation of Rolling Circle Amplifications Loading Flexibility for Protein Delivery. *In Preparation for Submission.* (2020)

Angell,Chava, Sibai Xie, and Yi Chen. “pH Responsive RCA Nanoparticles for Theranostic Delivery.” *Submitted to ACS Nano.* (2020)

FIELDS OF STUDY

Major Field: Nanoengineering

Studies in DNA Nanotechnology

Professor Yi Chen

ABSTRACT OF THE DISSERTATION

Co-opting Rolling Circle Amplification to Create Lower Cost DNA Nanostructures

by

Chava Angell

Doctor of Philosophy in Nanoengineering

University of California San Diego, 2020

Professor Yi Chen, Chair

In the field of DNA Nanotechnology, a field that utilizes synthetically designed DNA strands and their inherent complimentary nature to create two and three dimensional structures, there are many approaches to creating structures to act as vehicles for drug delivery and platforms for diagnostics. However, this field holds an expense due to the number of oligonucleotide strands that are required in order to form the structures. These structures are also limited by the amount of therapeutic load they can carry, the density of targeting modalities that can be attached to the surface, and the variability of other proteins or small molecules that we may wish to include. Our approach to this problem was to utilize a natural, bacterial DNA amplification process known as Rolling Circle Amplification, or RCA. With RCA, we can amplify a sequence into a long stranded DNA sequence carrying the complementary sequence repeating multiple times sequentially on one strand. Using these repetitive sequences, we can

create structures by binding them to themselves in certain manners. Any unbound sequences can be used to bind to, and capture, many different modalities and carry a large variety of materials or therapeutics to a designated target. They can also be of great use in capturing large quantities of an analyte in detection motifs and modalities. My RCA structures are capable of binding large quantities of materials, thusly delivering them to targeted cell populations through the use of binding many ligands on the surface. These structures are also capable of undergoing morphological changes in order to facilitate delivery or act as a diagnostic modality in the presence of the target analyte or environment. Thusly, these structures, created by amplifying a single DNA strand, as opposed to utilizing many, have a great advantage over current DNA Nanotechnology techniques for creating delivery and diagnostic vehicles due to their great flexibility in binding capabilities and the decreased cost for synthesis.

Chapter 1-Introduction

Abstract:

Nanomedicine has been growing exponentially due to its enhanced drug targeting and reduced drug toxicity. It uses the interactions where nanotechnological components and biological systems communicate with each other to facilitate the delivery performance. At this scale, the physiochemical properties of delivery systems strongly affect their capacities. Among current delivery systems, DNA nanotechnology shows many advantages because of its unprecedented engineering abilities. Through molecular recognition, DNA nanotechnology can be used to construct a variety of nanostructures with precisely controllable size, shape, and surface chemistry, which can be appreciated in the delivery process. In this chapter, different approaches that are currently used for the construction of DNA nanostructures are reported. Further, the utilization of these DNA nanostructures with the well-defined parameters for the precise control in drug delivery and gene therapy is discussed.

Introduction:

Naked therapeutic agents, which include small-molecule and biomolecular drugs, have some intrinsic issues that prevent the full realization of their functions in the body. This includes poor solubility, poor stability against chemical and enzymatic degradation, inability to pass the biologic barriers, unwanted side effects and toxicity. To overcome these challenges, many different drug delivery systems have been developed in the past decades.[1,2] They can be generally classified into two categories: natural and biomimetic delivery systems such as virus[3] and red blood cells mimicking carriers,[4] and synthetic delivery systems such as liposomes and polymeric particles.[5,6] These delivery platforms use natural or synthetic particles to carry

drugs and thus bypass their physiochemical limitations and barriers for effective delivery. Through appropriate parameter design, these delivery systems can effectively increase the drug loading efficacy, the circulation time in body, and improve the final therapeutic results.[7,8] Many of them have entered clinical trials and some have been approved for clinical use.

Although these drug carriers are actively being developed, there is still a measurable gap that has to be surmounted to achieve the ultimate goal of drug delivery: the maximal therapeutic efficacy with minimal toxic effects. In spite of different routes of administration, including oral, injection, transdermal and inhalation, the delivery systems and the therapeutic cargos can be traced to the cellular level. This stimulates the exponential development of nanomedicine which uses nanotechnology tools to enhance drug targeting, reduce drug toxicity, and enable reliable diagnosis.[9,10] Among these newly developed delivery systems, DNA nanostructures show high promise. DNA is a biopolymer that can self-assemble into double helices through by Watson–Crick base pairing and is stabilized by hydrogen bonds, p–p stacking, and hydrophobic interactions. They have well-defined structures: the helical turn is 3.4 nm and the diameter is ≈2.2 nm for the B-form double- helical molecules. Fueled by this base-pairing ability, DNA nanotechnology has enabled many strategies to form DNA nanostructures with well-controlled size, shape, and surface chemistry. In nanomedicine, these properties strongly affect the delivery capacities.[11,12] and thus give DNA nanostructures unique control abilities to address some of the unmet delivery requirements.

This introductory thesis chapter will discuss the applications and weigh the usefulness and viability of DNA nanostructures in precision nanomedicine. The discussion will begin with an introduction to DNA nanotechnology, including some of the types of structures that can be formed. Following this will be an elucidation of the DNA oligonucleotide approach, the original

strategy used to create DNA nanostructures, and current uses of this strategy for drug delivery. The next motif that will be discussed is the DNA origami strategy and what has currently been achieved with DNA origami in drug and gene therapy as well. Finally, we will touch on some of the unique shapes and modalities that have been created for the purpose of DNA drug delivery and finish with our remarks and thoughts on the future viability of this field.

DNA Nanotechnology:

DNA Nanotechnology is a branch of nanoengineering that utilizes the precise and predictable nature of complementary DNA base pairing to create 2D and 3D structures. This branch of nanotechnology has many applications in medicine and biotechnology as DNA can easily be functionalized with binding ligands and fluorescent dyes for signal readout.[13] The field was pioneered in the 80's by Ned Seeman, who proposed the construction of an immobile 4-way arm junction comprised of DNA and the connecting networks through sticky ends.[14]

After a few decades of development, this field has been exponentially explored. Varies of DNA nanostructures and applications have been successfully reported. Recently, DNA nanostructures start to be used as a creative solution to both the accumulation and off target effects of other drug delivery modalities as it is a nontoxic, biologically derived material that can be easily functionalized to target receptors on the cell surface and can also be covalently or electrostatically attached to metallic nanostructures.[15]

To create stable structures out of DNA, certain sequence symmetry has to be minimized to prevent the instability that is seen in many intermediate structures, such as Holliday junctions (**Figure 1.1** A).[14] There are also many design considerations such as the incorporation of sticky ends, and reciprocal exchanges for stability, also known as 'crossovers'.[16]

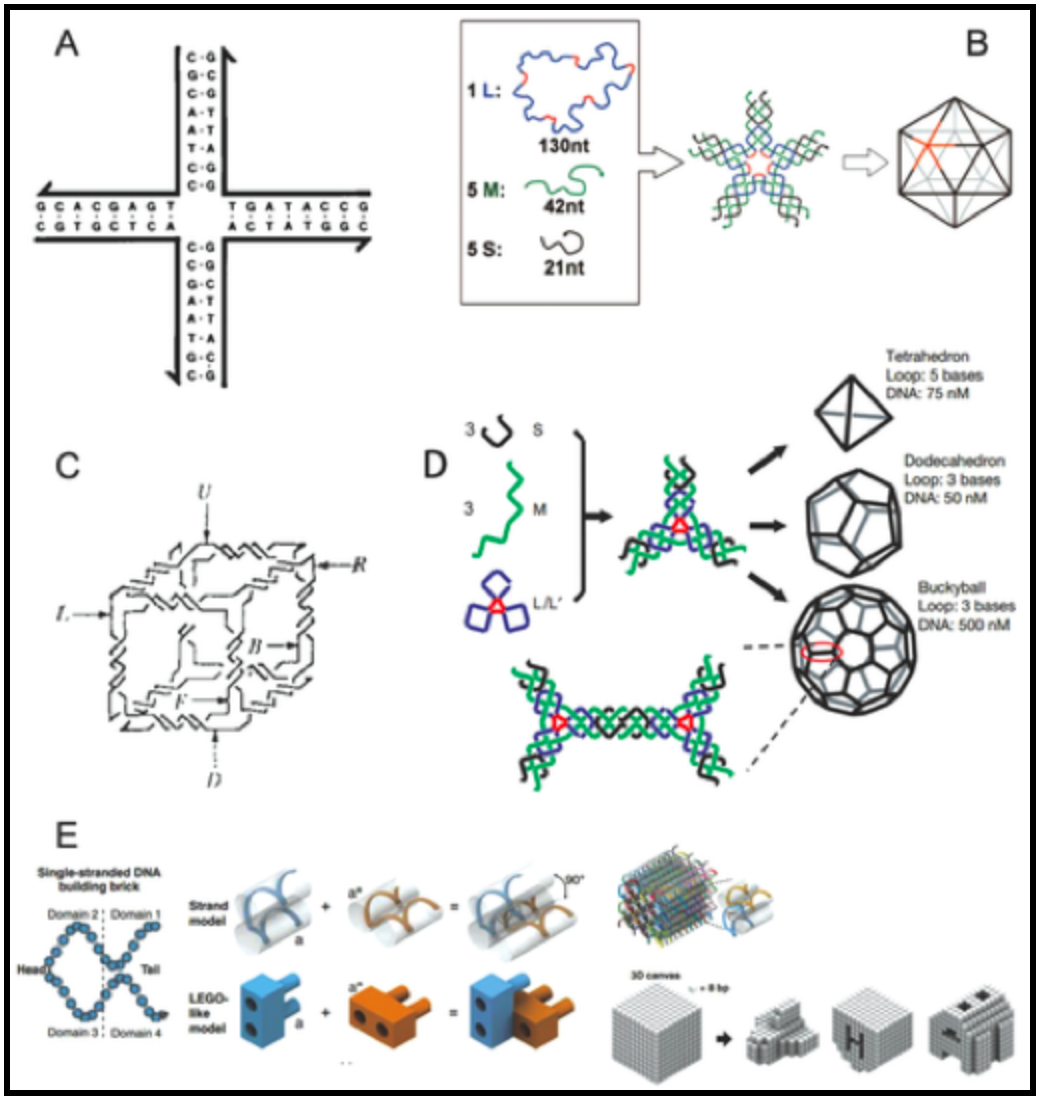

Figure 1.1. Demonstration of DNA nanostructures. A) immobile 4-strand junction proposed by Seeman. Reproduced with permission. [14] Copyright 1983, Cell Press. B) Icosahedral structure formed by flexible five-point-star motifs. Reproduced with permission. [22] Copyright 2008, National Academy of Sciences. C) Truncated cubic structure. Reproduced with permission. [17] Copyright 1991, Nature Publishing Group. D) Different structures formed by the same three-point-star motif with different "loop" length and concentration. Reproduced with permission.[19] Copyright 2008, Nature Publishing Group. [23] E) Single-stranded DNA bricks form 3D canvas. Reproduced with permission. [27] Copyright 2012, American Association for the Advancement of Science (AAAS).

DNA nanotechnology is a highly intriguing strategy for self-assembled drug delivery structures as it allows for the creation of precise structures that can mimic nanoparticles or viral capsids. Such structures include polyhedra of different sizes and shapes such as cubes,[17]

tetrahedra,[18–20] octahedra,[21] buckyballs,[19] and icosahedra.[22,23] Larger shapes based on the DNA origami method are also reported.[24]

Goodman et al. reported a facile way of building DNA tetrahedra using four different strands, with the struts less than 10 nm in length.[18] Under the simple process of cooling from 95 °C to 4 °C in 30 s, tetrahedra form under a yield of 95% and can be characterized by a single band on a native gel.

Another approach was proposed by He et al. to construct tetrahedra, dodecahedra, and buckyball structures through DNA tiles (**Figure 1.1 D**).[19] The proposed three-point star motif was used for 2D crystal formation.[25] In this approach, the flexibility of the long central strand was enhanced by elongating the non-binding hinge parts which they call “loops”, so that the motifs tend to bend and form closed structures. The concentration of the motif also affects the resulting structure. A loop length of 5 bases and a low concentration of 75 nm gives a final result of tetrahedra, while 3 bases loops and 50 nm gives dodecahedra, and 3 bases loops and 500 nm concentration gives buckyball structure. Each strut is around 14 nm.

Similar tile approach can also be used to form icosahedral DNA nanostructure (Figure 1.1 B).[22] The same group reported in 2008 a method to fabricate truncated icosahedra of diameter ≈20 nm. The five point star motif used in this method has a four base loop. They also reported that the concentration of the motif also has an effect on the predominant structure that can form: the samples form a big cage structure (≈115 nm in diameter) under higher concentration. The icosahedra sample was prepared in the concentration of 20 nm to prevent the formation of larger structures.

DNA nanostructures can also be formed through a step-by-step process. Chen et al. demonstrated this method by constructing a nano-scale cube structure (Figure 1.1 C).[17] In each step they hybridize two squares and in the last step the ends are connected to form a cube.

Bahtia et al. reported a three-step way to encapsulate gold nanoparticles into a truncated DNA nanostructure. [23] They first anneal DNA strands to form five-arm vertex motifs, and then combine the two “halves” form icosahedron with complementary binding sites. The two halves were put into a gold nanoparticle solution. The icosahedron with diameter of roughly 19 nm can successfully encapsulate 2–3 nm diameter gold nanoparticles. Other icosahedra have been reported that can intercalate doxorubicin (Dox).[26]

An important concept in DNA nanotechnology is ease of modular self-assembly. In 2012, Ke et al. reported the construction of short “DNA bricks” that can be used to create many different types of structures without having to redesign staple strands and scaffolding routing as is necessary in creating varying origami structures (Figure 1.1 E).[27] The authors reported essentially a lego-like modality in which each brick had a distinct shape and could bind to 4 neighbors just as a lego can fit into specific holes. These interactions are defined by the domains of the DNA bricks which have unique sequences. Therefore, each 32 nucleotide brick is distinctive and can be combined to create different 3D structures with both controllable surface features and precise cavities within the structure. 102 different structures were created using this method merely by selecting the bricks needed which greatly simplifies the process of creating 3D DNA nanostructures.[27]

There are several methods to make viable, stable structures comprised mostly or entirely of DNA: DNA origami, oligonucleotide design, and rolling circle amplification. In this review, we

will touch on the methodologies used to form DNA nanostructures and how those methodologies are being coupled with both gene silencing therapies and cancer therapeutic drugs to more successfully deliver and control the delivery of therapeutic modalities to site specific cells *in vivo*.

DNA-Based Approaches for Drug/Gene Delivery:

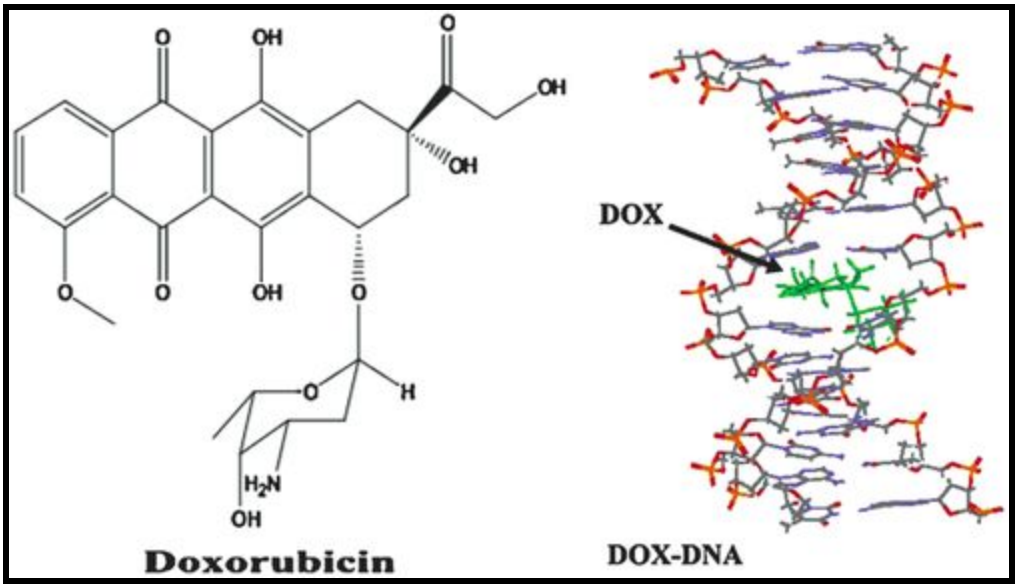

Figure 1.2. Reproduced with permission. [31] Copyright 2014, Elsevier.

There are many methods that have been coupled to DNA nanotechnology to effectively deliver therapeutic modalities, including drug modalities, gene-silencing modalities, and the incorporation of cellular targeting into DNA nanostructures. Many DNA drug delivery systems include the incorporation of doxorubicin (Dox), an anticancer therapeutic,[28,29] as the proof of concept for small molecular drug delivery. Dox can intercalate into the DNA structure and allow it to form properly by relieving torsional stress, as showed in **Figure 1. 2** [29–31] However, despite Dox's potency as an anticancer drug, it can have serious side effects when it

accumulates off-target such as cardiomyopathy, which can lead to congestive heart failure.[32] Therefore, avoiding off-target or premature delivery must be achieved.

Another therapeutic technique that many researchers have been taking advantage of is gene-silencing through RNA interference.[33] Small interfering RNA (siRNA) in particular has been utilized by many researchers for therapeutic gene silencing and can be modified to be target specific to avoid off target silencing effects.[34] RNA interference can usually be used without triggering the immune system. However, the introduction of the artificial siRNA can monopolize the natural interference pathway of the RNA silencing complex, which is an important part of the cellular function.[35] One of the biggest challenges in RNA delivery is stability *in vivo*, but chemical modifications of the oligomers can increase the stability.[36]

The targeting issue using DNA nanostructures can be achieved through the use of DNA aptamer sequences and also through the use of functionalizing the DNA with targeting ligands and can help avoid many of the undesirable off target effects.[32,37,38] For example, Zhu et al. created synthetic DNA adducts to allow for targeted anticancer delivery.[32] These take advantage of the overexpression of certain receptors during cancer.[39]

Once been uptake by cells, DNA nanostructure can be designed to respond to environmental triggers to release loaded drugs, such as incorporation of linkers that are responsible to changes in the pH.[29,30,40,41] This technique can also aid in mapping the pH changes inside the cells itself, as reported by Modi et al.[41]

There are several possible pathways for these DNA nanostructures to enter the cell and partially be explored by using inhibitors to block certain pathways.[42,43] These path- ways can be divided into two types: endocytotic pathways and non-endocytotic pathways.[44] The

endocytotic pathways include phagocytosis, clathrin mediated endocytosis, caveolae mediated endocytosis, and macropinocytosis. However, it is not well understood what mechanism is responsible for the successful uptake of DNA nanostructures. Preliminary data such as that demonstrated by Chen et al. suggested clathrin receptor mediated endocytosis.[43] They measured the mechanism of the uptake of their rolling circle amplification (RCA) nanoribbons through inhibitors such as chlorpromazine, a clathrin inhibitor, genistein, a caveolae mediated inhibitor, methyl-β-cyclodextrin, a lipid-raft endcytosis inhibitor, wortmannin, a macropinocytosis inhibitor, and NaN3, an energy dependent endocytosis inhibitor. Final results suggested that the uptake is clathrin mediated and lipid raft mediated endocytosis.

Chen et al. also studied the mechanism of transfection of DNA nanoparticle (DNPs) and suggested that nucleolin is a good target for non-viral gene delivery with the presence of glucocorticoid receptor (GCR).[45] Besides the disruption of a raft protein, flotillin also decrease the transfection of DNPs, while inhibition of other endocytic pathways barely affects the process.

Most of the cell membranes carry net negative charge and nucleic acids also carry a net negative charge.[46] As a result, some DNA nanostructures, not containing targeting modalities, may need some kind of cationic transfection agent, such as Lipofectamine, to increase the cellular uptake and therapeutic efficacy.[46] Positively charged intercalators or positively charged proteins, such as Dox, viral capsule proteins, or cationic polymers, may also help reduce the net negative charge thus reducing the electrostatic repulsion in the DNA structure itself and between the DNA nanotechnology and the cell membrane.[33,47–49]

For the purpose of this introductory chapter, I will discuss the different mechanisms of DNA nanostructure formation as separate categories. These mechanisms are integral to what can be achieved for the shape and size of the structures and can affect what can be delivered

and the release kinetics of delivery. Some large structures can only be created through the use of DNA origami and certain modularity can only be achieved using the oligonucleotide approach. However, some structures are hybrids of different fabrication methods and may fit multiple synthesis categories. Therefore, they will be categorized by their primary method of synthesis.

Oligonucleotide Approach:

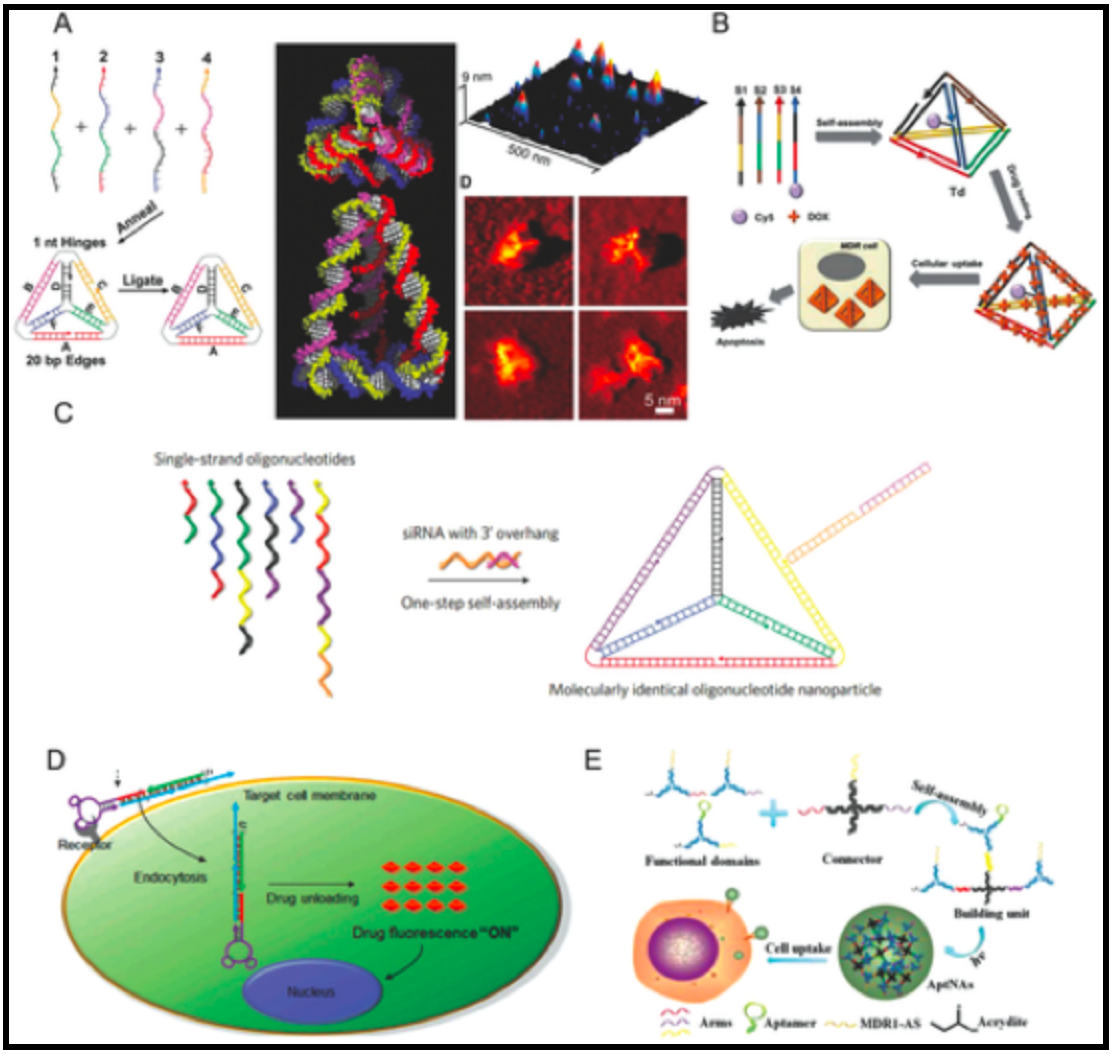

Figure 1.3. A) The original DNA tetrahedral structure proposed by Turberfield. Reproduced with permission. [18] Copyright 2005, AAAS. B) Modified DNA tetrahedral structure with Cy5 dye and Dox intercalation. Reproduced with permission. [13] Copyright 2013, Royal Society of Chemistry. C) Incorporation of siRNA onto the struts of the DNA nanotetrahedron. Reproduced with permission. [52] Copyright 2012, Nature Publishing Group. D) Proposed drug delivery route of DNA nanotrain. [53] E) Multifunctional aptamer-based nanoparticles. Reproduced with permission. [54] Copyright 2013, American Chemical Society.

Due to the precise and predictable pairing nature of DNA chains, the size and shape of the nanoscale DNA constructs can be designed to fit current drug delivery needs. Moreover, overhangs can be introduced on to the structures to allow easy functionalization of fluorescent dyes, targeting agents or even drugs.

The oligonucleotide strategy was reported first by Nadrian Seeman in 1983 and is widely considered the foundation of DNA nanotechnology. He synthesized a stable 4 arm junction with 4 sixteen base strands by minimizing the strand symmetry.[14] The oligonucleotide strategy requires more design consideration as there are no viable programs for designing these structures. Oligonucleotides have been used to create many types of structures such as nanotubes,[50] tetrahedra,[13,51] icosahedra,[23] and many other polyhedral structures.[19,21]

In 2010 Kim et al. reported a simple method of intercalating Dox into DNA tetrahedra as carriers to reverse drug resilience of cancer cells.[13] The dye Cy5 was incorporated into the tetrahedron for characterization purpose (**Figure 1.3** B). Results show that even without any targeting agent, the DNA tetrahedra are able to enhance uptake and bypass the efflux process in multidrug resistant breast cancer cell line (MCF-7 cancer cells). These results suggest certain shape dependence on transfection efficacy.

An example of DNA polyhedra assembled from oligonucleotides was reported by Chang et al. in 2011.[26] They designed a six-point-star motif with five sticky ends that are self-complementary and one end with targeting aptamer to assemble into icosahedra with diameter of around 28 nm, while the ends with aptamer erect. Dox was intercalated into the structure without affecting the shape. The Mucin-1 (MUC-1) aptamer was used to target MUC 1+ MCF-7 cells. The dox–apt–icosahedron complex shows great specificity and aptamer-mediated internalization for killing epithelial cancer cells. DNA polyhedral nanostructures have also been used in gene delivery.

Lee et al. reported a way to deliver siRNA using a tetrahedral DNA structure with a hydrodynamic size of 28.6 nm with narrow distribution (**Figure 1.3 C**).[52] Molecular identical oligonucleotide particles (ONPs) with six folic acid ligands per particle were injected in nude

mice with human epidermoid carcinoma cell (KB) xenograft tumors. Results show that the ODNs can accumulate primarily in the tumor and kidney. The circulation time of the ODNs is also a lot longer than the parent siRNA (blood half-life t1/2 ≈ 24.2 min vs 6 min).

A concept of nanotrain was reported by Zhu et al. in 2013.[53] Two strands of ODNs alternatively bind to each other triggered by an aptamer trigger to form a longer chain train-like structure with an aptamer sgc8 on one end to target specific cells (**Figure 1.3 D**). Dox is intercalated into the DNA double strand. The complex can be specifically transport the drug to target cancer cells, initiate endocytosis and unload the drugs within the cells. The complex was tested in vivo in NOD.Cg-Prkdc (scid) IL2 mice and showed reduced side effects and stronger therapeutic potency.

Wu et al. reported a modular aptamer based DNA nanoassembly (AptNA) approach (**Figure 1.3 E**).[54] Multifunctional DNA sequences are first assembled into Y-shaped functional domains and then connected to X shaped connectors. The connector has a photopolymerizable arm so that the building unit with different functional domains could be polymerized into spherical structure of diameter around 200 nm. The aptamer sgc8 was used to target CCRF-CEM (T cell acute lymphoblastic leukemia cell line) cancer cells. The cells showed increased viability compared to the treatment by free Dox. The DNA nanoparticles also showed selectivity on CEM cells rather than the non-target Ramos cells.

Li et al. developed a tetrahedron motif bearing unmethylated cytosine–phosphate–guanine (CpG) motifs which have immunostimulatory properties.[55] This is due to the fact that these motifs can bind to certain cellular receptors known as endosomal Toll-like receptor 9 and trigger an immunostimulatory response. After incubation with macrophage cell line (RAW264.7 cells), these structures were mostly localized in the cytoplasm

as imaged by confocal microscopy. Degradation studies were also conducted by incubating the tetrahedrons in fetal bovine serum (FBS). These structures remained stable at 4 hours whilst simple DNA duplexes degraded in the span of 2 hours.

Sellner et al. reported in 2015 an in vivo study of gene delivery by DNA nanotubes. The nanotubes were assembled by the single stranded tile (SST) method, in which each tile consists of four 10–11 bases domains and a total length of 42 bases.[50] Sticky ends of poly-As stick out of the tube side walls for functionalization. CpG and fluorescent dyes ATTO488-dUTP or Cy3-dUTP were conjugated onto the structure. The *in vivo* study on anesthetized mice showed that while plain nanotubes do not induce an immune response, CpG conjugated nanotubes can target tissue-resident macrophages and reach intact muscle tissue almost immediately, and elevate immune response strongly. The DNA nanotubes also had some stability against DNase I within muscle tissue.

Origami Approach:

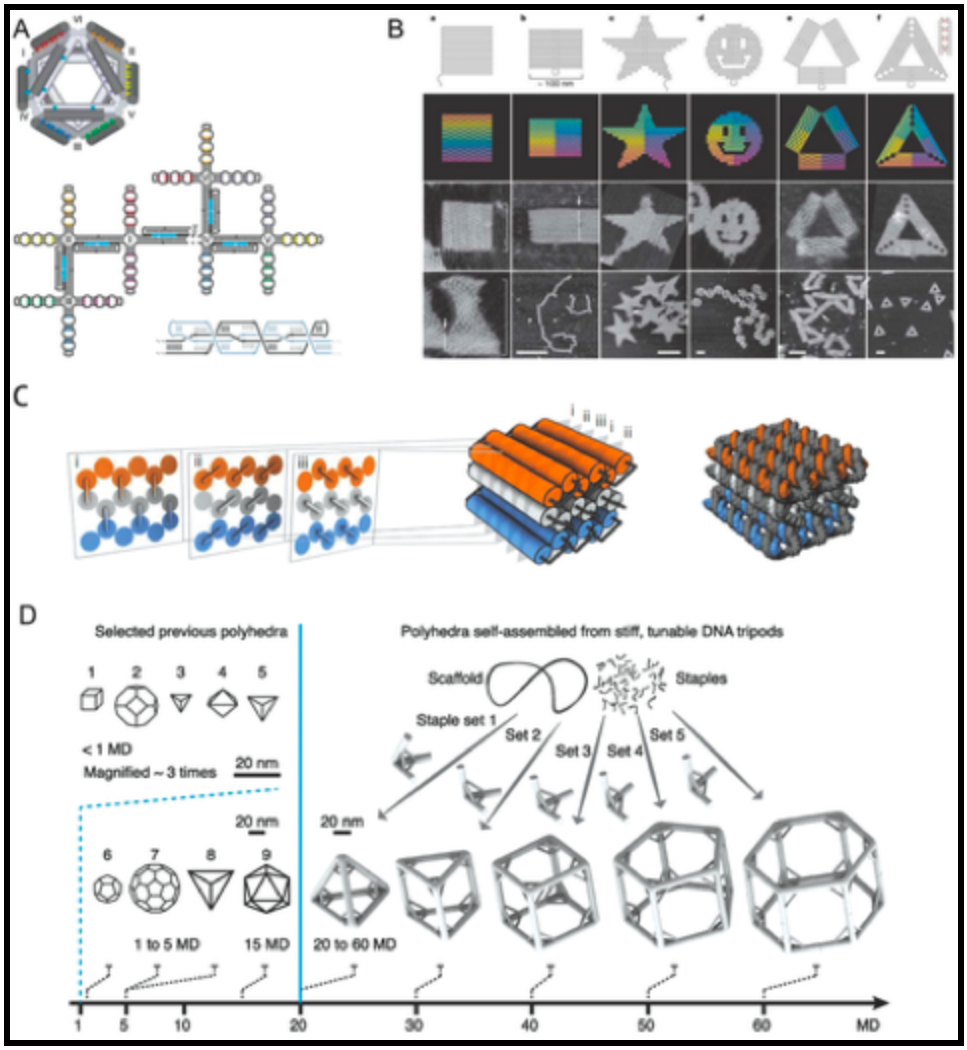

Figure 1.4. A) DNA octahedron obtained by folding a 1.7 kilobase backbone. Reproduced with permission. [63] Copyright 2004, Nature Publishing Group. B) Rothemund's DNA origami shapes. Reproduced with permission. [58] Copyright 2006, Nature Publishing Group. C) 3D DNA origami structures. Reproduced with permission. [60] Copyright 2009, Nature Publishing Group. D) Large 3D structures synthesized by Ilumina to carry therapeutic loads. Reproduced with permission. [24] Copyright 2014, AAAS.

As seen above, DNA oligonucleotides allow for the creation of precise structures that can be manipulated to deliver both gene therapies and anticancer therapeutics. Other than that, other strategies for synthesizing precision DNA nanotechnology are also extremely attractive for their shape control, control of flexibility and size, and ability to create larger, modular structures that can even be extended to include kinematic, movable joints.[27,56,57] This approach is

normally called DNA origami. It was pioneered by Paul Rothemund in 2006 (**Figure 1. 4**B).[58] DNA origami refers to the folding of a long stranded bacteriophage (7240 nt) through the use of over 200 complementary staple strands to fold the backbone. Paul Rothemund used the M13m18 bacteriophage and his original structures were 2D. Each oligonucleotide is considered a 6 nm pixel to build any pattern of desire. By putting sticky ends on the connection part of each construct, an extended array can also be formed. Since then, the DNA origami motif has been extended to three dimensions.[59,60]

There are now several programs that facilitate the design of DNA origami structures such as caDNAno and SARSE.[56,61] With DNA origami, structures such as smiley faces, tetrahedrons, DNA nanotubes, DNA barrels, DNA “dolphins” and many other shapes are possible.[20,28,56,58,62] Many groups have worked on extending this modality and facilitating its use for structural formation and drug delivery.

Shih et al. reported back in 2004 an idea similar to the later developed DNA approach, which is to fold a long backbone DNA chain by binding it at different points using staple strands (**Figure 1.4 A**).[63] In this example a 1669-nucleotide single-stranded DNA is used as the backbone and five 40-nucleotide strands are used to fold the backbone. Double-crossover and paranemic-crossover structures are designed to ensure the stiffness of the structure. It was proposed that the long backbone chain can be readily amplified. Douglas et al. reported that using the same DNA origami method, it is also possible to fabricate 3D structures.[61] They used honeycomb-pleat-based strategy to bring the helices together at a certain angle to construct 3D structures (**Figure 1.4 C**). They also developed a software called caDNAno, an easy tool to design 3D structures and program the staple strands. The whole design and synthesis process took 2 weeks as they reported. One of the largest challenges that faced DNA

origami was the time it takes to fold and hybridize the structures. In 2012, Sobczak et al. determined that a long annealing process is not necessary to create these structures in a "one-pot" reaction scheme as there is a distinct range where DNA will fold and hybridize.[64] These experiments also reported that DNA folding and unfolding are non-equilibrium processes as the temperature for unfolding is higher than the one at which the structures formed. This experiment allows DNA origami to be on a more feasible time scale.

There is the desire within this field to create large structures that mimic viral capsids. Iinuma et al. reported the construction of polyhedra from million daltons (MD) monomers (**Figure 1.4 D**).[24] These monomers created a 5-MD DNA origami three arm junction that was sixty times more massive than previously reported 3-arm motifs. These junctions have a "dynamic connector" design and Iinuma et al. created a DNA tetrahedron, a cube, a triangular prism, a pentagonal prism, and a hexagonal prism. All structures were on the order of 20–60 MD and had compartments that are similar in size to those of bacterial microcompartments and could be used to carry therapeutic loads. In drug delivery, the kinetics and controllability of release is an important factor for consideration. If the therapeutic is released in a burst mechanism as opposed to a slow, tunable release, there will be a higher initial delivery, however this can lead to high physiological damage and a lower lifetime of the therapy, which leads to the need for higher dosages.[65] DNA origami allows for either controlled or triggered release of a therapeutic modality through either the intercalation of positively charged molecules or the linking of certain peptides or proteins onto the surface of the DNA origami structure.

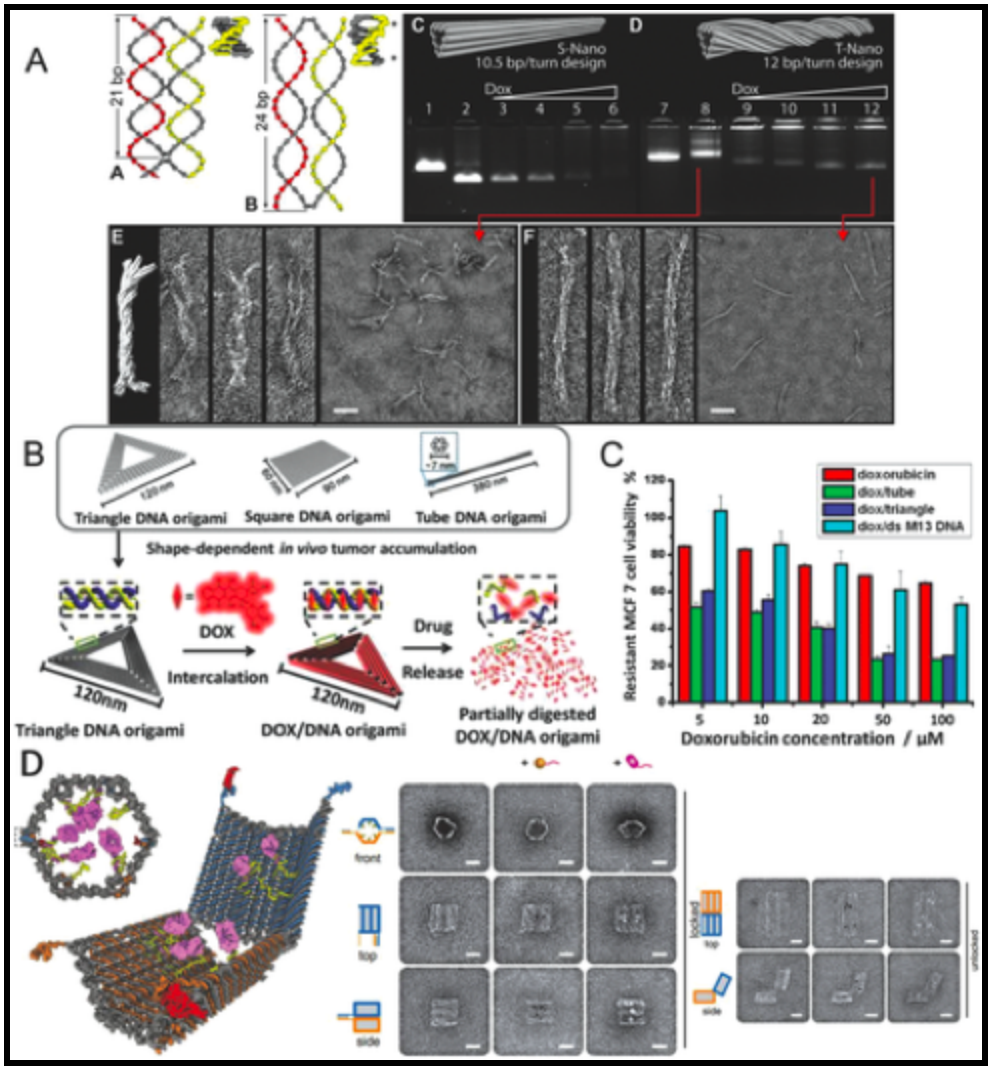

Figure 1.5. A) Doxorubicin-intercalating nanotubes. Reproduced with permission. [28] Copyright 2012, American Chemical Society. B) Doxorubicin intercalating nanostructures. Reproduced with permission. [62] Copyright 2014, American Chemical Society. C) Doxorubicin-intercalating nanostructures in combating drug resistance. Reproduced with permission. [66] Copyright 2012, American Chemical Society. D) DNA origami nanorobot. Reproduced with permission. [67] Copyright 2012, AAAS.

In 2012, Zhao et al. designed and fabricated a structure that has controllable release properties of Dox, a well-known anticancer therapeutic. These structures take advantage of the fact that DNA origami structures with a specific twist density will only correctly fold in the presence of an intercalating molecule such as Dox (**Figure 1.5** A).[28] This was origi- nally demonstrated by Ke et al. who inserted base pairs (bp) in between crossover junctions.[47]

These insertions, while relieving electrostatic repulsion, also increase torsional strain, thus destabilizing the structure and allowing for the intercalations to bind to the structure.[47] This binding relieves the stress and encourages the correct folding of the origami structures.

Zhao et al. created structures with 12 base pairs per turn that only fold correctly in the presence of Dox and compared them to structures with a natural twist density of 10.5 base pairs per turn. The increased binding affinity of the Dox also translates into both a higher loading and a slower and more sustainable release profile.[28]

Other groups have also reported utilizing DNA origami structure for Dox intercalation and controlled delivery. Zhang et al. reported the construction of varying shapes composed of DNA origami structures and loaded these structures with Dox to measure the *in vitro* drug release and the in vivo antitumor effects (**Figure 1.5 B**).[62] The shapes reported were a triangle, a square, and a tube. To test the accumulation, each structure was loaded with quantum dots and imaged fluorescently. The triangle shape demonstrated the highest efficacy of passive tumor targeting out of the three structures and maintained accumulation levels for 24 hours. Both the square and tube showed higher levels of off-target accumulation in the liver and kidney. The structures were stable in serum for 24 hours and demonstrated slow release properties with 20% released after 8 hours. In more acidic buffer conditions, which more closely mimic a tumor microenvironment, the release content was increased. When tumor-bearing mice were injected with saline, Dox, Dox/origami structures, and origami structures, the Dox/ origami structures were the most effective at reducing the tumor size. Earlier experiments reported by this group demonstrated that these nanostructures helped avoid multidrug resistance that Dox can induce by testing the Dox/origami structures in MCF 7 Dox resistant cells which were created by exposing the cells to increasing concentrations of Dox (**Figure 1.5 C**).[66]

As mentioned earlier during the course of this review, effective transfection and uptake of DNA nanostructures can be difficult and lead to low yield and therapeutic dose due to their net negative charge. Mikkilä et al. coated DNA origami structures with cowpea chlorotic mottle virus capsid proteins to allow for a more effective transfection as the proteins have a positively charge N-terminus.[48] This helps to combat the net negative charge of the DNA and allowed the structures to enter the cell. The DNA origami nanostructures "template" the self-assembly of the virus proteins with high yield through electrostatic binding. The results reported transfection efficiency higher than Lipofectamine 2000. The proposed uses for these structures are drug delivery applications.

Another method for utilizing DNA origami for delivery is covalently linking the small molecule drugs or nanoparticles to the structure. In 2012, Douglas et al. reported the construction of logic gated nanorobot with a hexagonal barrel shape (**Figure 1.5 D**).[67] This barrel can be loaded with therapeutics through the use of covalent linkers on the inside. The logic gate, or "lock", is a 23 base pair sequence that is antigen activated. This type of sequence is known as an aptamer and its sensitivity is directly related to the length of the sequence. In the presence of the correct antigen, the duplex will bind to the antigen and allow the barrel to open. The length of the sequence is tuned such that the risk of spontaneous activation is minimized (at around 16 bp) whilst the sensitivity is preserved as longer sequences are much less sensitive. These aptamer-based cues allow for triggering and targeted delivery based on local environments that are specific to certain disease modalities.

Rolling Circle Approach:

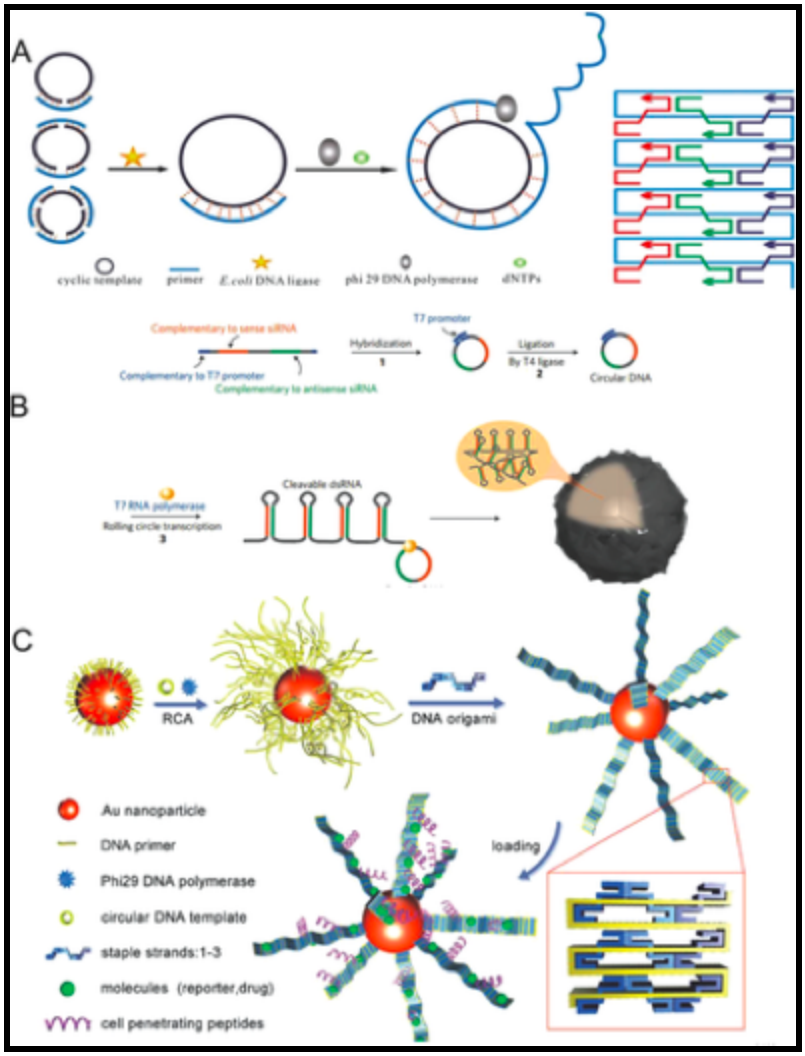

Figure 1.6. A) DNA origami using rolling circle amplification. Reproduced with permission. [69] Copyright 2013, Wiley-VCH. B) RNAi microsponge. Reproduced with permission. [73] Copyright 2012, Nature Publishing Group. C) DNA nanobelts loaded with reporter/therapeutic molecules and cell penetrating peptides. Reproduced with permission. [71] Copyright 2015, Wiley-VCH.

Rolling circle amplification (RCA) represents a novel way to approach precision DNA nanostructure construction. RCA creates long stranded structures with repeating DNA sequences through the use of a circular template and DNA polymerase, which copies the template thousands of times.[68] This allows for the precise templating of the RCA strand. The polymerase continually adds complementary nucleotides to the template until it is denatured or runs out of available nucleotides. This creates long stranded DNA with a known, repeating

sequence that is dependent on the sequence of the circular template.[49] This long stranded DNA can be manipulated through staple strands similarly to DNA origami.[43,69] The staple strands can also be manufactured through RCA and cleaved through a site-specific cleavage. RCA has been used to create nanotubes,[70] DNA nanoballs.[49] nanobelts that can intercalate dox and quantum dots,[71] and DNA nanoclews.[29] It has also been incorporated into DNA logic gates.[72] RCA can also be applied similarly to DNA origami, as demonstrated by Ouyang et al. who created a long stranded DNA template out of RCA instead of using a bacteriophage DNA (**Figure 1.6 A**).[69] These structures can easily be folded by fewer staple strands than DNA origami and can be utilized for therapeutic, drug delivery purposes as they are easily internalized by cells.[43,69]

Yan et al. has demonstrated a method to integrate nanoparticles and DNA strands produced in rolling circle amplification (RCA) utilizing a similar method to Ouyang (**Figure 1.6 C**).[71] DNAs are grown in-situ on gold nanoparticle surface, and the repetitive long chains are folded into so-called DNA belts while remaining at the particle surface. Drugs and targeting agents can be loaded on to the DNAs by either merging or intercalating mechanism for theranostic purposes. Merging was used to load quantum dots (QDs) for cellular imaging and intercalation was used to load Dox. Incorporation of the QDs and cellular penetration peptides (CPPs) on the nanoparticle (NP)–DNA conjugate gives QDs the ability to get into U87 MG cells, while maintaining the spacing so that QDs are not quenched by CPPs. Incorporation of Dox into the structure also shows a 2.5 times higher cell-killing efficacy in U87 MG cells than pure Dox.

Another proposed use for RCA is the self-degradable nanoclew reported by Sun et al.[29] The nanoclew is woven by RCA and includes DNase to degrade and release a therapeutic load inside the cells. To enhance the loading of the anticancer therapeutic Dox,

multiple G–C sequences were incorporated. The nanoclew is a composite structure including a polymeric capsule which contains the DNase and is degradable by acidic pH, allowing for triggered release by the cellular environment (i.e., the acidity of the late stage endosome) and protecting the Dox until it can have the most therapeutic effect. The capsule is positively charged to allow for incorporation into the structure. Finally, these structures were incorporated with folic acid to allow for the targeting of the folate receptors which are overexpressed in many cancers. These structures showed both efficient internalization and efficient nucleic accumulation.

Other DNA devices have taken advantage of this late stage endosomal pH shift.[30] Kim et al. created a DNA nanoball composed of an RCA template that was complimentary and hybridized to two types of antisense oligonucleotides.[49] These were then condensed by cationic Mu peptides and coated with hyaluronic acid to target the CD44 receptors. The addition of Mu decreased the size and increased the stability against nuclease.

In 2012, Lee et al. reported the construction of an RNAi microsponge that was synthesized by the self-assembly of siRNA polymers that are cleavable after cellular uptake, thus allowing for the protection of the siRNA until it has been successfully delivered (**Figure 1.6 B**).[73] The RNA is stable in the pleated nanosheets that form the microsponge as they exist in the hairpin modality. The long stranded RNA was produced through RCA but utilizing RNA polymerase instead of DNA polymerase. These microsponges, when combined with cationic polyethylenimine (PEI) were successfully transfected into cells and showed knock-down of luciferase expression. Rolling circle amplification is a very integrative process that allows for the creation of unique structures with repeating units. These repeating units are critical in allowing

the precise control of the nanostructure degradation, through the incorporation of regions with known responses to cellular environments, and therefore, therapeutic delivery.

DNA Nanoparticles:

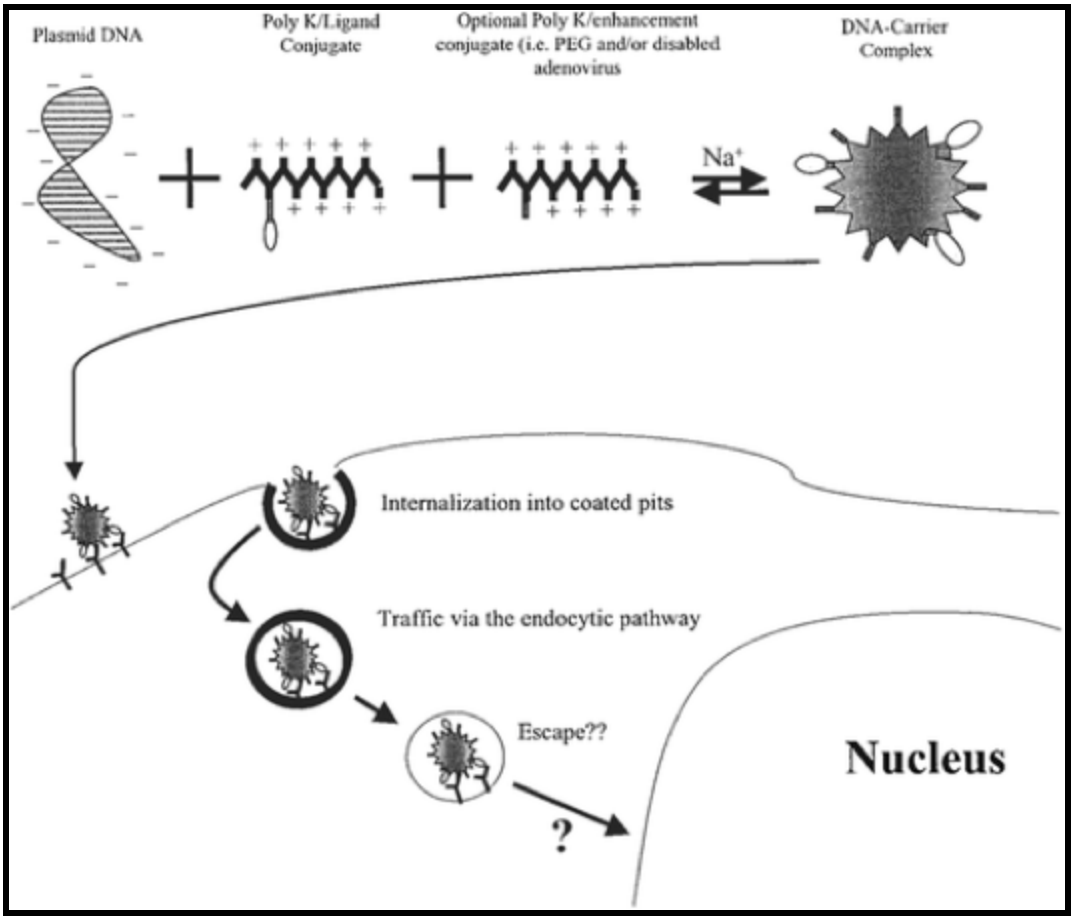

Figure 1.7. Proposed delivery path for DNA nanoparticles. Reproduced with permission. [79] Copyright 2002, Springer.

Another possible modality for utilizing DNA as a precision drug or gene delivery vehicle is to create nanoparticles comprised of the DNA itself (**Figure 1.7**), or a DNA nanoparticle.[45,74–89] DNA nanoparticles feature controllable sizes from ≈20 nm to ≈200 nm in diameter. The fabrication of the particles also allows a polyethylene glycol shell for longer circulation time.[80–84] It is also proved facile to functionalize the particle with targeting groups

like serpin enzyme complex receptor, SEC.[76] In this approach, DNA nanoparticles that were transformed from complexes of DNA to nanoparticles from 18–25 nm through the use of poly-l-lysine covalently coupled to a synthetic peptide.[74] Longer chain length (53.7 kDa poly-K) gives smaller particles and significantly more and longer duration of gene expression than short chain (9.7 kDa poly-K) complex. Moreover, shorter peptide chains give less protection from the DNase both in vitro and in vivo.[77] This complex allows the gene transfer into the cell via cer- tain cellular receptors. Cells containing the desired receptors showed the peak activity of the luciferase that was transfected. This receptor-targeting gene delivery can be apply on some emphysema patients, who has deficiency of alpha1–antitrypsin (A1AT), a specific kind of antiprotease, particularly in the lung.[75] In this treatment, alveolar macrophages (PAM) which reside within alveoli are targeted and mannose-terminal glycoprotein conjugates are used. Although the gene showed low expression in the cells, the gene transfer technique still appears promising once they have found proper receptor for this particular problem. This system is also used as a gene therapy for cystic fibrosis.[78,80–83,85] Utilizing the same serpin enzyme receptor targeting.[74,76] and condensing the plasmid DNA for the complementary DNA (cDNA) encoding human cystic fibrosis transmembrane conductance regulator (CFTR) with poly-l-lysine, these particles can be used to correct the chloride transfer defect.[78] These particles restored the expression of CFTR and of nitric oxide synthase-2 (NOS-2) in the nasal epithelium where the complexes were administered even with only 0.15 μg of DNA administered. Similar particles, with serpin targeting, that transfected the LacZ reporter gene showed galactosidase expression but no correction of the NOS-2 deficit. When these particles are poly(ethylene glycol)-modified (PEGylated), there is a higher avoidance of aggregation, higher circulation time, and effective transfection of the desired gene in the airway epithelium.[80] They also do not require the targeting ligand. The toxicity of these PEGylated

particles is minimal in vivo, stable in saline, and have a half-life of 2–4 hours in mouse serum.[81] These complexes also do not induce an antibody response when lacking PEG,[84] and when tested in human subjects, there were no adverse effects from the drug except in possibly one subject, and 8 out of the 12 subjects experienced at least partial, if not complete, CFTR chloride channel function.[83] Repeating dosing, at least three doses have been demonstrated as possible with the targeting, were also suggested as a possible to extend the lifetime of the transgene expression, despite the low levels of antibody formation to the ligand.[84] The PEGylated DNPs also showed long-term transgene expression in central nervous system in mice.[87] An intracer- ebral injection of DNPs can transfect both neuron and glia, and the transgene expression stayed active in the striatum for up to 8 weeks, at least 100-fold greater than naked DNA. Bioluminescent imaging (BLI) was also used 11 weeks after injection and significant higher transgene activity by DNPs than naked DNA was detected.Other than treatment, these particles are also useful in real-time imaging system: BLI, positron emission tomography (PET), and magnetic resonance imaging (MRI).[86] The efficacy of gene delivery using poly(ethylene glycol) (PEG)-stabilized DNPs was assessed using BLI of transgene expression in wild type and cystic fibrosis mouse models[88] and in long-term tracking of transgene activity in brain in 2011.[89]

Another kind of DNA nanoparticle includes the combination of interfering RNA with actual metallic nanoparticles to increase the density and the uptake of the siRNA.[15] These particles, reported by Jensen et al., showed significant down-regulation of their target: the oncoprotein, Bcl2Like12 which inhibits apoptosis, thus allowing for higher cytotoxicity of the cancer cells.

Other DNA Nanostructures:

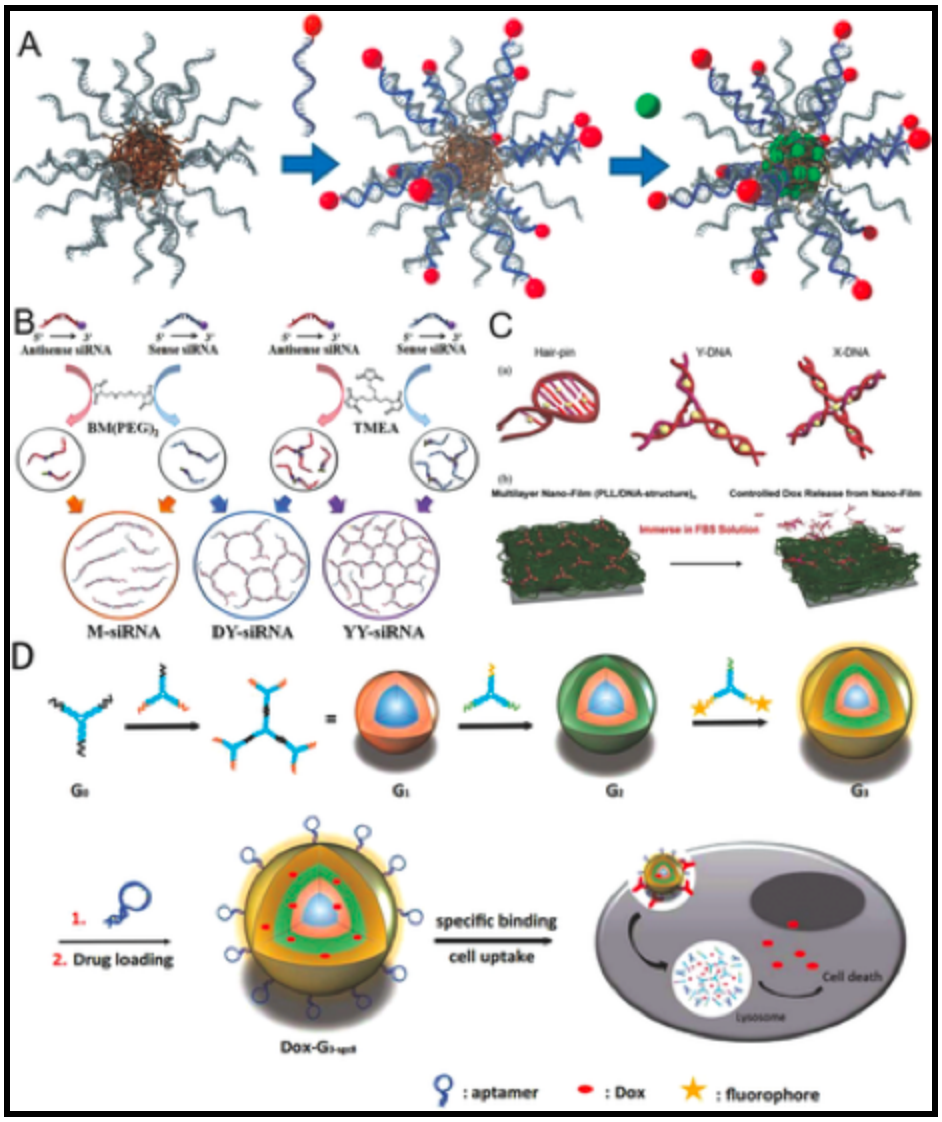

Figure 1.8. A) DNA block copolymer system. Reproduced with permission. [90] Copyright 2008, Wiley-VCH. B) DNA nanogel. Reproduced with permission. [91] Copyright 2011, American Chemical Society. C) DNA-structured nanofilm synthesized by layer by layer deposition. Reproduced with permission. [93] Copyright 2014, Nature Publishing Group. D) DNA dendrimer layered particles. Reproduced with permission. [94] Copyright 2015, Nature Publishing Group.

It is also worthwhile to review some other unique DNA nanostructures that have been used for drug delivery that don't fall entirely within any particular category of synthesis. These

methods also possess the potential of shape control, ease of functionalization of targeting agents, and incorporation of drugs.

DNA block copolymer system was introduced by Alemdaroglu et al. in 2008 (**Figure 1.8 A**). [90] The hydrophobic core made of polypropylene oxide (PPO) is designated for incorporating hydrophobic drugs like doxorubicin (**Figure 1.8 A**). The DNA shell makes it easier for functionalization of targeting groups, in this case, folic acid. The diameter of the final particles is roughly 10 nm. Human colon adenocarcinoma (Caco-2) cells were used to test this delivery system. Fluorescence labeling showed that the particles are readily uptaken by the cells and loading of Dox showed efficient cytotoxicity.

DNA can also be used to create hydrogels for targeted delivery that can be environmentally triggerable by including aptamers and disulfide linkages.[91,92] As Hong et al. reported, one can utilize siRNA to create nanogels through polymeric condensation.[91] These siRNA modalities contained Y-branched antisense siRNA to act as a cross-linker for the short stranded sense and antisense siRNA strand. Three modalities were synthesized: M-siRNA, which mixed the sense and antisense, DY-siRNA, which mixed the sense and the antisense strand with the Y-shaped linkers, and YY-siRNA which combined the Y-shaped sense and anti-sense strand (Figure 8B). The gels were condensed through the use of cationic linear polyethylenimine (LPEI) and without the Y-shaped linker (M-siRNA) condensed particles were not formed. However,unlike other nanogels discussed in this review, there were no acidic cleavable modalities and so the nanogels must be cleaved by RNA enzymes inside the cell, specifically Dicer which can cleave artificial siRNA within the cell.

Cho et al. reported the construction of DNA structured nanofilm with controllable release properties.[93] Three types of film were assembled from hairpin shaped, Y-shaped, and

X-shaped DNA that contained “sticky ends” and each film was assembled, layer-by-layer, through the use of poly-l-Lysine (**Figure 1.8 C**). Each layer of DNA film contained Dox as an intercalating agent and demonstrated different release profiles, in serum, of the drug depended on the shape of the DNA used. X-DNA films showed a low burst initial release with a slower and more controlled release than the other two films, H-DNA had a larger initial burst release and a faster release overall. Thus, this modality can control the release of the doxorubicin based on the type of film. Y shaped aptamers can also be used to for big multilayered DNA dendrimers (Figure 8D).[94] By designing each layer of aptamers differently, the DNA dendrimers contain fluorophores, targeting ligands (sgc8) and anticancer drugs (Dox) for imaging, cell recognition and drug delivery. This complex also showed potent toxicity towards target cancer cells (human T cell acute lymphoblastic leukemia cell line) while having low side effects for the non-target cells (human Burkitt’s lymphoma cell line).

Summary and Future Outlook:

Table 1.1. Comparison of different DNA nanotechnology approaches

Approach	Advantage	Disadvantage
ODN	Commercially available short strands; less types of strands involved in structure construction.	Less structurally stable than origami; no available programmable designing tool.
DNA origami	Programmable tools (e.g., caDNAno); More condensed for intercalation of drugs.	Safety concern about the virus DNA backbone; hundreds of types of staple strands.
RCA	Economic and easy large-scale fabrication.	Lack of precise control in length and structure.
DNA nanoparticles	Integration of different materials properties (e.g., polymer and DNA).	Safety issue regarding combinations of materials.

DNA nanotechnology has shown great potential in controlling drug/gene delivery. DNA based particles of a vast variety of sizes and shapes have been fabricated either through oligonucleotide, RCA or origami methods, along with other hybrid nanostructures. Their advantages and disadvantages are summarized in **Table 1.1**. They can be readily functionalized to target specific cells, elongate circulation time, respond to environmental cues, and incorporate drug, gene and imaging agents. Therefore, as demonstrated in this review, DNA nanotechnology has become a robust platform to bring controls in a lot of different aspects into drug and gene delivery. DNA can also be easily functionalized, as discussed earlier in this review, which allows for the combination of DNA nanostructures with other nanostructures. This can lead to creative solutions for therapeutics such as the combination DNA/gold nanoparticle therapy of Jensen et al.[15]

DNA can also be situated onto structures that are not metallic, such as polymeric structures allowing for codelivery. The examples we discussed demonstrate the wide breadth of how DNA can be used to create versatile, precision nanostructures for controllable, targeted delivery of molecular therapeutics and gene therapeutics. While DNA nanotechnology holds high promise for precision nanomedicine, it is still in very early stage. So far to the authors' knowledge, there is no significant clinical trial in progress regarding DNA nanotechnology. Some key issues need to be considered prior to its clinical translation. i) Unclear working mechanism. Although DNA nanostructures have been tested in drug delivery, further exploration into the mechanisms of transfection is urgently needed as the actual mechanism of uptake and how important factors like size and shape affect the uptake are still not fully understood. As these mechanisms are explored, more targeting modalities will become available and will allow for a higher uptake of the DNA nanostructures thus allowing for a lower dosage of therapeutics and a lower possible chance of detrimental off-target effects. As a novel delivery platform, most of the current reports on drug delivery applications are using Dox as a model drug, given the easy intercalation process and the fluorescence property when released. To broaden their applications, it is vital to investigate the use of DNA nanotechnology on other drug systems to expand the horizon of the application.

Another important issue is the controlled release. Although it has been reported that the release profile can be tuned in DNA origami,[28] it is still important to control the release profile to make a sustainable drug concentration for certain treatment purposes, some of which should be based on the incorporation of multiple types of drugs. For this purpose, incorporation of multiple release mechanisms, e.g., environmental stimuli and slow degradation of the structure can be explored. ii) Further testing of safety profile. As a naturally biodegradable and biocompatible polymer, DNA shows quite promising performance in certain types of cells and in

mouse,[52] In these early studies, there was no antibody response against DNA nanostructures. However, given the complexity of the human body, the influence of particle physiochemical properties on renal systems, and the unlikely but essentially harmful genome recombination, further investigation on DNA nanostructures in different types of organs are needed for their clinic application translation. iii) Undetermined large scale production. Compared with polymer and lipid delivery systems, DNA nanostructures have added cost, given the synthesis challenges. A few methods, including PCR, RCA and in-cell production,[95] are used to amplify the DNA strands using relatively cheap costs. However, considering the complexity of DNA nanostructures, there is still a gap that needs to be filled. To enlarge the production scale, besides what discussed in this review, new approaches to synthesis DNA strands and DNA nanostructures are also needed. We believe that with the further development in drug delivery and resolution of scalability issues, DNA nanotechnology can bring a new concept into carrier systems and generate useful clinic results.

Chapter 1, in full, is a reprint of the material as it appears in Small 2016. Angell, Chava; Smith, Sibai X; Liangfang Z; Yi C.. The dissertation author was co-first author with Sibai Xie.

Chapter 1 BIBLIOGRAPHY

[1] Langer, R., 1990. New methods of drug delivery. *Science*, *249*(4976), pp.1527-1533.

[2] Langer, R., 1998. Drug delivery and targeting. *NATURE-LONDON-*, pp.5-10.

[3] Steidler, L., Hans, W., Schotte, L., Neirynck, S., Obermeier, F., Falk, W., Fiers, W. and Remaut, E., 2000. Treatment of murine colitis by Lactococcus lactis secreting interleukin-10. *Science*, *289*(5483), pp.1352-1355

[4] Hu, C.M.J., Zhang, L., Aryal, S., Cheung, C., Fang, R.H. and Zhang, L., 2011. Erythrocyte membrane-camouflaged polymeric nanoparticles as a biomimetic delivery platform. *Proceedings of the National Academy of Sciences*, *108*(27), pp.10980-10985.

[5] Felgner, P.L. and Ringold, G.M., 1989. Cationic liposome-mediated transfection. *Nature*, *337*(6205), pp.387-388.

[6] Torchilin, V.P., 2005. Recent advances with liposomes as pharmaceutical carriers. *Nature reviews Drug discovery*, *4*(2), pp.145-160.

[7] Alexis, F., Pridgen, E., Molnar, L.K. and Farokhzad, O.C., 2008. Factors affecting the clearance and biodistribution of polymeric nanoparticles. *Molecular pharmaceutics*, *5*(4), pp.505-515.

[8] Sun, T., Zhang, Y.S., Pang, B., Hyun, D.C., Yang, M. and Xia, Y., 2014. Engineered nanoparticles for drug delivery in cancer therapy. *Angewandte Chemie International Edition*, *53*(46), pp.12320-12364.

[9] Farokhzad, O.C. and Langer, R., 2009. Impact of nanotechnology on drug delivery. *ACS nano*, *3*(1), pp.16-20.

[10] Peer, D., Karp, J.M., Hong, S., Farokhzad, O.C., Margalit, R. and Langer, R., 2007. Nanocarriers as an emerging platform for cancer therapy. *Nature nanotechnology*, *2*(12), p.751.

[11] Geng, Y.A.N., Dalhaimer, P., Cai, S., Tsai, R., Tewari, M., Minko, T. and Discher, D.E., 2007. Shape effects of filaments versus spherical particles in flow and drug delivery. *Nature nanotechnology*, *2*(4), pp.249-255.

[12] Champion, J.A. and Mitragotri, S., 2006. Role of target geometry in phagocytosis. *Proceedings of the National Academy of Sciences*, *103*(13), pp.4930-4934.

[13] Kim, K.R., Kim, D.R., Lee, T., Yhee, J.Y., Kim, B.S., Kwon, I.C. and Ahn, D.R., 2013. Drug delivery by a self-assembled DNA tetrahedron for overcoming drug resistance in breast cancer cells. *Chemical Communications*, *49*(20), pp.2010-2012.

[14] Seeman, N.C. and Kallenbach, N.R., 1983. Design of immobile nucleic acid junctions. *Biophysical journal*, *44*(2), p.201.

[15] Jensen, S.A., Day, E.S., Ko, C.H., Hurley, L.A., Luciano, J.P., Kouri, F.M., Merkel, T.J., Luthi, A.J., Patel, P.C., Cutler, J.I. and Daniel, W.L., 2013. Spherical nucleic acid nanoparticle conjugates as an RNAi-based therapy for glioblastoma. Sci Transl Med 5 (209): 209ra152.

[16] Seeman, N.C., 2003. Biochemistry and structural DNA nanotechnology: an evolving symbiotic relationship. *Biochemistry*, *42*(24), pp.7259-7269.

[17] Chen, J. and Seeman, N.C., 1991. Synthesis from DNA of a molecule with the connectivity of a cube. *Nature*, *350*(6319), pp.631-633.

[18] Goodman, R.P., Schaap, I.A., Tardin, C.F., Erben, C.M., Berry, R.M., Schmidt, C.F. and Turberfield, A.J., 2005. Rapid chiral assembly of rigid DNA building blocks for molecular nanofabrication. *Science*, *310*(5754), pp.1661-1665.

[19] He, Y., Ye, T., Su, M., Zhang, C., Ribbe, A.E., Jiang, W. and Mao, C., 2008. Hierarchical self-assembly of DNA into symmetric supramolecular polyhedra. *Nature*, *452*(7184), pp.198-201.

[20] Smith, D.M., Schüller, V., Forthmann, C., Schreiber, R., Tinnefeld, P. and Liedl, T., 2011. A structurally variable hinged tetrahedron framework from DNA origami. *Journal of nucleic acids*, *2011*.

[21] Zhang, Y. and Seeman, N.C., 1994. Construction of a DNA-truncated octahedron. *Journal of the American Chemical Society*, *116*(5), pp.1661-1669.

[22] Zhang, C., Su, M., He, Y., Zhao, X., Fang, P.A., Ribbe, A.E., Jiang, W. and Mao, C., 2008. Conformational flexibility facilitates self-assembly of complex DNA nanostructures. *Proceedings of the National Academy of Sciences*, *105*(31), pp.10665-10669.

[23] Bhatia, D., Mehtab, S., Krishnan, R., Indi, S.S., Basu, A. and Krishnan, Y., 2009. Icosahedral DNA nanocapsules by modular assembly. *Angewandte Chemie International Edition*, *48*(23), pp.4134-4137.

[24] Iinuma, R., Ke, Y., Jungmann, R., Schlichthaerle, T., Woehrstein, J.B. and Yin, P., 2014. Polyhedra self-assembled from DNA tripods and characterized with 3D DNA-PAINT. *science*, *344*(6179), pp.65-69.

[25] He, Y., Chen, Y., Liu, H., Ribbe, A.E. and Mao, C., 2005. Self-assembly of hexagonal DNA two-dimensional (2D) arrays. *Journal of the American Chemical Society*, *127*(35), pp.12202-12203.

[26] Chang, M., Yang, C.S. and Huang, D.M., 2011. Aptamer-conjugated DNA icosahedral nanoparticles as a carrier of doxorubicin for cancer therapy. *ACS nano*, *5*(8), pp.6156-6163.

[27] Ke, Y., Ong, L.L., Shih, W.M. and Yin, P., 2012. Three-dimensional structures self-assembled from DNA bricks. *science*, *338*(6111), pp.1177-1183.

[28] Zhao, Y.X., Shaw, A., Zeng, X., Benson, E., Nyström, A.M. and Högberg, B., 2012. DNA origami delivery system for cancer therapy with tunable release properties. *ACS nano*, *6*(10), pp.8684-8691.

[29] Sun, W., Jiang, T., Lu, Y., Reiff, M., Mo, R. and Gu, Z., 2014. Cocoon-like self-degradable DNA nanoclew for anticancer drug delivery. *Journal of the American Chemical Society*, *136*(42), pp.14722-14725.

[30] Surana, S., Bhat, J.M., Koushika, S.P. and Krishnan, Y., 2011. An autonomous DNA nanomachine maps spatiotemporal pH changes in a multicellular living organism. *Nature communications*, *2*(1), pp.1-7.

[31] Agudelo, D., Bourassa, P., Bérubé, G. and Tajmir-Riahi, H.A., 2014. Intercalation of antitumor drug doxorubicin and its analogue by DNA duplex: structural features and biological implications. *International journal of biological macromolecules*, *66*, pp.144-150.

[32] Zhu, G., Cansiz, S., You, M., Qiu, L., Han, D., Zhang, L., Mei, L., Fu, T., Chen, Z. and Tan, W., 2015. Nuclease-resistant synthetic drug-DNA adducts: programmable drug-DNA conjugation for targeted anticancer drug delivery. *NPG Asia Materials*, *7*(3), pp.e169-e169.

[33] Fellmann, C. and Lowe, S.W., 2014. Stable RNA interference rules for silencing. *Nature cell biology*, *16*(1), pp.10-18.

[34] Naito, Y. and Ui-Tei, K., 2012. siRNA design software for a target gene-specific RNA interference. *Frontiers in genetics*, *3*, p.102.

[35] Castanotto, D. and Rossi, J.J., 2009. The promises and pitfalls of RNA-interference-based therapeutics. *Nature*, *457*(7228), pp.426-433.

[36] Guo, P., Coban, O., Snead, N.M., Trebley, J., Hoeprich, S., Guo, S. and Shu, Y., 2010. Engineering RNA for targeted siRNA delivery and medical application. *Advanced drug delivery reviews*, *62*(6), pp.650-666.

[37] Liu, L., Xu, K., Wang, H., Tan, P.J., Fan, W., Venkatraman, S.S., Li, L. and Yang, Y.Y., 2009. Self-assembled cationic peptide nanoparticles as an efficient antimicrobial agent. *Nature nanotechnology*, *4*(7), pp.457-463.

[38] Wilner, O.I. and Willner, I., 2012. Functionalized DNA nanostructures. *Chemical reviews*, *112*(4), pp.2528-2556.

[39] Allen, T.M., 2002. Ligand-targeted therapeutics in anticancer therapy. *Nature Reviews Cancer*, *2*(10), pp.750-763.

[40] Cheng, E., Xing, Y., Chen, P., Yang, Y., Sun, Y., Zhou, D., Xu, L., Fan, Q. and Liu, D., 2009. A pH-triggered, fast-responding DNA hydrogel. *Angewandte Chemie International Edition*, *48*(41), pp.7660-7663.

[41] Modi, S., Swetha, M.G., Goswami, D., Gupta, G.D., Mayor, S. and Krishnan, Y., 2009. A DNA nanomachine that maps spatial and temporal pH changes inside living cells. *Nature nanotechnology*, *4*(5), pp.325-330.

[42] Lühmann, T., Rimann, M., Bittermann, A.G. and Hall, H., 2008. Cellular uptake and intracellular pathways of PLL-g-PEG-DNA nanoparticles. *Bioconjugate chemistry*, *19*(9), pp.1907-1916.

[43] Chen, G., Liu, D., He, C., Gannett, T.R., Lin, W. and Weizmann, Y., 2015. Enzymatic synthesis of periodic DNA nanoribbons for intracellular pH sensing and gene silencing. *Journal of the American Chemical Society*, *137*(11), pp.3844-3851.

[44] Xiang, S., Tong, H., Shi, Q., Fernandes, J.C., Jin, T., Dai, K. and Zhang, X., 2012. Uptake mechanisms of non-viral gene delivery. *Journal of controlled release*, *158*(3), pp.371-378.

[45] Chen, X., Shank, S., Davis, P.B. and Ziady, A.G., 2011. Nucleolin-mediated cellular trafficking of DNA nanoparticle is lipid raft and microtubule dependent and can be modulated by glucocorticoid. *Molecular Therapy*, *19*(1), pp.93-102.

[46] Dalby, B., Cates, S., Harris, A., Ohki, E.C., Tilkins, M.L., Price, P.J. and Ciccarone, V.C., 2004. Advanced transfection with Lipofectamine 2000 reagent: primary neurons, siRNA, and high-throughput applications. *Methods*, *33*(2), pp.95-103.

[47] Ke, Y., Bellot, G., Voigt, N.V., Fradkov, E. and Shih, W.M., 2012. Two design strategies for enhancement of multilayer–DNA-origami folding: underwinding for specific intercalator rescue and staple-break positioning. *Chemical science*, *3*(8), pp.2587-2597.

[48] Mikkila, J., Eskelinen, A.P., Niemela, E.H., Linko, V., Frilander, M.J., Torma, P. and Kostiainen, M.A., 2014. Virus-encapsulated DNA origami nanostructures for cellular delivery. *Nano letters*, *14*(4), pp.2196-2200.

[49] Kim, M.G., Park, J.Y., Shim, G., Choi, H.G. and Oh, Y.K., 2015. Biomimetic DNA nanoballs for oligonucleotide delivery. *Biomaterials*, *62*, pp.155-163.

[50] Sellner, S., Kocabey, S., Nekolla, K., Krombach, F., Liedl, T. and Rehberg, M., 2015. DNA nanotubes as intracellular delivery vehicles in vivo. *Biomaterials*, *53*, pp.453-463.

[51] Goodman, R.P., Berry, R.M. and Turberfield, A.J., 2004. The single-step synthesis of a DNA tetrahedron. *Chemical Communications*, (12), pp.1372-1373.

[52] Lee, H., Lytton-Jean, A.K., Chen, Y., Love, K.T., Park, A.I., Karagiannis, E.D., Sehgal, A., Querbes, W., Zurenko, C.S., Jayaraman, M. and Peng, C.G., 2012. Molecularly self-assembled nucleic acid nanoparticles for targeted in vivo siRNA delivery. *Nature nanotechnology*, *7*(6), pp.389-393.

[53] Zhu, G., Zheng, J., Song, E., Donovan, M., Zhang, K., Liu, C. and Tan, W., 2013. Self-assembled, aptamer-tethered DNA nanotrains for targeted transport of molecular drugs in cancer theranostics. *Proceedings of the national academy of sciences*, *110*(20), pp.7998-8003.

[54] Wu, C., Han, D., Chen, T., Peng, L., Zhu, G., You, M., Qiu, L., Sefah, K., Zhang, X. and Tan, W., 2013. Building a multifunctional aptamer-based DNA nanoassembly for targeted cancer therapy. *Journal of the American Chemical Society*, *135*(49), pp.18644-18650.

[55] Li, J., Pei, H., Zhu, B., Liang, L., Wei, M., He, Y., Chen, N., Li, D., Huang, Q. and Fan, C., 2011. Self-assembled multivalent DNA nanostructures for noninvasive intracellular delivery of immunostimulatory CpG oligonucleotides. *ACS nano*, *5*(11), pp.8783-8789.

[56] Andersen, E.S., Dong, M., Nielsen, M.M., Jahn, K., Lind-Thomsen, A., Mamdouh, W., Gothelf, K.V., Besenbacher, F. and Kjems, J., 2008. DNA origami design of dolphin-shaped structures with flexible tails. *ACS nano*, *2*(6), pp.1213-1218.

[57] Marras, A.E., Zhou, L., Su, H.J. and Castro, C.E., 2015. Programmable motion of DNA origami mechanisms. *Proceedings of the National Academy of Sciences*, *112*(3), pp.713-718.

[58] Rothemund, P.W., 2006. Folding DNA to create nanoscale shapes and patterns. *Nature*, *440*(7082), pp.297-302.

[59] Tørring, T., Voigt, N.V., Nangreave, J., Yan, H. and Gothelf, K.V., 2011. DNA origami: a quantum leap for self-assembly of complex structures. *Chemical Society Reviews*, *40*(12), pp.5636-5646.

[60] Douglas, S.M., Dietz, H., Liedl, T., Högberg, B., Graf, F. and Shih, W.M., 2009. Self-assembly of DNA into nanoscale three-dimensional shapes. *Nature*, *459*(7245), pp.414-418.

[61] Douglas, S.M., Marblestone, A.H., Teerapittayanon, S., Vazquez, A., Church, G.M. and Shih, W.M., 2009. Rapid prototyping of 3D DNA-origami shapes with caDNAno. *Nucleic acids research*, *37*(15), pp.5001-5006.

[62] Zhang, Q., Jiang, Q., Li, N., Dai, L., Liu, Q., Song, L., Wang, J., Li, Y., Tian, J., Ding, B. and Du, Y., 2014. DNA origami as an in vivo drug delivery vehicle for cancer therapy. *ACS nano*, *8*(7), pp.6633-6643.

[63] Shih, W.M., Quispe, J.D. and Joyce, G.F., 2004. A 1.7-kilobase single-stranded DNA that folds into a nanoscale octahedron. *Nature*, *427*(6975), pp.618-621.

[64] Sobczak, J.P.J., Martin, T.G., Gerling, T. and Dietz, H., 2012. Rapid folding of DNA into nanoscale shapes at constant temperature. *Science*, *338*(6113), pp.1458-1461.

[65] Huang, X. and Brazel, C.S., 2001. On the importance and mechanisms of burst release in matrix-controlled drug delivery systems. *Journal of controlled release*, *73*(2-3), pp.121-136.

[66] Jiang, Q., Song, C., Nangreave, J., Liu, X., Lin, L., Qiu, D., Wang, Z.G., Zou, G., Liang, X., Yan, H. and Ding, B., 2012. DNA origami as a carrier for circumvention of drug resistance. *Journal of the American Chemical Society*, *134*(32), pp.13396-13403.

[67] Douglas, S.M., Bachelet, I. and Church, G.M., 2012. A logic-gated nanorobot for targeted transport of molecular payloads. *Science*, *335*(6070), pp.831-834.

[68] Mao, Y., Liu, M., Tram, K., Gu, J., Salena, B.J., Jiang, Y. and Li, Y., 2015. Optimal DNA templates for rolling circle amplification revealed by in vitro selection. *Chemistry–A European Journal*, *21*(22), pp.8069-8074.

[69] Ouyang, X., Li, J., Liu, H., Zhao, B., Yan, J., Ma, Y., Xiao, S., Song, S., Huang, Q., Chao, J. and Fan, C., 2013. Rolling circle amplification‐based DNA origami nanostructrures for intracellular delivery of immunostimulatory drugs. *Small*, *9*(18), pp.3082-3087.

[70] Hamblin, G.D., Carneiro, K.M., Fakhoury, J.F., Bujold, K.E. and Sleiman, H.F., 2012. Rolling circle amplification-templated DNA nanotubes show increased stability and cell penetration ability. *Journal of the American Chemical Society*, *134*(6), pp.2888-2891.

[71] Yan, J., Hu, C., Wang, P., Zhao, B., Ouyang, X., Zhou, J., Liu, R., He, D., Fan, C. and Song, S., 2015. Growth and Origami Folding of DNA on Nanoparticles for High‐Efficiency Molecular Transport in Cellular Imaging and Drug Delivery. *Angewandte Chemie International Edition*, *54*(8), pp.2431-2435.

[72] Xu, W., Deng, R., Wang, L. and Li, J., 2014. Multiresponsive rolling circle amplification for DNA logic gates mediated by endonuclease. *Analytical chemistry*, *86*(15), pp.7813-7818.

[73] Lee, J.B., Hong, J., Bonner, D.K., Poon, Z. and Hammond, P.T., 2012. Self-assembled RNA interference microsponges for efficient siRNA delivery. *Nature materials*, *11*(4), pp.316-322.

[74] Ziady, A.G., Perales, J.C., Ferkol, T.H.O.M.A.S., Gerken, T.H.O.M.A.S., Beegen, H., Perlmutter, D.H. and Davis, P.B., 1997. Gene transfer into hepatoma cell lines via the serpin enzyme complex receptor. *American Journal of Physiology-Gastrointestinal and Liver Physiology*, *273*(2), pp.G545-G552.

[75] Ferkol, T., Mularo, F., Hilliard, J., Lodish, S., Perales, J.C., Ziady, A. and Konstan, M., 1998. Transfer of the human alpha1-antitrypsin gene into pulmonary macrophages in vivo. *American journal of respiratory cell and molecular biology*, *18*(5), pp.591-601.

[76] Ziady, A.G., Ferkol, T., Gerken, T., Dawson, D.V., Perlmutter, D.H. and Davis, P.B., 1998. Ligand substitution of receptor targeted DNA complexes affects gene transfer into hepatoma cells. *Gene therapy*, *5*(12), pp.1685-1697.

[77] Ziady, A.G., Ferkol, T., Dawson, D.V., Perlmutter, D.H. and Davis, P.B., 1999. Chain length of the polylysine in receptor-targeted gene transfer complexes affects duration of reporter gene expression both in vitro and in vivo. *Journal of Biological Chemistry*, *274*(8), pp.4908-4916.

[78] Ziady, A.G., Kelley, T.J., Milliken, E., Ferkol, T. and Davis, P.B., 2002. Functional evidence of CFTR gene transfer in nasal epithelium of cystic fibrosis mice in vivo following luminal application of DNA complexes targeted to the serpin-enzyme complex receptor. *Molecular Therapy*, *5*(4), pp.413-419.

[79] Morgan, J.R. ed., 2002. *Gene therapy protocols* (Vol. 69). Springer Science & Business Media.pp. 25.

[80] Ziady, A.G., Gedeon, C.R., Miller, T., Quan, W., Payne, J.M., Hyatt, S.L., Fink, T.L., Muhammad, O., Oette, S., Kowalczyk, T. and Pasumarthy, M.K., 2003. Transfection of airway epithelium by stable PEGylated poly-L-lysine DNA nanoparticles in vivo. *Molecular Therapy*, *8*(6), pp.936-947.

[81] Ziady, A.G., Gedeon, C.R., Muhammad, O., Stillwell, V., Oette, S.M., Fink, T.L., Quan, W., Kowalczyk, T.H., Hyatt, S.L., Payne, J. and Peischl, A., 2003. Minimal toxicity of stabilized compacted DNA nanoparticles in the murine lung. *Molecular Therapy*, *8*(6), pp.948-956.

[82] Ziady, A.G., Davis, P.B. and Konstan, M.W., 2003. Non-viral gene transfer therapy for cystic fibrosis. *Expert opinion on biological therapy*, *3*(3), pp.449-458.

[83] Konstan, Michael W., Pamela B. Davis, Jeffrey S. Wagener, Kathleen A. Hilliard, Robert C. Stern, Laura JH Milgram, Tomasz H. Kowalczyk et al. "Compacted DNA nanoparticles administered to the nasal mucosa of cystic fibrosis subjects are safe and demonstrate partial to complete cystic fibrosis transmembrane regulator reconstitution." *Human gene therapy* 15, no. 12 (2004): 1255-1269.

[84] Ziady, A.G., Kim, J., Colla, J. and Davis, P.B., 2004. Defining strategies to extend duration of gene expression from targeted compacted DNA vectors. *Gene therapy*, *11*(18), pp.1378-1390.

[85] Ziady, A.G. and Davis, P.B., 2006. Current prospects for gene therapy of cystic fibrosis. *Current opinion in pharmacology*, *6*(5), pp.515-521.

[86] Lee, J.W. and Foote, R.S., 2009. *Micro and nano technologies in bioanalysis*. Humana Press, University of Michigan, MI, USA. pp. 525.

[87] Yurek, D.M., Fletcher, A.M., Smith, G.M., Seroogy, K.B., Ziady, A.G., Molter, J., Kowalczyk, T.H., Padegimas, L. and Cooper, M.J., 2009. Long-term transgene expression in the central nervous system using DNA nanoparticles. *Molecular Therapy*, *17*(4), pp.641-650.

[88] Ziady, A.G., Kotlarchyk, M., Bryant, L., McShane, M. and Lee, Z., 2010. Bioluminescent imaging of reporter gene expression in the lungs of wildtype and model mice following the administration of PEG-stabilized DNA nanoparticles. *Microscopy research and technique*, *73*(9), pp.918-928.

[89] Yurek, D.M., Fletcher, A.M., McShane, M., Kowalczyk, T.H., Padegimas, L., Weatherspoon, M.R., Kaytor, M.D., Cooper, M.J. and Ziady, A.G., 2011. DNA nanoparticles: detection of long-term transgene activity in brain using bioluminescence imaging. *Molecular imaging*, *10*(5), pp.7290-2010.

[90] Alemdaroglu, F.E., Alemdaroglu, N.C., Langguth, P. and Herrmann, A., 2008. DNA block copolymer micelles–a combinatorial tool for cancer nanotechnology. *Advanced Materials*, *20*(5), pp.899-902.

[91] Hong, C.A., Lee, S.H., Kim, J.S., Park, J.W., Bae, K.H., Mok, H., Park, T.G. and Lee, H., 2011. Gene silencing by siRNA microhydrogels via polymeric nanoscale condensation. *Journal of the American Chemical Society*, *133*(35), pp.13914-13917.

[92] Li, J., Zheng, C., Cansiz, S., Wu, C., Xu, J., Cui, C., Liu, Y., Hou, W., Wang, Y., Zhang, L. and Teng, I.T., 2015. Self-assembly of DNA nanohydrogels with controllable size and stimuli-responsive property for targeted gene regulation therapy. *Journal of the American Chemical Society*, *137*(4), pp.1412-1415.

[93] Cho, Y., Lee, J.B. and Hong, J., 2014. Controlled release of an anti-cancer drug from DNA structured nano-films. *Scientific reports*, *4*, p.4078.

[94] Zhang, H., Ma, Y., Xie, Y., An, Y., Huang, Y., Zhu, Z. and Yang, C.J., 2015. A controllable aptamer-based self-assembled DNA dendrimer for high affinity targeting, bioimaging and drug delivery. *Scientific reports*, *5*, p.10099.

[95] Lin, C., Rinker, S., Wang, X., Liu, Y., Seeman, N.C. and Yan, H., 2008. In vivo cloning of artificial DNA nanostructures. *Proceedings of the National Academy of Sciences*, *105*(46), pp.17626-17631.

Chapter 2-DNA Nanomachines Derived from Natural Sequences

Abstract:

Beside its genomic properties, DNA is also recognized as a novel material in the field of nanoengineering. The specific bonding of base pairs can be used to direct the assembly of highly structured materials with specific nanoscale features such as periodic 2D arrays, 3D nanostructures, assembly of nanomaterials, and DNA nanomachines. In recent years, a variety of DNA nanomachines are developed because of their many potential applications in biosensing, diagnostics, and therapeutic applications. In this review, the fuel-powered motors and secondary structure motors, whose working mechanisms are inspired or derived from natural phenomena and nanomachines, are discussed. The combination of DNA motors with other platforms is then discussed. In each section of these motors, their mechanisms and their usage in the biomedical field are described. Finally, it is believed that these DNA-based nanomachines and hybrid motifs will become an integral point-of-care diagnostics and smart, site-specific therapeutic delivery.

i-motif:

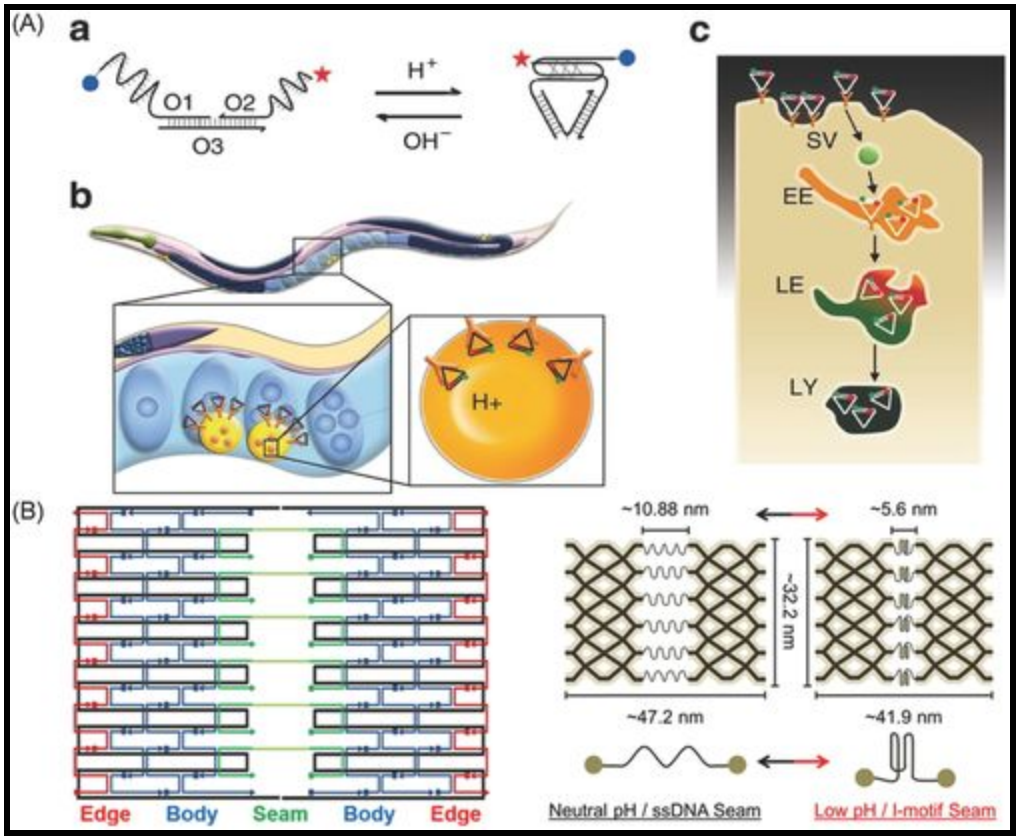

Figure 2.1. A) i-Motif switched used to map pH inside a living organisms. Reproduced with permission.[7] Copyright 2011, Nature Publishing Group. B) DNA origami actuated through the incorporation of the i-motif sequence. Reproduced with permission.[4] Copyright 2017, American Chemical Society.

Not only can we draw inspiration from nature to create functioning DNA nanomachines, we can also incorporate natural DNA sequences within our synthetic designs in order to create responsive functionality and conformational changes that react to specific microenvironments in order to allow eventual responsiveness for targeted action. There are DNA sequences, which are unique secondary structures, that respond to pH stimuli in the environment and DNA sequences whose unique structures allow them to bind with specific small molecules, proteins, and certain elements.[1] The initial inspiration for these types came from a motor synthesized in

1999 by Seeman and co-workers, which underwent a conformational change from B DNA to Z DNA based on environmental conditions.[2] DNA sequences that are rich in cytosine can form two intercalated parallel duplexes under low pH through the hemiprotonation of a cytosine–cytosine pair.[3]This structure has a height proportional to the length of the ssDNA sequence.[4] Consequently, this structural formation change can be incorporated into DNA nanodevices for usage in biomapping and therapeutic delivery due to the acidification of late stage endosomes.[5]

In 2009, the lab of Krishnan and co-workers[6] utilized this motif which is known as an i-motif, or intercalated motif and created a DNA nanomotor that mapped pH change from early to late stage endosome. This nanoswitch closed in response to low pH and displayed fluorescent signal. The switch was cyclic, which demonstrates the ability of DNA nanodevices to be robust and work within functioning cells and further demonstrated the ability of DNA nanodevices to take advantage of cellular microenvironment changes.[6] The same lab extended this work to living organisms, specifically the nematode *Caenorhabditis elegans* [7] as shown in **Figure 2.1 A**. This work thus demonstrated that their i-motif-based nanomachine can maintain function within a living organism.[7]

In 2009, Zhou and co-workers[8] synthesized a nanomotor similar to that of the nanomotor of Krishnan and co-workers,[6], [7] which was a nanotriangle that can open and close in response to environmental stimulation. However, they utilized an i-motif structure as the trigger strand with another strand able to bind to it under higher pH, thus allowing the motor to close under low pH and reopen when the pH is switched back. This device has potential for drug delivery under cellular or extracellular microenvironment conditions due to both endocytotic acidification and tumor acidification. The authors also posit that by combining multiple

machines, they could create a structure that functions similarly to muscle fiber as the i-motif structure formation would act as a contraction.[8]

The lab of Willner and co-workers[9] also created a DNA tweezer that utilized the properties of the i-motif to change machine conformation with respect to pH. When the pH was lowered, the tweezers released a strand that was holding them in a closed position by forming two i-motif structures. This strand was actually able to function as a closing strand for a second pair of DNA tweezers, such that by lowering the pH, the first set of tweezers would open and the second set of tweezers would close. This is reversible as the fuel strand to close both tweezers is more favorable to hybridize with the pH-responsive tweezers but is forced to release during the formation of the i-motif.[9]

The i-motif was also utilized by Fan and co-workers, who created an adaptable DNA tetrahedron that could function as logic gates.[10] One edge of the tetrahedron functioned as a sensor that is responsive to microenvironment conditions and during the annealing process, was flexible enough that the sensing strand could be switched out for other potential sensing DNA sequences. Depending on the sequence, or sequences, used in the responsive strand, various types of DNA logic gates were constructed. The i-motif sequence allowed for the construction of an INH gate. Gates such as an OR gate, XOR gate, and an AND gate were constructed using various DNA sequences that are responsive. The flexibility of this system, and the fact that this work proved the functionality of the tetrahedral sensors in vivo, allow a wide range of smart biosensing and detection at the cellular level.[10]

Recently, LaBean and co-workers[4] synthesized DNA origami that was able to actuate spatially through the incorporation of i-motif sequences (**Figure 2.1 B**). The authors mentioned that the length of the actuation can be designed through the length of the i-motif sequence.[4]

Thus, the incorporation of pH-responsive DNA i-motifs have many potential benefits to help understand and map cellular pH on a deeper level. These motifs also clearly have potential in targeted release due to tumor acidification and late stage endosome acidification.

In contrast to the usage of the i-motif, the Lab of Lee and DeRosa[11] created a pH-responsive DNA nanostructure that took advantage of the unique nature of the adenine–guanine (A–G) mismatch, which becomes more stable under low pH, as confirmed by melting temperature data. This property allowed Lee and DeRosa to create a simple motor that cycles between an opened and closed conformation based on pH changes. The A–G mismatch has advantages over the i-motif as it requires less space within the DNA design and could potentially decrease the limitations on other sequence designs as it does not require a repeating cytosine motif.[11]

DNA Triplex-Based Motors:

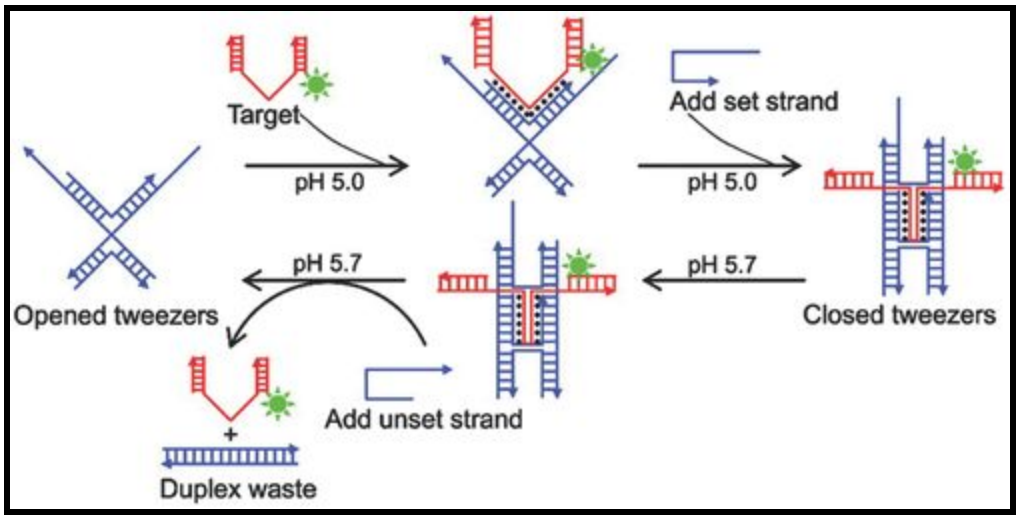

Figure 2.2. DNA tweezers powered through triplex binding and fuel strand-mediated displacement. Reproduced with permission.[15] Copyright 2008, American Chemical Society

Another potential pH-responsive DNA structure, existing in nature, is that of the DNA triplex. Triplex DNA is stabilized through Hoogstein hydrogen bonding in the major groove of B DNA.[12] Depending on the type of triplex, purine or pyrimidine, we can design the structure to be responsive to low pH as purine triplexes are stable at physiological pH, whereas pyrimidine triplexes form at low pH. Thus, with the incorporation of pyrimidine triplexes, we can create pH-responsive DNA nanomachines.[13]

The lab of Mao and co-workers[14] created a DNA nanomachine by utilizing the pH responsiveness of a C+G-C DNA triplex sequence. The three strand design formed a triplex under low pH, thus closing the machine, and reopened under higher pH. The machine did not require any external fuel strand DNA and thus did not create DNA waste within the system.[14]

In 2008, Deng and co-workers[15] utilized the pH-responsive DNA triplex motif and fuel strand-mediated displacement to create DNA tweezers that can actually capture and hold a target, similar to actual tweezers as shown in **Figure 2.2**. The target DNA sequence contains a ssDNA region nestled between two duplexes that can form a triplex with the tweezer complex under low pH (5). The full tweezer complex structure is set through the addition of another strand which closes the tweezer motif, effectively trapping the target DNA. With an increase in pH, to 5.7, and the addition of a strand that is more fully complementary to the set strand, the target DNA sequence is released. This concept was tested through FRET quenching experiments.[15]

Similar to the motor created by Krishnan and co-workers, Tan and co-workers[16] created a device to map intracellular pH by utilizing the DNA triplex motif and FRET. This work utilized polyethylenimine (PEI) (PEI) to protect the DNA switch from enzymatic degradation and

to aid in cellular internalization, although their motif was able to enter the cell without the PEI entirely.[16]

In 2013, the lab of Mao and co-workers[17] created a DNA tetrahedron that can assemble into a 3D structure in response to pH, utilizing a combination of the CGC DNA triplex motif, which is pH responsive, and the TAT triplex motif, which is unresponsive. This three stranded motif formed a DNA star under alkaline pH, however, as the pH decreased, the cytosine hemi-protonated and transformed the star motif into a tetrahedron. As with the other pH-responsive motifs discussed during the review, this motif could potentially be utilized for pH-triggered therapeutic release or pH related biodiagnostics.

Recently, Ricci and co-workers[18] synthesized a DNA nanodevice that opened and closed in response to an antibody cue due to the attachment on an antigen. The machine functioned by binding to an antibody cue which forces dissociation of a triplex structure holding the device closed by destabilizing the Hoogstein bonding that is essential to triplex formation. This reaction allowed a DNA payload sequence to be rapidly released in direct, proportional response to that specific antibody key, including, but not limited to, an anti-human immunodeficiency virus (HIV) antibody, an anti-Digoxigenin antibody, and an anti-dinitrophenol (DNP) antibody. This would allow potential delivery of therapeutic nucleic acid sequences such as siRNA or microRNA.[18]

Inspired by hemoglobin functionality, Ricci and co-workers[19] also developed a DNA-based nanodevice with multiple binding sites for cargo loading and release, which is a process that is well controlled by allosteric effectors or environmental conditions like pH and temperature. This machine functions utilizing triplex interactions. They built up an in vitro system with molecule beacons to characterize the cargo loading and release profile. The project was

able successfully mimic heterotropic allosteric effects, inverted Bohr effect, and temperature dependence in the artificial system. It is the first artificial DNA nanodevice which mimics complex nature-inspired control mechanisms, which is potentially useful for diagnostics and drug delivery.[19]

G-Quadruplex-/Aptamer-Based Motors:

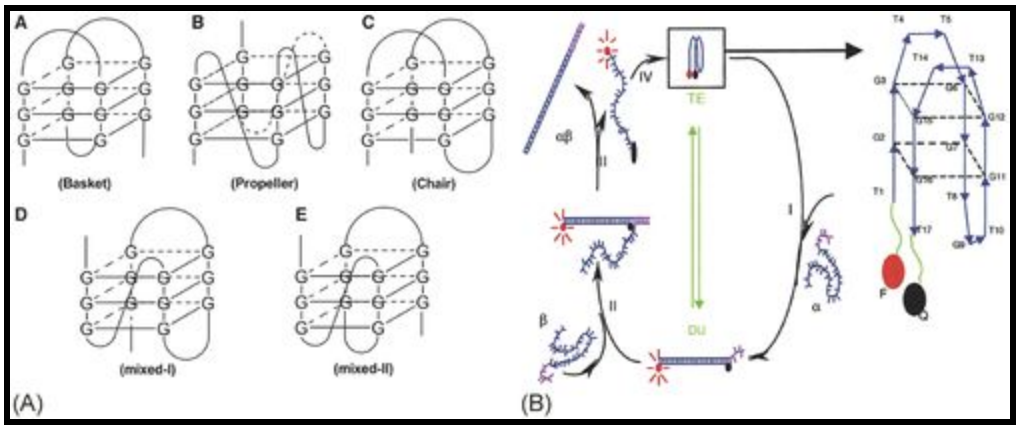

Figure 2.3. A) Guanine quadruplex configurations. Reproduced with permission.[20] Copyright 2013, Oxford University Press. B) Fuel strand-mediated powered Guanine quadruplex-powered motor. Reproduced with permission.[21] Copyright 2002, American Chemical Society.

It is also necessary to examine the DNA structure that has been used for DNA nanomachines known as the guanine quadruplex or G-quadruplex. A G-quadruplex (**Figure 2.3 A**) is a DNA secondary structure that forms when two or more guanine tetrads stack in a planar fashion through π-stacking. The guanine tetrads themselves are held together through a combination of Hoogstein and Watson–Crick bonding. The quadruplex can be contained to a single strand or can be formed by multiple strands and there are many potential orientations of G-quadruplexes based on factors such as loop length and quantity of tetrads.[20]

In the early 2000s, Li and Tan[21] created a simple motor based off of the G-quadruplex and fuel strand-mediated displacement as shown in **Figure 2.3 B**. Similar to the i-motif motor

created by Zhou and co-workers in 2006[22] discussed later in this paper, this motor functioned through binding to another strand, forcing the G-quadruplex to straighten out. The G-quadruplex was allowed to reform when a third strand was flowed that is more complementary to the strand bound to the G-quadruplex.[21]

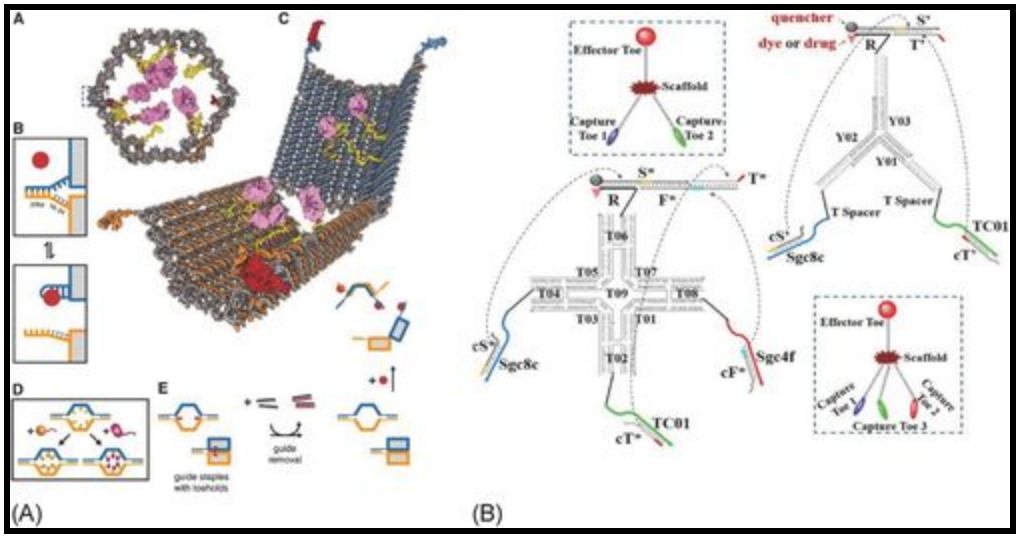

Figure 2.4. A) Aptamer logic gate keyed nanorobot for drug delivery. Reproduced with permission.[28] Copyright 2012, The American Association for the Advancement of Science. B) Logic-gated "Nano-Claw" for delivery and diagnostics. Reproduced with permission.[27] Copyright 2014, American Chemical Society.

G-quadruplexes are often the functional component of DNA sequences known as aptamers, which are nucleic acid sequences that target and bind to small molecules, proteins, and certain elements.[23] Aptamer-based sensors are less expensive and more stable than antibodies, giving them distinct advantages in biosensing and diagnostics.[24] Similarly, aptamers also demonstrate high thermostability and have "similar target-binding specificities to antibody–antigen interactions.[25]

In 2004, the Lab of Simmel and co-workers[26] created a nanomachine based on the G-quadruplex thrombin binding aptamer which can bind and release thrombin by utilizing fuel

strand-mediated displacement. A fuel strand, called the opening strand, with an overhang was introduced into the system and bound to the majority of the sequence that includes the thrombin binding aptamer. This binding disrupted the guanine tetrads and forced the aptamer to release the protein. The aptamer structure can be recovered when a second strand is introduced into the system that is completely complementary to the opening strand. Like other fuel strand motifs, this does generate waste in the system, however this aptamer motor experiment was the basis for other catch and release thrombin and protein motifs that can be used for sorting, biodiagnostics, and smart delivery.[26]

Cancer cells often demonstrate changes in regulation and expression of cellular membrane receptors. We can use this knowledge and DNA nanodevices to target those cancer cells, whether they overexpress or under express certain signals.[27] Perhaps one of the most interesting nanorobots that takes advantage of this phenomenon would be the aptamer logic-gated nanorobot that was fabricated in 2012 by Church and co-workers.[28] As seen in **Figure 2.4 A** DNA origami has been used in many different cases to construct DNA nanomachines, including DNA boxes and hatches used to encapsulate a payload.[29] The origami nanorobot, fabricated by Church and co-workers, contained binding regions inside for cargo transport and was locked by aptamer locks that only opened when both protein cues were available, thus functioning as an AND gate and removing the possibility for delivery under false positive conditions. The aptamer locks were specifically designed to be sensitive, but also to avoid spontaneous activation through tailoring the length of the binding duplex. The highly sensitive locks were tested against specific cell lines that expressed combinations of antigens that activated whatever aptamers were included in the locks. They found that the locks were highly specific and only activated in the presence of the cell population that expressed that precise combination of antigens. This robot showed potential in targeted drug delivery as it was

able to stop growth in leukemia cells and induce T cell signaling pathways as the robot was able to collect flagellin from solution. This would allow the robot to potentially be used for scavenging applications as well as drug delivery.[28]

Similar to the nanorobot demonstrated by Church and co-workers, the Lab of Tan and co-workers (**Figure 2.4 B**)[27] created a “Nano-Claw” to interact with various levels of cellular membrane markers and perform therapeutic actions autonomously. This functional DNA nanodevice was able to both generate diagnostic signals and release therapeutic modalities. Similar to the robot of Church and co-workers, this robot requires multiple inputs, i.e., AND gate or INH gate, to avoid false positives in reporting and release. It can be designed to require two or more inputs to bind to aptamer-based “capture toes” which consist of aptamer sequences bound to complementary DNA. Once the target is available, the complementary DNA is released and binds to an “effector toe,” causing a diagnostic or therapeutic action to occur. This type of technology provides a level of specificity and guarding against false negatives in theranostics.[27]

In 2015, the Lab of Tan and co-workers[30] also created a highly specific, logic-gated aptamer-based Boolean cascade with “12 three input conditions and 2 four-input conditions” for cancer diagnostics and to allow for incredibly selective delivery based on either the presence or absence of necessary cell markers.[30]

Funabashi and co-workers[31] utilized the G-quadruplex motif to create a DNA nanosensor for nucleic acid sequences that could demonstrate a colorimetric readout. The three stranded design contained two strands with sites to recognize the nucleic acid target and a strand that contains a split G-quadruplex, with half of the sequence on one end of the strand and the other half on the other end of the strand. When the desired target hybridizes to the

target recognition sequence, it closes the device and allows the split strand G-quadruplex to form its secondary structure, thus allowing it to function as an aptamer and bind to hemin. This allows 2,2′-azino-bis(3-ethylbenzothiazoline-6-sulfonic acid) (ABTS) to be oxidized in the presence of hydrogen peroxide and produces a colorimetric signal. With this design, the authors were able to detect norovirus mRNA with a minimum concentration of 4 × 10−9 m. The potential of this device to act a sensor for many nucleic acid indicators for disease is flexible and could easily be modified to whatever target sequence is desired. There are some drawbacks relating to free hemin in solution which limits the device sensitivity.[31]

In 2017, Tanner and co-workers[32] demonstrated a colorimetric aptamer-based sensor to detect a malarial biomarker by incorporating a split version (similar to that of Funabashi and co-workers) of the *Plasmodium falciparum* lactate dehydrogenase aptamer within DNA tweezers. In the presence of the protein, the split aptamer binds the protein and forces a split G-quadruplex to form and bind to hemin, which, in the presence of hydrogen peroxide, can oxidize ABTS, thus allowing a colorimetric readout.[32] Consequently, it is easy to visualize the massive advantage that smart DNA nanomachines have in site-specific, targeted therapeutic delivery and diagnostics when they incorporate these natural aptamer sequences.

Recently, in 2017, Li and co-workers[33] combined both aptamer DNA and G-quadruplex DNA to synthesize a DNA-based ATP nano-biosensor. This system consisted of a three strand design that, without the presence of indicator Thioflavin T, or ATP, forms a single strand triangle in the middle, surrounded by three pairs of duplexes. The single-stranded region of this three way junction contained three ATP aptamers in order to capture the target molecule of ATP. Thioflavin, a ligand that binds to the ATP aptamer, acts as a fluorescent indicator for the binding of ATP to the aptamer, by competitively binding to the aptamer in the absence of ATP,

and releasing once ATP is present. Once a release strand, that contains a G-quadruplex sequence, hybridizes to the ATP aptamer, the ATP is released and the Thioflavin is captured by the release strand. The system can be reset with the addition of another strand.[33]

At the beginning of 2017, Qiu and co-workers[34] modified exosomes with an aptamer-based nanoarchitecture. Exosomes, which are extracellular vesicles, are biocompatible and carry many biomarkers, thus allowing for potential usage in disease diagnostics and drug delivery. Exosomes present challenges in modifying the surface, however, aptamers can allow researchers to overcome that challenge by binding to molecules expressed on the surface of the exosomes.[34] Consequently, the potential of incorporating natural motifs into our DNA nanomachines is easily visualized as they can function as detection modalities, delivery modalities, and as a surface modification technique. During the course of this thesis, you will see some of these techniques included to add the ability to deliver and sense certain microenvironment techniques.

Summary and Future Outlook:

Bioinspired DNA nanomachines have revolutionized biodiagnostics and have great future potential to revolutionize targeted, smart therapeutic delivery. By combining bioderived mechanisms and natural DNA motifs with special properties, researchers are able to create uniquely sensitive devices with the ability to smartly diagnose and treat specific diseases in a targeted fashion. DNA nanomachines have the capacity to greatly increase diagnostic sensitivity through amplification reactions that are triggered by small quantities of disease analyte. The incorporation of natural DNA motifs can also be used to create diagnostic readouts for the detection of often fatal diseases. Due to their unique flexibility and ease of functionalization, DNA nanostructures and machines can be made to target specific cellular populations due to

irregularities in their microenvironments or on their cellular surface or carry very high loads of therapeutic or diagnostic motifs. The future of bioderivative DNA nanomachines for biological applications is incredibly wide and varied and there are many motifs and machines that could be used eventually in a clinical aspect, however there is still a dearth of translational DNA nanomachines used clinically. However, we believe that through their ability to both derive inspiration for functionality from mimicking natural nanomachines and their ability to incorporate natural motifs, these DNA-based nanomachines and hybrid motifs will become an integral point-of-care diagnostics and smart, site-specific therapeutic delivery.

Chapter 2, is a partial reprint of the material as it appears in Advanced Healthcare Materials, 2018, Angell, Chava; Sibai X;.Mingxuan K; Xiangyi D;Yi C. The dissertation author was the primary author of this paper.

Chapter 2-BIBLIOGRAPHY

[1] Ruscito, A. and DeRosa, M.C., 2016. Small-molecule binding aptamers: Selection strategies, characterization, and applications. *Frontiers in chemistry*, *4*, p.14.

[2] Mao, C., Sun, W., Shen, Z. and Seeman, N.C., 1999. A nanomechanical device based on the B–Z transition of DNA. *Nature*, *397*(6715), pp.144-146.

[3] Leroy, J.L., Gueron, M., Mergny, J.L. and Helene, C., 1994. Intramolecular folding of a fragment of the cytosine-rich strand of telomeric DNA into an i-motif. *Nucleic acids research*, *22*(9), pp.1600-1606.

[4] Majikes, J.M., Ferraz, L.C. and LaBean, T.H., 2017. pH-driven actuation of DNA origami via parallel I-motif sequences in solution and on surfaces. *Bioconjugate chemistry*, *28*(7), pp.1821-1825.

[5] Dong, Y., Yang, Z. and Liu, D., 2014. DNA nanotechnology based on i-motif structures. *Accounts of chemical research*, *47*(6), pp.1853-1860.

[6] Modi, S., Swetha, M.G., Goswami, D., Gupta, G.D., Mayor, S. and Krishnan, Y., 2009. A DNA nanomachine that maps spatial and temporal pH changes inside living cells. *Nature nanotechnology*, *4*(5), pp.325-330.

[7] Surana, S., Bhat, J.M., Koushika, S.P. and Krishnan, Y., 2011. An autonomous DNA nanomachine maps spatiotemporal pH changes in a multicellular living organism. *Nature communications*, *2*(1), pp.1-7.

[8] Wang, W., Yang, Y., Cheng, E., Zhao, M., Meng, H., Liu, D. and Zhou, D., 2009. A pH-driven, reconfigurable DNA nanotriangle. *Chemical Communications*, (7), pp.824-826.

[9] Elbaz, J., Wang, Z.G., Orbach, R. and Willner, I., 2009. pH-stimulated concurrent mechanical activation of two DNA “tweezers”. A “SET− RESET” logic gate system. *Nano letters*, *9*(12), pp.4510-4514.

[10] Pei, H., Liang, L., Yao, G., Li, J., Huang, Q. and Fan, C., 2012. Reconfigurable three-dimensional DNA nanostructures for the construction of intracellular logic sensors. *Angewandte Chemie International Edition*, *51*(36), pp.9020-9024.

[11] Lee, J.A. and DeRosa, M.C., 2010. A pH-driven DNA switch based on the A+· G mispair. *Chemical Communications*, *46*(3), pp.418-420.

[12] Rich, A., 1993. DNA comes in many forms. *Gene*, *135*(1), pp.99-110.

[13] Mills, M., Arimondo, P.B., Lacroix, L., Garestier, T., Hélène, C., Klump, H. and Mergny, J.L., 1999. Energetics of strand-displacement reactions in triple helices: a spectroscopic study. *Journal of molecular biology*, *291*(5), pp.1035-1054.

[14] Chen, Y., Lee, S.H. and Mao, C., 2004. A DNA nanomachine based on a duplex–triplex transition. *Angewandte Chemie International Edition*, *43*(40), pp.5335-5338.

[15] Han, X., Zhou, Z., Yang, F. and Deng, Z., 2008. Catch and release: DNA tweezers that can capture, hold, and release an object under control. *Journal of the American Chemical Society*, *130*(44), pp.14414-14415.

[16] Yang, M., Zhang, X., Liu, H., Kang, H., Zhu, Z., Yang, W. and Tan, W., 2015. Stable DNA nanomachine based on duplex–triplex transition for ratiometric imaging instantaneous pH changes in living cells. *Analytical chemistry*, *87*(12), pp.5854-5859.

[17] Liu, Z., Li, Y., Tian, C. and Mao, C., 2013. A smart DNA tetrahedron that isothermally assembles or dissociates in response to the solution pH value changes. *Biomacromolecules*, *14*(6), pp.1711-1714.

[18] Ranallo, S., Prévost-Tremblay, C., Idili, A., Vallée-Bélisle, A. and Ricci, F., 2017. Antibody-powered nucleic acid release using a DNA-based nanomachine. *Nature communications*, *8*(1), pp.1-9.

[19] Mariottini, D., Idili, A., Vallée-Bélisle, A., Plaxco, K.W. and Ricci, F., 2017. A DNA nanodevice that loads and releases a cargo with hemoglobin-like allosteric control and cooperativity. *Nano letters*, *17*(5), pp.3225-3230.

[20] He, H.Z., Chan, D.S.H., Leung, C.H. and Ma, D.L., 2013. G-quadruplexes for luminescent sensing and logic gates. *Nucleic acids research*, *41*(8), pp.4345-4359.

[21] Li, J.J. and Tan, W., 2002. A single DNA molecule nanomotor. *Nano Letters*, *2*(4), pp.315-318.

[22] Liu, D., Bruckbauer, A., Abell, C., Balasubramanian, S., Kang, D.J., Klenerman, D. and Zhou, D., 2006. A reversible pH-driven DNA nanoswitch array. *Journal of the American Chemical Society*, *128*(6), pp.2067-2071.

[23] O Tucker, W., T Shum, K. and A Tanner, J., 2012. G-quadruplex DNA aptamers and their ligands: structure, function and application. *Current pharmaceutical design*, *18*(14), pp.2014-2026.

[24] Wu, Y., Zou, L., Lei, S., Yu, Q. and Ye, B., 2017. Highly sensitive electrochemical thrombin aptasensor based on peptide-enhanced electrocatalysis of hemin/G-quadruplex and nanocomposite as nanocarrier. *Biosensors and Bioelectronics*, *97*, pp.317-324.

[25] Wei, B., Cheng, I., Luo, K.Q. and Mi, Y., 2008. Capture and Release of Protein by a Reversible DNA‐Induced Sol–Gel Transition System. *Angewandte Chemie International Edition*, *47*(2), pp.331-333.

[26] Dittmer, W.U., Reuter, A. and Simmel, F.C., 2004. A DNA‐based machine that can cyclically bind and release thrombin. *Angewandte Chemie International Edition*, *43*(27), pp.3550-3553.

[27] You, M., Peng, L., Shao, N., Zhang, L., Qiu, L., Cui, C. and Tan, W., 2014. DNA “nano-claw”: logic-based autonomous cancer targeting and therapy. *Journal of the American Chemical Society*, *136*(4), pp.1256-1259.

[28] Douglas, S.M., Bachelet, I. and Church, G.M., 2012. A logic-gated nanorobot for targeted transport of molecular payloads. *Science*, *335*(6070), pp.831-834.

[29] Kuzuya, A. and Ohya, Y., 2014. Nanomechanical molecular devices made of DNA origami. *Accounts of chemical research*, *47*(6), pp.1742-1749.

[30] You, M., Zhu, G., Chen, T., Donovan, M.J. and Tan, W., 2015. Programmable and multiparameter DNA-based logic platform for cancer recognition and targeted therapy. *Journal of the American Chemical Society*, *137*(2), pp.667-674.

[31] Nakatsuka, K., Shigeto, H., Kuroda, A. and Funabashi, H., 2015. A split G-quadruplex-based DNA nano-tweezers structure as a signal-transducing molecule for the homogeneous detection of specific nucleic acids. *Biosensors and Bioelectronics*, *74*, pp.222-226.

[32] Shiu, S.C.C., Cheung, Y.W., Dirkzwager, R.M., Liang, S., Kinghorn, A.B., Fraser, L.A., Tang, M.S. and Tanner, J.A., 2017. Aptamer‐Mediated Protein Molecular Recognition Driving a DNA Tweezer Nanomachine. *Advanced Biosystems*, *1*(1-2), p.1600006.

[33] Peng, P., Shi, L., Wang, H. and Li, T., 2017. A DNA nanoswitch-controlled reversible nanosensor. *Nucleic acids research*, *45*(2), pp.541-546.

[34] Wan, S., Zhang, L., Wang, S., Liu, Y., Wu, C., Cui, C., Sun, H., Shi, M., Jiang, Y., Li, L. and Qiu, L., 2017. Molecular recognition-based DNA nanoassemblies on the surfaces of nanosized exosomes. *Journal of the American Chemical Society*, *139*(15), pp.5289-5292.

Chapter 3-RCA Wrapped Nanomotors for siRNA Delivery

Abstract:

An effective intracellular gene silencing strategy based on acoustically propelled nanowires modified with an interfering RNA's (siRNA) payload is described. The gold nanowires (AuNW) are wrapped with a Rolling Circle Amplification (RCA) DNA strand, which serves to anchor the siRNA therapy. The ultrasound (US)-powered propulsion of the AuNW leads to fast internalization and rapid intracellular movement and hence to an accelerated siRNA delivery and silencing response. To optimize the micromotor gene silencing procedure, the influence of motion, time, and siRNA dosage was investigated, leading up to a 94% silencing after few minutes treatment with US-propelled siRNA–AuNWs, and to a dramatic (~13-fold) improvement in the silencing response compared to the static modified nanowires. The ability of the nanomotor-based method for gene silencing has been demonstrated by measuring the GFP silencing response in two different cell lines (HEK-293 and MCF-7) and using detailed control experiments. The viability of the cells after the nanomotors treatment was examined using the MCF-7 cancer cell line. The use of DNA structures carried by the US-propelled nanomotors for gene silencing represents an efficient tool that addresses the challenges associated with RNA transportation and intracellular delivery. Future implementation of nanomachines in gene therapy applications can be expanded into a co-delivery platform for therapeutics.

Introduction

Small interfering RNA (siRNA) therapy is a promising tool for gene suppression and knockdown, offering an attractive, alternative route for treating various diseases.[1,2] Such knockdown occurs once the siRNA strand is incorporated into the RNA-induced silencing

complex, which is then guided to the target mRNA sequence to be excised,[3] ensuring that certain undesirable target proteins will no longer be expressed within the cell.[4]However, widespread use of RNA transfection agents is challenging due to the lack of targeting modalities, limited loading efficiency, internalization barriers, and biocompatibility issues.[5] Thus, future work focusing on the development of safe and effective delivery materials is needed to ensure the broad clinical application of siRNA.[6]

However, due to the negatively charged cell membrane surface and the anionic nature of siRNA, the use of cationic transfection agents or targeting ligands is necessary to ensure safe, efficient intracellular uptake and knockdown. This pitfall in RNA interference (RNAi) therapy, and more specifically siRNA delivery, has been circumvented through different strategies, including the use of metal nanoparticles (NPs),[4,7] cationic lipid NPs,[8] cationically condensed siRNA microhydrogels,[9] and polymerization along with subsequent conjugation of siRNA to receptor targeted ligands.[5]

An attractive solution to design siRNA carriers is to approach it from the framework of DNA nanotechnology.[10−14] As discussed in the Introductory chapter, DNA is well-known as a genomic carrier and as a building material for supramolecular assemblies. The specific bonding of base pairs makes DNA strands particularly suited as building blocks to assemble highly structured materials with specific nanoscale features. In drug delivery field, DNA nanotechnology enables the precise control of morphology and loading efficacy of delivery cargos and offers a creative approach to delivering small molecules, siRNA, and diagnostic agents.[10,15,16]

Alternately, the attractive cargo-towing, movement and navigation capabilities of modern self-propelled and externally powered micro/nanomotors[17−21] have permitted their use for

enhanced transport and delivery of therapeutic payloads, compared to common diffusion based approaches.[22−26] In particular, recent efforts have demonstrated the use of lipoplexes-modified microengines for plasmid DNA delivery[27] and of ultrasound (US)-propelled nanomotors for intracellular monitoring of miRNA expression.[28]

In this paper, we describe the use of self-propelled nanowires (AuNWs) for selective and rapid intracellular siRNA delivery utilizing a hybrid siRNA−DNA nanotechnology platform. This gene-silencing approach relies on the accelerated intracellular delivery of Green Fluorescence Protein targeted siRNA (siGFP), hybridized to Rolling Circle Amplification (RCA) DNA structures carried by the US-propelled gold nanowires. Once inside the cell, the siGFP is responsible for silencing the formation of new fluorescent proteins, as indicated by the rapid loss of the green fluorescence, which reflects an effective intracellular siRNA delivery. Different from other approaches using either membrane fusion[1,7,8] or receptor related endocytosis[5,15,16] to enter the cell, these ultrasound-powered nanomotors pierce and travel inside the cell. Different parameters related with the silencing efficiency (US propulsion time and siRNA dosage) were studied. The versatility of the nanomotor-based gene silencing method was demonstrated using different cell lines (HEK-293-GFP and MCF-7-GFP). Cell viability tests were conducted with the MCF-7-GFP cell line, demonstrating that most of the cells remained alive after the nanomotor treatment.

US-propelled nanomotors are attractive candidates to overcome biological barriers and physical limitations commonly faced by siRNA carrier methods. These nanoscale motors have been used recently in a wide range of applications, including triggered drug release,[29,30] decontamination,[31,32] and intra- cellular motion[33] and miRNA detection.[28] The latter

studies demonstrate that the ultrasound propulsion facilitates the internalization of functionalized nanowire motors into cells.[28,33]

3.2-Results and Discussion

Figure 3.1. Schematic of the nanomotor-based gene silencing approach including fluorescence images and optical images of the acoustic movement of the motors inside living cells. Schematic of the (A) GFP/RCA-AuNW penetration inside a HEK293-GFP cell due to the nanomotor movement under an US field, and (B) natural process for gene-mRNA silencing inside living cells (observed in the images by the cell-fluorescence decrease after have been treated during 5 min with US-propelled GFP/RCA-modified nanomotors, and following an overnight incubation; 200 ng of GFP/RCA; scale bar, 1000 μm). (C) Actual time-lapse images taken at 10 s intervals (from Supporting Information Video S1) illustrating the preconcentration of GFP/RCA-AuNWs (black dots) and HEK293-GFP cells (light spheres) under the US field. (D) Actual time-lapse images taken at 4 s intervals (from Supporting Information Video S2) illustrating the penetration of a GFP/ RCA-AuNW into a HEK293-GFP cell. (E) Actual time-lapse images taken at 1 s intervals (from Supporting Information Video S3) showing the spinning motion of a GFP/RCA-AuNW inside a HEK293-GFP cell; arrows indicate the direction of the motion. US field, 6 V, and 2.66 MHz.

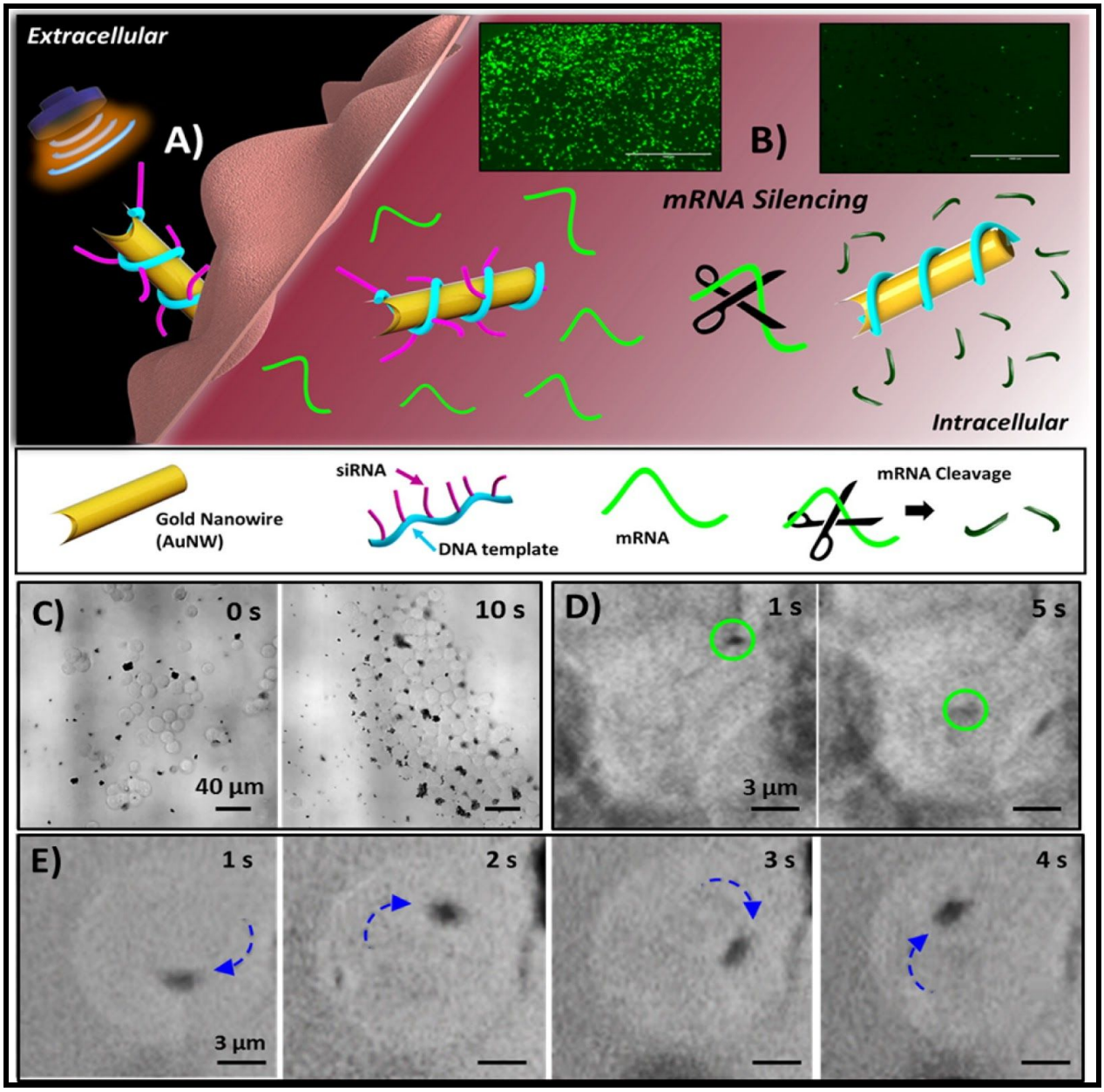
Extracellular
A)
B)
mRNA Silencing
Intracellular
Gold Nanowire
(AuNW)
siRNA
DNA template
mRNA
mRNA Cleavage
C)
0 s
10 s
40 µm
D)
1 s
5 s
3 µm
E)
1 s
2 s
3 s
4 s
3 µm

A schematic of the siRNA nanomotor-based gene silencing approach is illustrated in **Figure 3.1**. The hybrid DNA-motor motif has been illustrated for gene-mRNA-silencing inside living Human Embryonic Kidney 293 cells that express GFP (HEK293-GFP). The fast propulsion thrust and force of the US-propelled siRNA-wrapped AuNWs lead to efficient piercing and penetration into these HEK293-GFP cells (**Figure 3.1 A**). Coupling the rapid intracellular motion, fast release of the siRNA, and optimal siRNA loading capacity, this approach results in efficient and rapid suppression of target gene expression when compared to existing gene-silencing methods.[34,35] Such acceleration represents an important advantage for the potential treatment of many diseases. The short silencing time, efficient knockdown, high selectivity, and other characteristics of the nanomotor approach are described in the following sections.

As is illustrated in **Figure 3.1 B**, upon entry into the cell, the GFP/RCA sequence, attached to a positive cysteamine- functionalized AuNWs surface via electrostatic interactions and wrapping, starts to suppress the gene-mRNA expression and thus turns the cell-fluorescence “OFF” (**Figure 3.1 B**, top-part fluorescence images) confirming the intracellular siRNA delivery. Such process is allowed by the US-induced preconcentration of AuNWs and cells into localized pressure nodes (**Figure 3.1 C** and Supporting Video S1). Once concentrated in these nodes, the US-propelled nanomotors bombard the cell wall, leading to aggregation, piercing and penetration (**Figure 3.1 D** and Supporting Video S2), enabling intracellular delivery of siRNA. Further evidence of internalization is illustrated by the spinning motion of AuNWs inside the cell, which is shown in **Figure 3.1 E** and corresponding Supporting Video S3. Once inside the cell, the speed of the US- propelled nanomotors is dependent on several parameters, such as higher intracellular viscosity,[33] imperfection in the nano- motor’s shape,[30] and the applied voltage.[29]

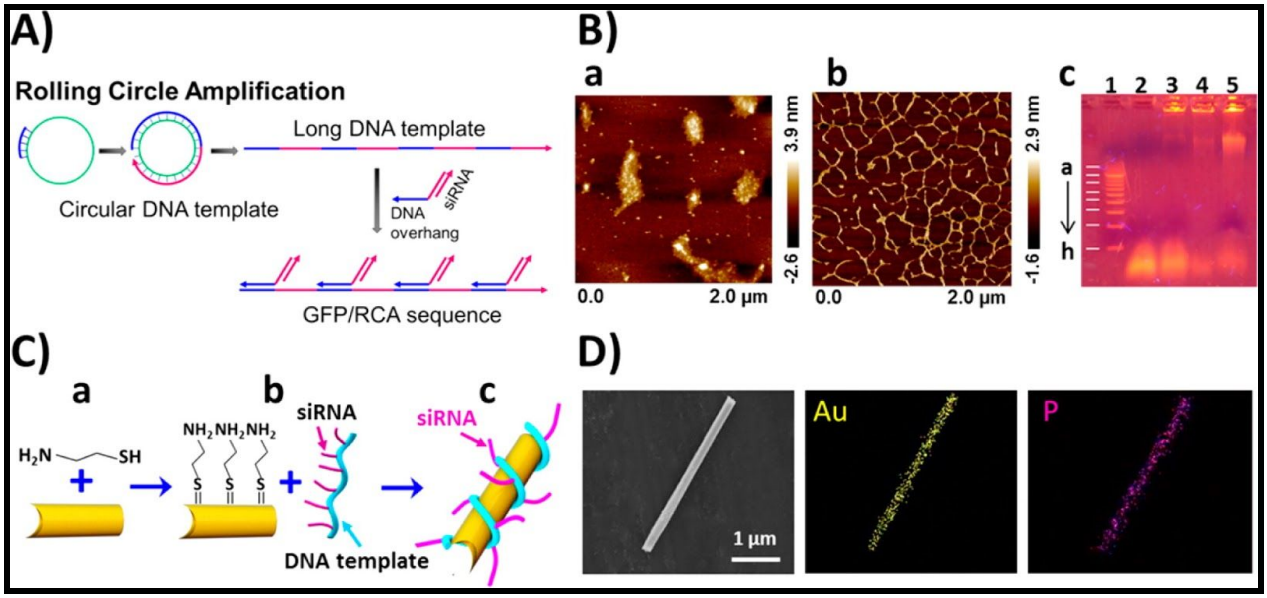

Figure 3.2. (A) Rolling circle amplification technique where a short DNA sequence is amplified to form a long single-stranded DNA using a circular DNA template with repeating units, and subsequently modified with a complementary DNA overhang-siRNA sequence. (B) AFM image of a 2 µm scan of the RCA strand (a) without siRNA and (b) with siRNA; (c) 0.5% native agarose gel to confirm the binding of the siRNA to the RCA product (well 1 corresponds to marker ladders, from a to h: 8 Kb, 5 Kb, 3.5 Kb, 2.5 Kb, 2 Kb, 1.5 Kb, 1 Kb, 500 bp, respectively; wells 2−5 contains 1 µg of siRNA and 0, 5, 10, and 20 µL of RCA, respectively). (C) Functionalization of the AuNWs with GFP/ RCA: (a) coating with cysteamine, (b) amine activation and conjugation with GFP/RCA sequence, (c) the resulting GFP/RCA-modified AuNW. (D) Characterization of a GFP/RCA-AuNW: SEM image and EDX analysis of Au and P (corresponding to the GFP/RCA phosphate backbone).

RCA is a process that utilizes a circular nucleic acid template, created by ligating a single strand of DNA or RNA closed with ligase and then amplifying that template through the use of polymerase.[36,37] The length of the final product is determined by the polymerase concentration and its reaction time. This process can be extrapolated to develop sensors[36] or complex 3D DNA structures via origami techniques that are used to deliver therapeutics and diagnostic agents.[38] The circular template for the RCA product used in these experiments contains two repeating units, a noncoding spacer region, and a binding region of 20 A base pairs (bp) that binds to the target siRNA (GFP). When amplified by RCA, these segments repeat and allow for the binding of multiple units of siRNA (**Figure 3.2 A**). The 20 A bp region, when transcribed by phi29 DNA polymerase, through RCA, creates a 20 T region which can then bind

to the GFP-targeting siRNA which is modified with an additional 20 A DNA nucleotide region on the sense strand. Once the siRNA has bound to the long stranded RCA product, the RCA product transitions from a large clump of DNA and straightens out into long stranded regions, resulting in the final GFP/RCA product. This can be clearly seen in the AFM images of **Figure 3.2 B**, which show the RCA product without the siRNA as large coiled balls of long-stranded DNA (**Figure 3.2 B(a)**), and, when hybridized to the siRNA, as a spread out network of strands (**Figure 3.2 B(b)**). This expanded structure leads to a smaller diameter that facilitates a higher volume of the RCA/siRNA product entering into a 0.5% agarose gel in **Figure 3.2 B(c)**. Each volume of RCA in the gel was hybridized with the same amount of the double-stranded siRNA product. As shown, the upper RCA/siRNA bands (2−5 wells) become more intense with increasing amounts of RCA, due to the fact that the siRNA acts as a “declumping” agent, thus allowing more bound product to enter the gel. The intensity change in the lower siRNA bands (2−5 wells) becomes fainter upon adding more RCA, indicating the successful binding of the siRNA and subsequent shift in size. Once bound, an alternating single and double-stranded RCA product is created, which allows the product to wrap onto the positively charged surface of the gold nanomotor. This provides the ability to localize siRNA in a controlled fashion onto the motor and increase the knockdown efficiency.

AuNWs were synthesized by template electrodeposition method and further functionalized with cysteamine to obtain the appropriate self-assembly monolayer (SAM), and later with the GFP/RCA sequence (procedures are detailed in the Experimental Section). Briefly, the template-directed electrodeposition protocol consists on depositing the gold within the cylindrical micropores of an alumina membrane template, followed by dissolution of the membrane and release of the AuNWs.

We have characterized the nanomotor design and functionalization to ensure an efficient siRNA loading and intracellular delivery. Scanning electron microscopy (SEM) image was obtained to examine the structural morphology of the GFP/RCA-AuNWs. **Figure 3.2 D** shows the SEM image of a GFP/RCA-modified AuNW with ~4 μm length and a diameter of 200 nm, which reflects the electrical charge and pore size, respectively, of the anodic aluminum oxide (AAO) membrane template used in the fabrication process. Furthermore, the acoustic propulsion mechanism relies on ultrasound streaming over the rigid metallic surface of the asymmetric AuNW,[39,40] which contains a concave end essential for the motion. This, combined with fluid streaming,[41] leads to enhanced propulsion thrust capable of piercing and internalization of AuNWs into cells.

The AuNWs were modified via self-assembly of the cysteamine bifunctional agent on the gold surface35 to obtain a positively charged nanomotors surface and allow an electrostatic interaction with the negative charge of the GFP/RCA sequence. The EDX analysis also demonstrates the composition of the gold-nanomotor and the successful modification of motor with the GFP/RCA sequence, as confirmed by the phosphate content of the AuNW, corresponding to the phosphate backbone of the GFP/RCA sequence (images shown in Figure 2D).

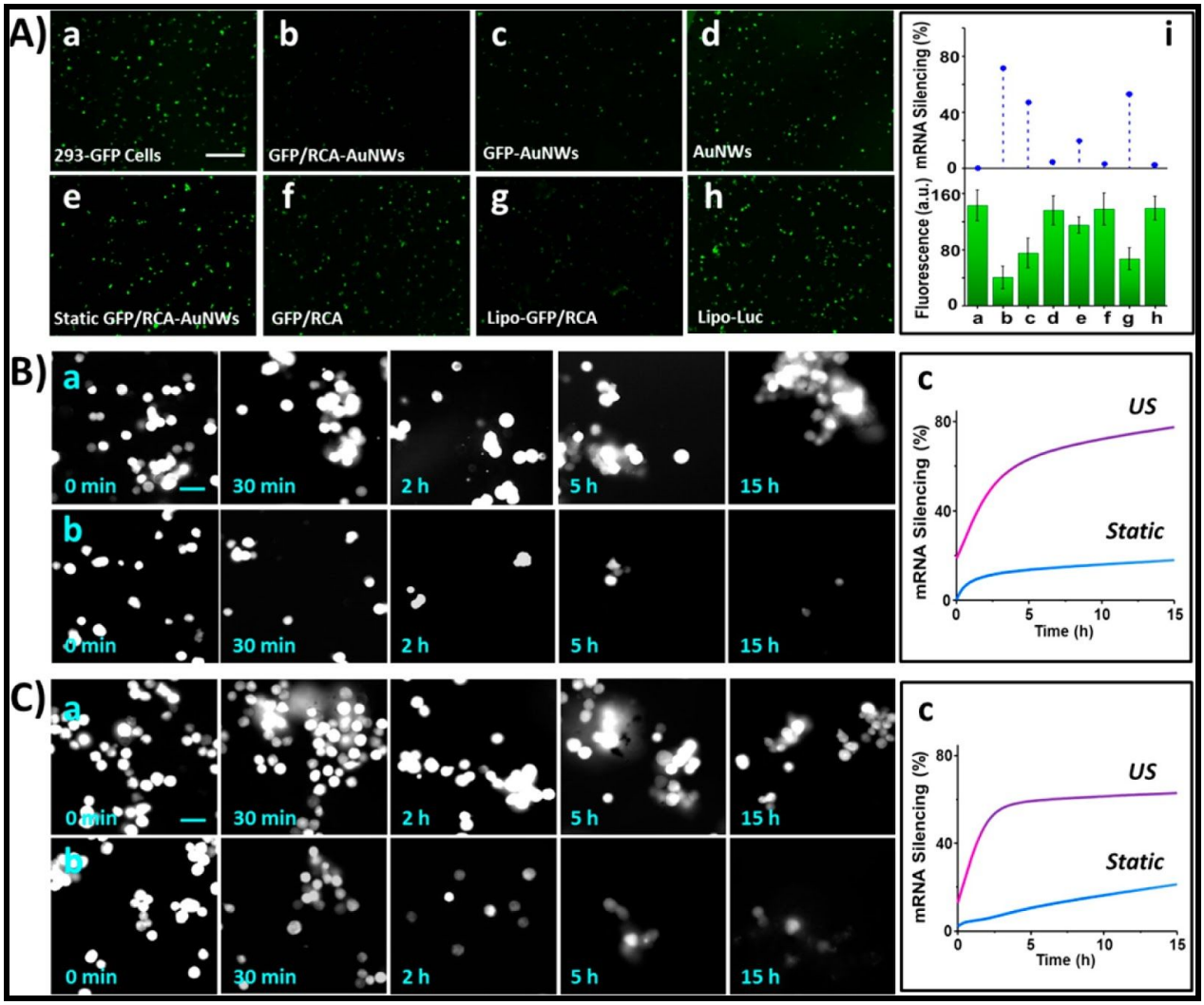

Figure 3.3. (A) Fluorescence images of the HEK293-GFP cells obtained after exposure to different experimental (control) conditions (a−h): (a) untreated cells, (b) cells treated with the US-powered-GFP/RCA-AuNWs, (c) cells treated with US-powered-GFP-AuNWs, (d) cells treated with US-powered-unmodified-AuNWs, (e) cells treated with static-GFP/RCA-AuNWs, (f) cells treated with free GFP/RCA, (g) cells treated with free lipofectamine/GFP/RCA, and (h) cells treated with free lipofectamine-luciferase. (i) Gene-mRNA silencing percentage and fluorescence quantification corresponding to each control. US conditions: 6 V, 2.66 MHz, and 5 min; all cells were incubated overnight; scale bar, 500 μm. Time-silencing study with (B) HEK293-GFP cells and (C) MCF7-GFP cells comparing in both cell lines: (a) static GFP/RCA AuNWs and (b) US-propelled GFP/RCA-AuNWs after different incubation times (0, 0.5, 2, 5, and 15 h); scale bar, 50 μm. (c) Dependence of the mRNA silencing percentage upon the incubation time after treating the HEK293-GFP cells and MCF7-GFP cells (B and C, respectively) with the GFP/RCA-AuNWs in the absence and presence of the US field. US conditions: 6 V, 2.66 MHz, and 5 min.

To demonstrate the feasibility of the nanomotors-based approach toward enhanced mRNA silencing, various controls (**Figure 3.3 A**) and time-silencing dependence studies were

carried out under static and US conditions (**Figure 3.3 B,C**) to investigate and optimize the in vitro intracellular mRNA silencing mechanism involved in the miRNA knockdown. **Figure 3.3 A** shows the fluorescence results of HEK293-GFP cells (corresponding optical images shown in Supporting Figure S1) after they have been exposed to different conditions and incubated overnight in the adequate cellular media (all the controls were compared to fluorescence signal of untreated HEK293-GFP cells (**Figure 3.3 A(a)**), and AuNWs were modified with 80 ng of GFP/RCA sequence).

The HEK 293 cell line was chosen due to its common ability to easily express recombinant proteins, such as the GFP, which can be then targeted with known siRNA sequences such as GFP-targeting siRNA.[42] As illustrated in the fluorescence image of **Figure 3.3 A(b)**, a 74% gene-silencing is obtained with the US-powered-GFP/RCA- AuNWs (6 V, 2.66 MHz for 5 min) (**Figure 3.3 A(i): line b**), as compared to 20% achieved with the GFP/RCA-AuNWs under static conditions (**Figure 3.3 A(e),A(i): line e**), i.e., ~3.7 times higher silencing when US is applied. It has been also demonstrated that the propulsion of the nanomotors greatly facilitates the siRNA internalization process, as this nanomotor route offers a 21-fold enhanced silencing when compared to GFP/RCA free in solution at the same concentration level (**Figure 3.3 A(i): lines b vs f**). Such enhancement and performance are extremely important since current intracellular mRNA silencing strategies commonly require prolonged incubation times (24−48 h) and complex systems to overcome the problems related to escape from endosome to cytoplasm.[34,35,38] Furthermore, to ensure that the silencing efficiency was a result of the RCA surface template, we also analyzed cells treated with US-powered-AuNWs modified with plain GFP lacking the RCA template (**Figure 3.3 A(c)**). This control experiment resulted in a significantly lower silencing efficiency compared to the use of RCA-loaded GFP (**Figure 3.3 A(i): line c**). Consequently, we can determine that the RCA

template offers a higher siRNA loading capacity and leads to an increased transfection efficiency. This reflects the strong preferential binding of the siRNA to the RCA template, allowing for more siRNA to be confined on the nanomotors as they enter the cells. Such efficient modification of the gold nanomotor surface has a profound effect upon the efficiency of the siRNA delivery. Cells were also treated with US-powered unmodified-AuNWs (**Figure 3.3 A(d),(i)**) to exclude the possibility of any off fluorescence switching effects resulting from the nanomotor motion. To finalize the control experiments, we compared the silencing achieved with commonly used cationic transfection agent Lipofectamine 2000 with two types of siRNA: the target GFP siRNA and Luciferase siRNA, as positive and negative controls, respectively (**Figure 3.3 A (g vs h)**). While, as expected, the Lipofectamine-GFP siRNA induced knockdown, it did not lead to the same efficacy as the RCA/ GFP-modified nanomotors. This phenomenon was also confirmed with a dosage-silencing dependence study using both Lipofectamine-modified siRNAs (Supporting Figure S2). The mRNA silencing percentage increased first with the Lipofectamine-GFP siRNA dosage up to 60% knockdown with 80 ng sample, leveling off above this dosage. However, the Luciferase siRNA did not display the dosage silencing-response effect, demonstrating again the importance of the siRNA-RCA template.

To demonstrate the feasibility of the nanomotors approach toward mRNA silencing, we compared the fluorescence signals of HEK293-GFP and MCF7-GFP cells (**Figure 3.3, panels B and C, respectively**) after different incubation times, following a 5 min treatment with the GFP/RCA-AuNWs in the absence (a) and presence (b) of the US field (6 V, 2.66 MHz). As illustrated in **Figure 3.3 B(a)**, the fluorescence of the cell did not change significantly using the static conditions, compared to the fast (50%) silencing response after 2 h of the nanomotors treatment (**Figure 3.3 B(b)**; corresponding optical images are shown in Supporting Figure S3).

These results indicate that the movement of the siRNA-modified motors leads to a ~4.3-fold enhancement in the siRNA silencing after an overnight incubation (**Figure 3.3 B(c)**), which confirms the knockdown results obtained in the previous control studies. Similar results were obtained with the MCF7-GFP cancer cell line (**Figure 3.3 C**; corresponding optical images are shown in Supporting Figure S4), confirming the viability and versatility of the hybrid DNA-nanomotor-based silencing strategy. In view of the results shown in **Figure 3.3 B(c),C(c)**, it can be said that the major advantage of the nanomotor-based siRNA delivery approach is the accelerated silencing response, with both cell lines reaching a silencing percentage plateau after 5 h nanomotor treatment.

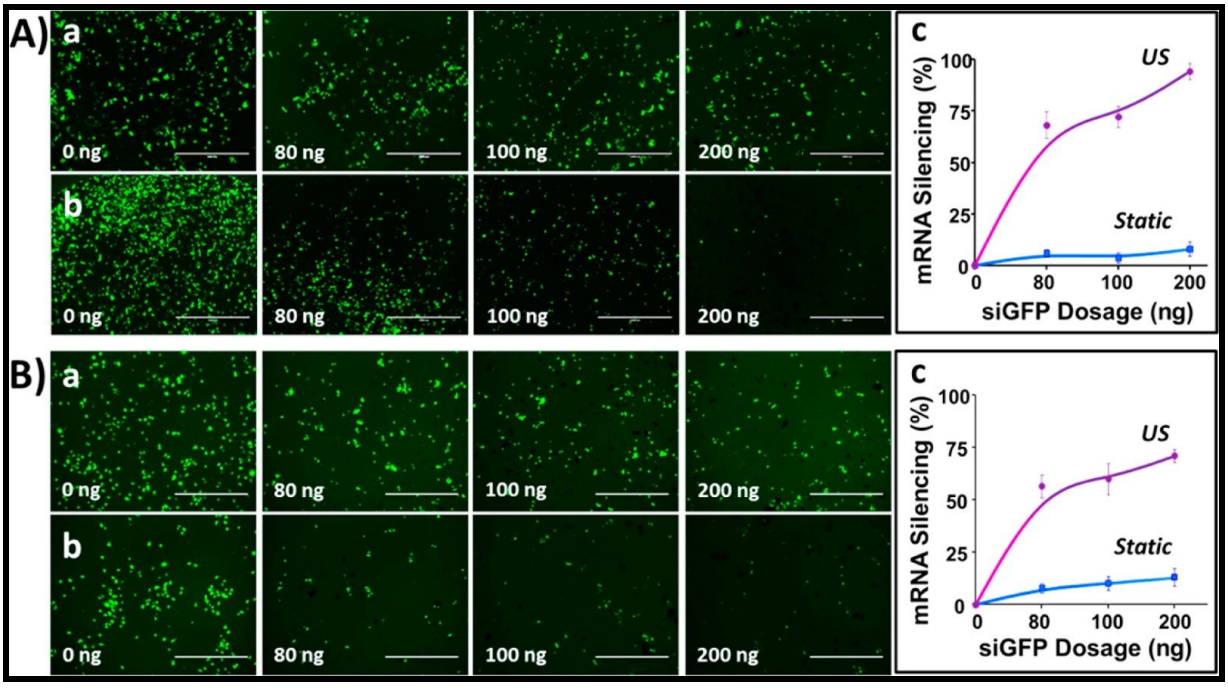

Figure 3.4. siRNA dosage study. Effect of the amount of siGFP (0, 80, 100, and 200 ng) immobilized on AuNWs onto the efficiency of the genemRNA silencing inside HEK293-GFP cells (A) and MCF7-GFP cells (B), using (a) static conditions and (b) US-propelled micromotors; (c) dependence of the mRNA silencing percentage in both cell lines upon the GFP/RCA dosage (ng) in the absence and presence of the US field (6 V, 2.66 MHz, 5 min).

Further improvement of the silencing effect has been achieved by modifying the siGFP dosage for enhancing the amount of intracellular siRNA (**Figure 3.4**). For this purpose, a concentrated RCA-siRNA product was synthesized to modify the motors, and was then diluted according to the desired dosage (0, 80, 100, or 200 ng). Subsequently, both cell lines were treated with motors loaded with different dosages of siGFP (siRNA dosages), and the silencing effect between static and US propulsion conditions was compared (**Figure 3.4 A,B: (a) vs (b)**). Using US-propelled motors, the silencing response of HEK293-GFP cells increased from a 68% to a 94% upon raising the dosage from 80 ng (used in previous studies) to 200 ng of siGFP, respectively (**Figure 3.4 B(c)**). In contrast, static conditions resulted in a significantly lower change of the silencing percentage (6−12%) over the same 80−200 ng GFP/ RCA dosage range (**Figure 3.4 A(c)** and Supporting Figure S5). As illustrated in **Figure 3.4 A(c)**, loading the nanomotors with 100 ng of the siRNA/RCA template and propelling them for 5 min resulted in ~13-fold higher silencing compared to the static wires. Such major improvement reflects the efficient siRNA delivery associated with the fast internalization of the motor and rapid intracellular movement under the US field. Similar silencing responses were observed with the MCF7-GFP cancer cell line (**Figure 3.4 B**), demonstrating a 70% silencing when using US-propelled nanomotors loaded with 200 ng of the siRNA/ RCA template, compared to the 13% silencing obtained with static nanorods (**Figure 3.4 B(c)**). Overall, the results presented in **Figure 3.4** demonstrate the clear advantages of speed and efficiency of the nanomotor mRNA-gene silencing approach in terms of knockdown method in both cell lines, which make it a competitive gene-delivery platform for the treatment of various diseases.

To exclude the possibility that the silencing of GFP signal comes from the death of cells, we examined the cell viability after the different treatments with static and US-propelled nanomotors, choosing the MCF7-GFP as the model cell line (see Experimental Section for

details). The results obtained indicated that neither the nonmodified AuNWs nor the GFP/ RCA-AuNWs (using different GFP/RCA dosages) affected significantly the cell viability. These findings are in good agreement with earlier reports[33,43,44] that indicate that the presence of micro/nanomotors does not exhibit acute toxicity toward the cells. These data demonstrate that after the nanomotors treatment, the cells were still alive, but had specifically reduced their expression of the target protein (Supporting Figure S7). The detailed mechanism of this rapid GFP silencing is under investigation. We believe that it takes advantage of the nanomotors movement within the cells. Compared with commonly used delivery cargos, such as lipid nanoparticles, which take a few hours for cell uptake and endosome escape,[45,46] the acoustically propelled nanowires enter the cell rapidly (within few minutes) and travel inside it. The spinning motion inside the cells accelerates the siRNA's release and diffusion at multiple locations, and thus leads to a faster mRNA silencing

Materials and Methods

Cysteamine hydrochloride was purchased from Sigma-Aldrich. All RCA products were purchased from Core Bio Services. Phosphate buffered saline (PBS) solution was purchased from Gibco, Invitrogen.

Human Embryonic Kidney 293 cells imaged with Green Fluorescent Protein (HEK293-GFP) and Michigan Cancer Foundation-7 (MCF7-GFP) were obtained from the University of California, San Diego (UCSD), Nanomaterials & Nanomedicine Laboratory. The cell lines were grown in Corning cellular DMEM media with 4.5 g/L glucose, L-glutamine, and sodium pyruvate purchased from Fisher Scientific; 10% HyClone Bovine Growth Serum (FBS) purchased from VWR International; and 1% penicillin streptomycin purchased from Core Bio Services, and the cells were used immediately for the experiments. To prepare the cells

suspension, after removing the cell culture media, cells were detached from the flask by treating them with 2 mL of Trypsin-EDTA (0.25%), obtained from Core Bio Services, for 2 min. The trypsin was then inactivated using the supplemented media, centrifuged for 5 min at 0.7 RCF, and resuspended to the correct concentration in media using a hemocytometer.

Milli-Q water was used for the modification step of AuNWs with cysteamine. PBS solution pH 7.5, prepared with Milli-Q water, was used during the incubation of the cysteamine-modified AuNWs and siRNA samples, to perform the washing steps and during the US experiments.

All chemicals used were of analytical-grade reagents, and deionized water was obtained from a Millipore Milli-Q purification system (18.2 MΩ cm at 25 °C).

Synthesis of RCA. All DNA sequences were purchased from Integrated DNA Technologies. The circle strand (Circle-20A) and the primer strand (Primer-Poly-T) were ligated together in a 1:10 molar ratio using 148 μL of quick ligation buffer, 150 μL of DI water, and 15 μL of quick ligase for at least 16 h at 14 °C. Two picomoles of the ligated circle was combined with the nucleotides (12 μL, 120 nmol of dNTPS), water (up to 60 μL), the polymerase buffer (6 μL), bovine serum albumin (1.6 μL of 10 mg/mL), and the polymerase (3 μL, 30 units). This procedure was adapted and modified from Lin et al.37 This was reacted for 2 h at 37 °C and then the polymerase was inactivated at 70 °C for 10 min. The GFP sense and antisense strands were combined in an equimolar ratio and diluted to 1 μg/μL using water and 10× TAE Mg diluted to a 1× concentration in the final volume. Then, 1.5 μg of GFP siRNA was added to 30 μL of RCA product and 3.44 μL of 10× TAE Mg. This was annealed using an annealing program we have titled the “native 30” program using an Eppendorf Mastercycler (hold for 5 min at 90 °C,

ramp down to 65 °C, hold for 30 min, ramp down to 50 °C, hold for 30 min, ramp down to 37 °C, hold for 30 min, and then ramp down to 22 °C and hold).

Synthesis of Concentrated RCA for Dosage Experiment. Six times the normal volume of RCA was created and then the phi29 polymerase was deactivated at 70 °C for 35 min. The DNA was precipitated out of solution using ethanol precipitation and then resuspended in 50 μL of 18.2 MΩ cm water, 6.66 μL of 10× TAE Mg, and 10 μg of 1 μg/μL GFP siRNA. This was annealed using the native 30 program. Once annealed, the RCA/GFP was combined with the nanomotors and diluted according to the desired dosage.

Characterization of GFP/RCA. The morphology of the RCA strand with and without the siRNA was analyzed by AFM (Credit Sibai Xie). AFM imaging was performed under room temperature in dry conditions. Three μL of sample DNA solution was dropped onto freshly cleaved mica surface, and incubated at room temperature for 1−2 min for surface adsorption. The drop was washed off by 30 μL of 2 mM Mg(Ac)2 solution, and was dried by compressed air. Scanasyst- Air tip (Bruker, Camarillo, CA) with a spring constant of 0.4 N/m was used on a Multimode AFM (Vecco Metrology, Santa Barbara, CA). Amplitude setpoint was controlled at the lowest possible value to avoid scratching on the structure. A 0.5% native TBE agarose gel was performed to confirm the binding of the siRNA to the RCA product as well. The gel was stained with 0.01% ethidium bromide in the gel before running at 100 V for 1 h and 20 min in 1× TBE buffer and exposed to ultraviolet light for imaging.

Lipofectamine 2000. A volume of 200 μL of OPTI-MEM was combined with 0.8 μg of “native 30” annealed 1 μg/μL GFP siRNA and 5 μL of Lipofectamine 2000. Approximately, 7 × 103cells were seeded in a 96 well plate and incubated overnight at 37 °C. The media was removed, and each well was treated with 80 ng of the GFP siRNA with the Lipofectamine 2000

and additional media. After 18 h incubation at 37 °C, the wells were imaged using the EVOS FL microscope. The Lipofectamine used in the dosage experiment was prepared in the same method, by increasing the amount of siRNA added into the original mixture.

Nanomotors Fabrication. The gold nanowire (AuNWs) motors were prepared by a common template-directed electrodeposition protocol. A thin gold film was first sputtered on one side of the porous alumina membrane template containing 200 nm diameter cylindrical nanopores (Catalogue No. 6809-6022; Whatman, Maidstone, U.K.) to serve as a working electrode. The membrane was assembled in a Teflon plating cell with aluminum foil serving as an electrical contact for the subsequent electrodeposition. A sacrificial copper layer was electrodeposited into the branched area of the membrane using a 1 M cupric sulfate pentahydrate solution (CuSO4·5H2O, Sigma-Aldrich, St. Louis, MO), using a charge of 8 C and a potential of −0.90 V (vs a Ag/ AgCl reference electrode, along with a Pt-wire as a counter electrode). The removal of this sacrificial layer helps to create the concave shape in one end of the gold wire motor. Subsequently, Au was plated using a commercial gold plating solution (Orotemp 24 RTU RACK; Technic, Inc., Anaheim, CA) at −1 V (vs Ag/AgCl), using a charge of 4 C. The resulting AuNWs had a length of around 4 μm. The sputtered gold layer and the copper sacrificial layer were simultaneously removed by mechanical polishing using cotton tip applicators soaked with 0.5 M CuCl2 solution in 20% HCl. The membrane was then dissolved in a 3 M NaOH solution for 30 min to completely release the nanowires. The resulting nanomotors were separated from solution by centrifugation at 7000 rpm for 5 min and washed repeatedly with ultrapure water (18.2 MΩ cm) until a neutral pH was achieved. Between washing steps, the nanomotors solution was mixed with ultrapure water and briefly sonicated (2−5 s) to ensure complete dispersion of nanomotors in the washing water. All AuNWs were stored in 1 mL of ultrapure water at room temperature.

Nanomotors Modification. The external gold surface of the AuNWs was modified by an overnight immersion in a 2 mM cysteamine hydrochloride solution prepared in water, to obtain an appropriate self-assembly monolayer (SAM). After a wash with ultrapure water (by centrifugation at 7000 rpm for 5 min), the cysteamine-modified AuNWs were incubated with the corresponding sample during 1 h under gently shaking. After another washing step with ultrapure water, the GFP/RCA-modified ANWs were washed twice with PBS solution pH 7.5. All incubation steps were carried out at room temperature.

AuNWs were prepared using the same protocol to perform the corresponding control experiments.

In Vitro Intracellular mRNA Silencing. The intracellular mRNA silencing mechanism involved the knockdown of the mRNA target by the siRNA (GFP/RCA) immobilized on the motors surface. To determine the percentage of mRNA silencing in intact HEK293-GFP cells, a mixture of 2 μL of the cell suspension (~1750 cells/μL) and 2 μL of the GFP/RCA-AuNWs was prepared and put into the US holder, applying 6 V and 2.66 MHz during 5 min. After each study, the total volume (~7.0 × 103 cells) of the mixture solution was placed in a well containing Corning cellar DMEM media with 4.5 g/L glucose, L- glutamine, and sodium pyruvate; 10% Hylcone Bovine Growth Serum (FBS); and 1% penicillin streptomycin, and incubated at 37 °C for 24 h. Each well was imaged using an EVOS fluorescent cell imaging system. Also, for the study of the fluorescence signal dependence upon the incubation time under static or US conditions, the fluorescence signal of each sample (static conditions or US) was checked in the microscope after different times (0, 30, 120 min, and 5, 15 h). All the experiments were carried out at room temperature.

Videos were captured using Cool SNAP HQ2 camera, 20× and 40× objectives (unless mentioned otherwise) and acquired at the frame rate of 10 using the Metamorph 7.1 software (Molecular Devices, Sunnyvale, CA). A Nikon Eclipse 80i upright microscope with AT- GFP/F LP filter was used to capture fluorescence images and videos. The fluorescence intensities were estimated by analyzing the corresponding time lapse images using the software ImageJ.

Ultrasound Equipment. The acoustic cell setup consisted of a piezoelectric transducer (Ferroperm PZ26 disk 10 mm diameter, 0.5 mm thickness) responsible for the generation of ultrasound waves, attached by conductive epoxy glue to the bottom center of a steel plate (50 × 50 × 0.94 mm3); then the steel plate was covered with a 240 μm kapton tape protective layer and a sample reservoir at the center (5 mm). A glass slide was used to cover the reservoir for ultrasound reflection and to protect the sample. The continuous ultrasound sine wave was applied via a piezoelectric transducer, through an Agilent 15 MHz arbitrary waveform generator, in connection to a homemade power amplifier. The applied continuous sine waveform had a frequency of 2.66 MHz and voltage amplitude, which varied between 3 and 9 V, to modulate the intensity of the acoustic wave.

Cell Viability Assay. Cell viability testing was conducted using MTT (3-(4,5-dimethylthiazolyl-2)-2,5-diphenyltetrazolium bromide) cell viability reagent (VWR International) to evaluate the effect of the acoustic exposure. After 20 h of cell incubation, the media from the wells was removed and replaced with 110 μL of a mixture of 100 μL of DMEM with 10% FBS and 1% PST and 10 μL of the Biotium MTT assay kit. This work was performed in a hood with the light turned off due to the light sensitive nature of MTT. The 96 well-plate was then incubated for 4 h at 37 °C. The MTT mixture was then carefully removed using a small

needle, replaced with 100 μL of DMSO, and then incubated for 10 min at 37 °C. The absorbance was then read from 540 to 580 nm.

The percentage of viability was calculated assuming that the average absorbance of the wells containing pure cells represented 100% viability. Subsequent t-values were obtained by performing two-tailed, paired t tests between each set of wells and the cells themselves. From these t-values, p-values have been calculated. In our case, all of the p- values showed that we could not state a significant difference between the pure cells and the treated samples (see Supporting Table S2).

Conclusion

In conclusion, we have demonstrated that the combination of synthetic nanomotors with DNA nanotechnology leads to a powerful therapeutic option for siRNA delivery that greatly enhances intracellular gene delivery compared to existing gene- silencing methods. We have shown that GFP/RCA wrapped AuNWs can be propelled rapidly into different cell lines and can dramatically accelerate the siRNA delivery and gene-mRNA silencing compared with static nanowires. Up to a 94% silencing has been observed after 5 min treatment with US- propelled siRNA/RCA-nanomotors and HEK293-GFP cells. Such improvement reflects the fast internalization and rapid intracellular movement, along with the large siRNA payloads. The latter relies on creating DNA GFP/RCA nanostructures on the motor surface. The RCA template could be modified, in the future, to contain different binding regions in order to allow for the quantitative co-delivery of multiple types of siRNA that are associated with various cancer phenotypes. Cell viability tests indicate no significant cell damage after the acoustic nano-motors treatment, even when using high nanomotor concentration. Further investigation into the size and shape of the nanomotor and the siRNA surface loading should enhance further future

targeted in vivo RNAi therapies. Furthermore, with the use of the localization ability of ultrasound, this nanomotor-driven platform could address the challenge of targeted delivery in vivo. Accordingly, we expect that the micromotor-based gene-silencing strategy will find considerable interest in the fields of cancer biology, drug development, functional genomics, and nanomedicine.

Chapter 3, in full, is a reprint of the material as it appears in ACS Nano, 2016. Esteban-Fernández de Ávila, Berta; Chava A; Fernando S; Miguel ALR; Daniela B; Sibai X; Joseph W; Yi C. The dissertation author was the co-first author and investigator of this material.

APPENDIX

Chapter 3 Sequences:

Sequence Name	Sequence
Circle 20A	5′-/phos/ATA CAT ACA TA AAA AAA AAA AAA AAA AAA AA -3′
Primer-polyT	5′-TAT GTA TTT TTT TT -3′
sense-GFP-20A	5’-rArCrArUrGrArArGrCrArGrCrArCrGrArCrUrUTT AAA AAA AAA AAA AAA AAA AA-3’
antisense-GFP	5’-rArArGrUrCrGrUrGrCrUrGrCrUrUrCrArUrGrUTT-3’
sense-Luc	5'-rCrUrUrArCrGrCrUrGrArGrUrArCrUrUrCrGrATT-3'
antisense-Luc	5’-rUrCrGrArArGrUrArCrUrCrArGrCrGrUrArArGTT AAA AAA AAA AAA AAA AAA AA-3’

Supplementary Figures for Chapter Three:

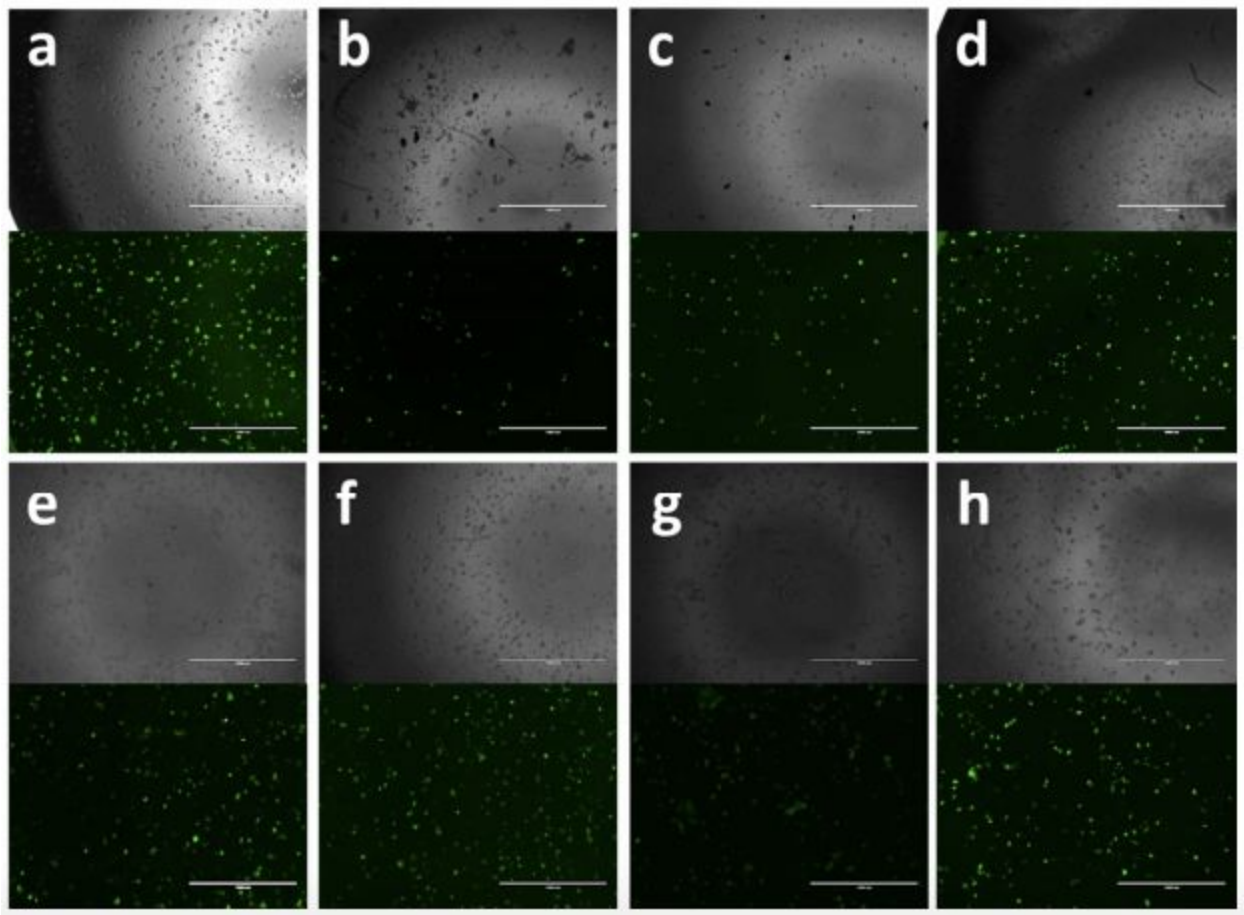

Supporting Figure S1. Optical and fluorescence images corresponding to the control experiments shown in Figure 3A: (a) cells without treatment, (b) cells previously treated with the US-powered-GFP/RCA-modified AuNWs, (c) cells treated with US-powered-GFP-AuNWs, (d) cells treated with US-powered-unmodified-AuNWs, (e) cells treated with static-GFP/RCAAuNWs, (f) cells incubated with free GFP/RCA, (g) cells incubated with free lipofectamine/GFP/RCA, and (h) cells treated with free lipofectamine-luciferase.

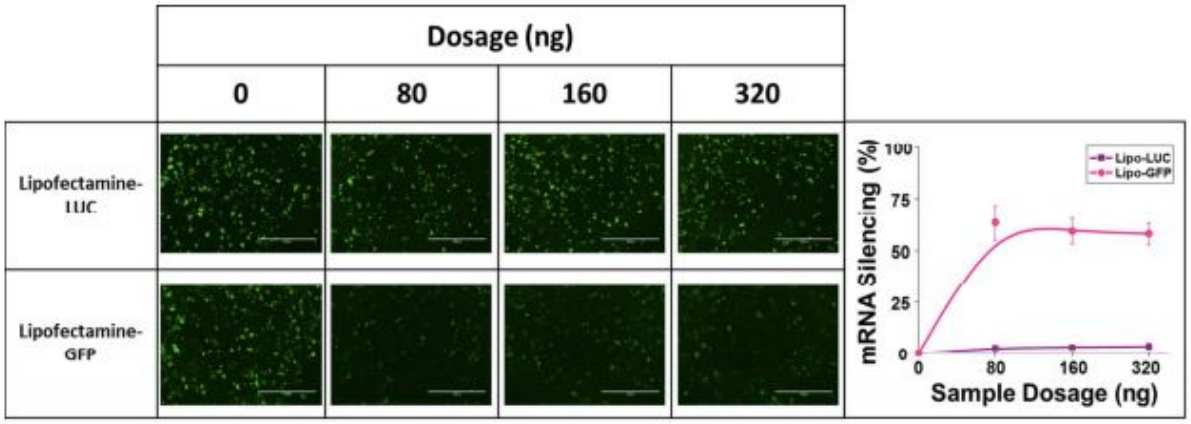

Supporting Figure S2. Effect of amount of lipofectamine-luciferase or lipofectamine-GFP (ng) onto the gene-mRNA silencing.

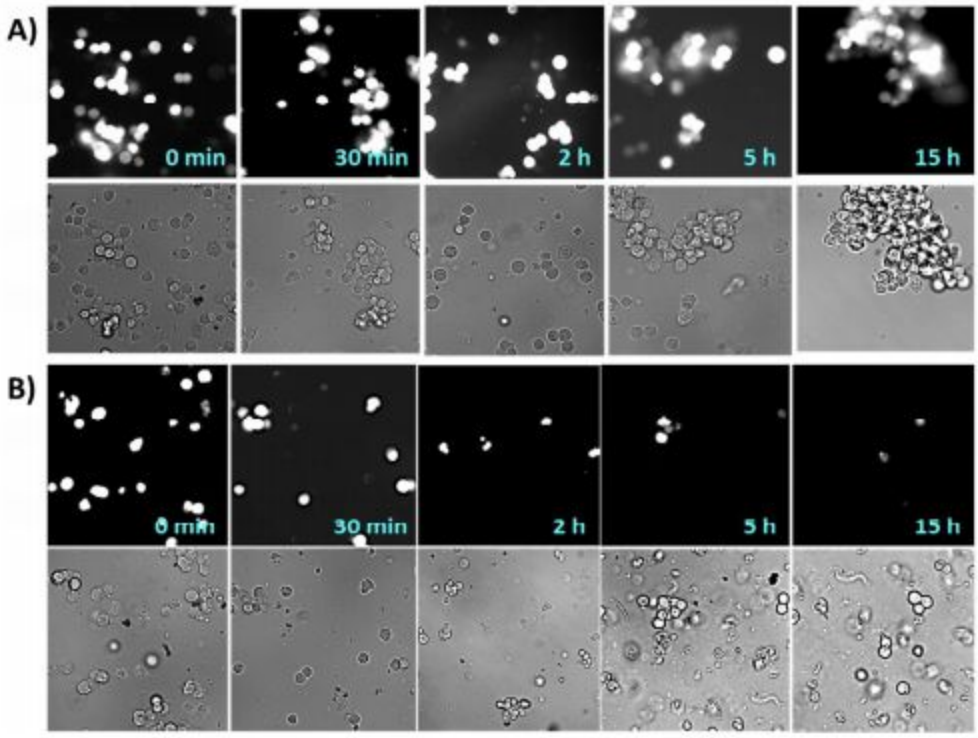

Supporting Figure S3. Optical and fluorescence images corresponding to the time-fluorescence lost dependence study shown in Figure 3B, performed after applying static conditions (A) or the US field (B) to HEK293-GFP cells.

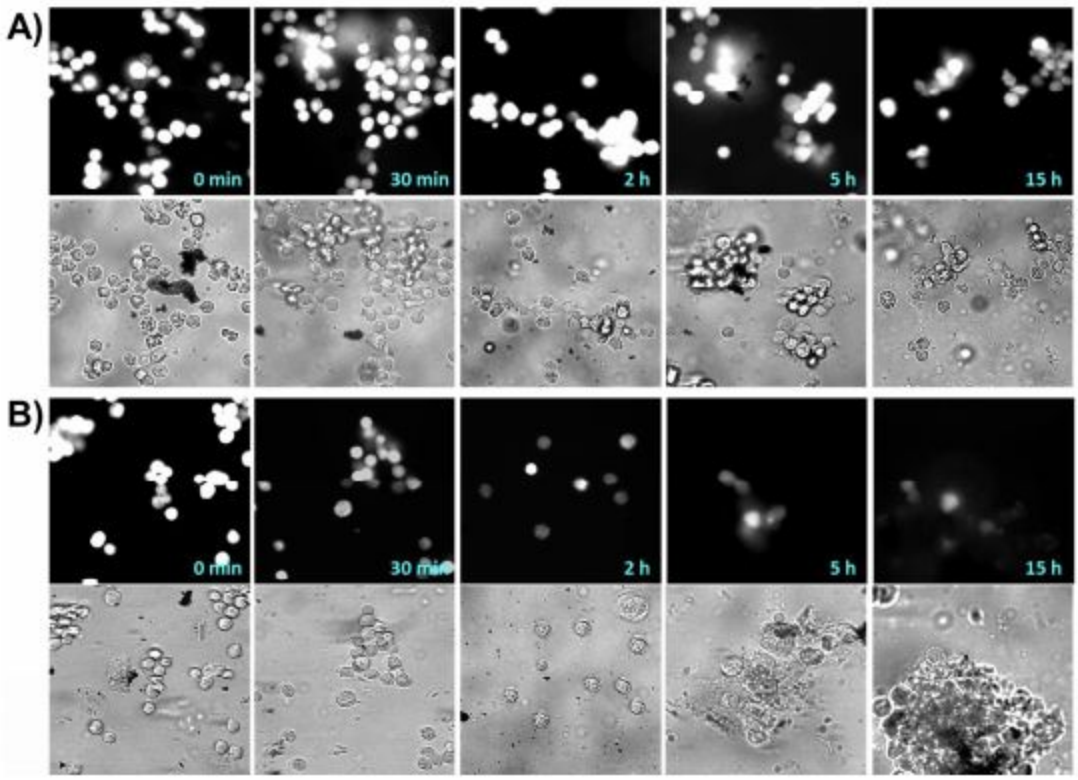

Supporting Figure S4. Optical and fluorescence images corresponding to the time-fluorescence lost dependence study shown in Figure 3C, performed after applying static conditions (A) or the US field (B) to MCF7-GFP cells.

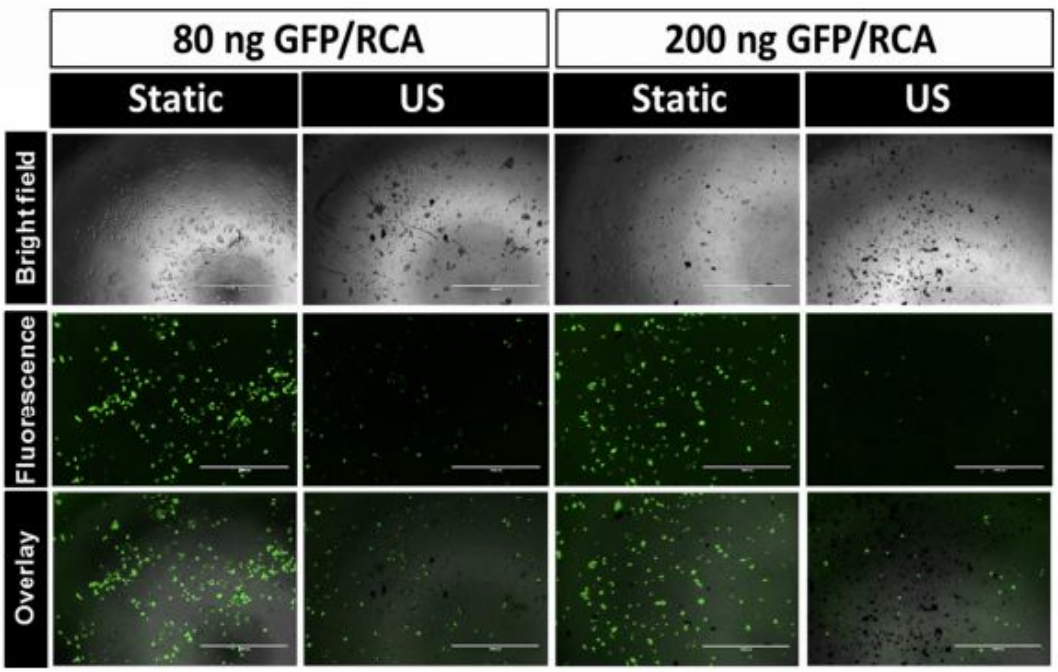

Supporting Figure S5. Bright-field, fluorescence, and overlay images of HEK293-GFP cells after have been treated with AuNWs modified with 80 or 200 ng of GFP/RCA, comparing static conditions and US (6V, 2.66 MHz, 5 min) for both sample concentrations.

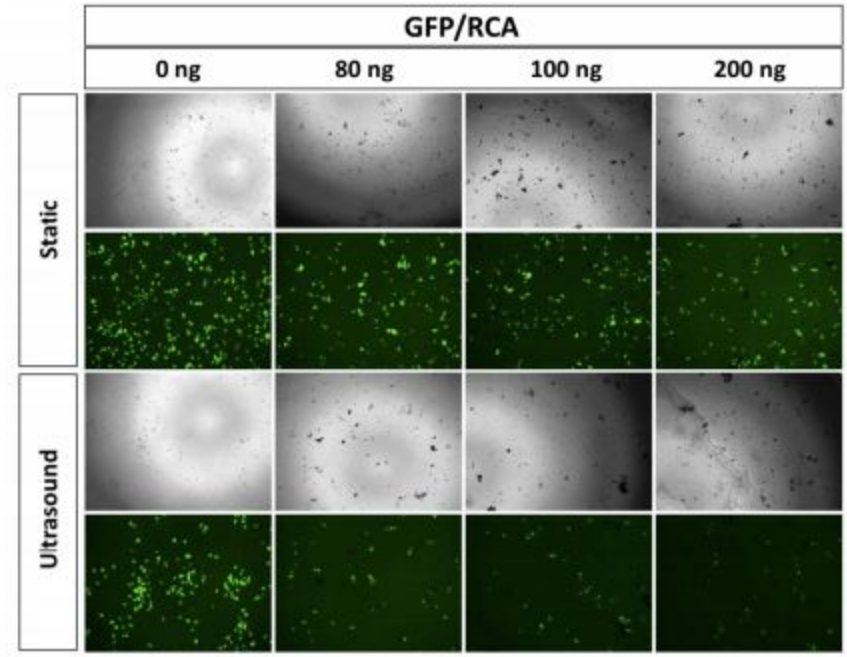

Supporting Figure S6. Bright-field and fluorescence images of MCF7-GFP cells corresponding to the GFP/RCA dose study shown in Figure 3D.

\

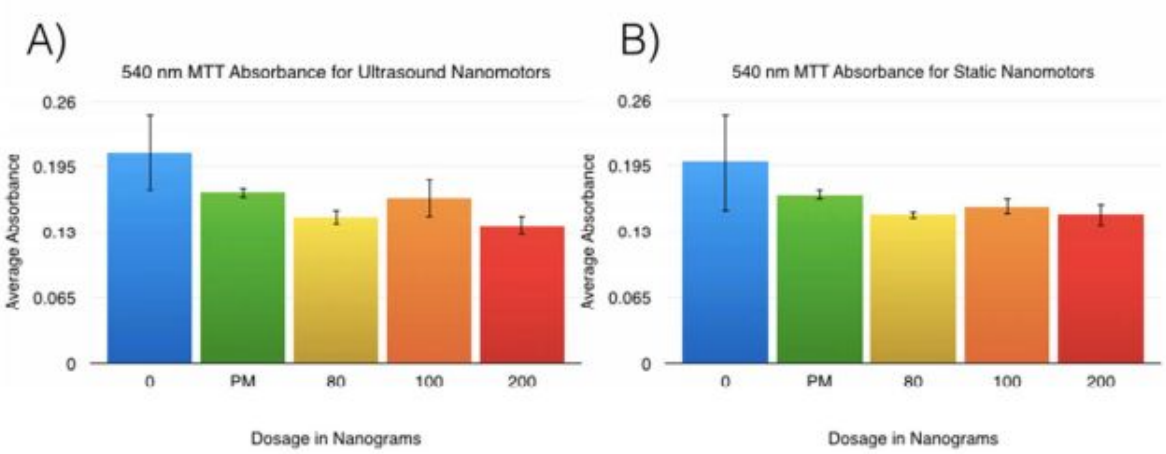

Supporting Figure S7. Results of the cell viability test. Graphs correspond to the average absorbance at 540 nm using an MTT assay across three wells of MCF-7-GFP cells treated with A) GFP/RCA-modified nanomotors propelled by ultrasound and B) static GFP/RCA-modified nanomotors. GFP/RCA dosage: 0, 80, 100 and 200 ng. US conditions: 6 V, 2.66 MHz and 5 min. (PM: plain motors).

Supporting Table S2. GFP/RCA dosages: 0, 80, 100 and 200 ng. PM: plain motors (gold nanorods without modification). α = 0.05

Ultrasound (540 nm)	**200**	**100**	**80**	**PM**	**cells**
Well 1	0.147	0.154	0.153	0.166	0.234
Well 2	0.127	0.185	0.143	0.175	0.23
Well 3	0.137	0.152	0.14	0.167	0.166
Average	**0.1370**	**0.1637**	**0.1453**	**0.1603**	**0.2100**
Standard Deviation	*0.0100*	*0.0185*	*0.0068*	*0.0049*	*0.0382*
Percent	65.24	77.94	69.21	76.35	100.00
T-Test	**0.0832**	**0.1357**	**0.0795**	**0.1947**	
P-value	0.9472	0.9142	0.9495	0.8644	

Static (540 nm)	**200**	**100**	**80**	**PM**	**cells**
Well 1	0.152	0.146	0.148	0.172	0.25
Well 2	0.154	0.162	0.15	0.162	0.155
Well 3	0.135	0.158	0.143	0.165	0.191
Average	**0.1470**	**0.1553**	**0.1470**	**0.1663**	**0.1987**
Standard Deviation	*0.0104*	*0.0083*	*0.0036*	*0.0051*	*0.0480*
Percent	73.99	78.19	73.99	83.72	100.00
T-Test	**0.2072**	**0.3135**	**0.2069**	**0.3213**	
P-value	0.8700	0.8066	0.8701	0.8021	

Chapter 3 BIBLIOGRAPHY

[1] McClellan, J. and King, M.C., 2010. Genetic heterogeneity in human disease. *Cell*, *141*(2), pp.210-217.

[2] Castanotto, D. and Rossi, J.J., 2009. The promises and pitfalls of RNA-interference-based therapeutics. *Nature*, *457*(7228), pp.426-433.

[3] Agrawal, N., Dasaradhi, P.V.N., Mohmmed, A., Malhotra, P., Bhatnagar, R.K. and Mukherjee, S.K., 2003. RNA interference: biology, mechanism, and applications. *Microbiol. Mol. Biol. Rev.*, *67*(4), pp.657-685.

[4] Jensen, S.A., Day, E.S., Ko, C.H., Hurley, L.A., Luciano, J.P., Kouri, F.M., Merkel, T.J., Luthi, A.J., Patel, P.C., Cutler, J.I. and Daniel, W.L., 2013. Spherical nucleic acid nanoparticle conjugates as an RNAi-based therapy for glioblastoma. *Science translational medicine*, *5*(209), pp.209ra152-209ra152.

[5] Jang, M., Kim, J.H., Nam, H.Y., Kwon, I.C. and Ahn, H.J., 2015. Design of a platform technology for systemic delivery of siRNA to tumours using rolling circle transcription. *Nature communications*, *6*, p.7930.

[6] Lytton-Jean, A.K., Langer, R. and Anderson, D.G., 2011. Five years of siRNA delivery: spotlight on gold nanoparticles. *Small*, *7*(14), pp.1932-1937.

[7] Lee, J.S., Green, J.J., Love, K.T., Sunshine, J., Langer, R. and Anderson, D.G., 2009. Gold, poly (β-amino ester) nanoparticles for small interfering RNA delivery. *Nano letters*, *9*(6), pp.2402-2406.

[8] Semple, S.C., Akinc, A., Chen, J., Sandhu, A.P., Mui, B.L., Cho, C.K., Sah, D.W., Stebbing, D., Crosley, E.J., Yaworski, E. and Hafez, I.M., 2010. Rational design of cationic lipids for siRNA delivery. *Nature biotechnology*, *28*(2), pp.172-176.

[9] Hong, C.A., Lee, S.H., Kim, J.S., Park, J.W., Bae, K.H., Mok, H., Park, T.G. and Lee, H., 2011. Gene silencing by siRNA microhydrogels via polymeric nanoscale condensation. *Journal of the American Chemical Society*, *133*(35), pp.13914-13917.

[10] Zhao, Y.X., Shaw, A., Zeng, X., Benson, E., Nyström, A.M. and Högberg, B., 2012. DNA origami delivery system for cancer therapy with tunable release properties. *ACS nano*, *6*(10), pp.8684-8691.

[11] Kim, K.R., Kim, D.R., Lee, T., Yhee, J.Y., Kim, B.S., Kwon, I.C. and Ahn, D.R., 2013. Drug delivery by a self-assembled DNA tetrahedron for overcoming drug resistance in breast cancer cells. *Chemical Communications*, *49*(20), pp.2010-2012.

[12] Angell, C., Xie, S., Zhang, L. and Chen, Y., 2016. DNA nanotechnology for precise control over drug delivery and gene therapy. *Small*, *12*(9), pp.1117-1132.

[13] Zhu, G., Zheng, J., Song, E., Donovan, M., Zhang, K., Liu, C. and Tan, W., 2013. Self-assembled, aptamer-tethered DNA nanotrains for targeted transport of molecular drugs in cancer theranostics. *Proceedings of the national academy of sciences*, *110*(20), pp.7998-8003.

[14] Yan, J., Hu, C., Wang, P., Zhao, B., Ouyang, X., Zhou, J., Liu, R., He, D., Fan, C. and Song, S., 2015. Growth and Origami Folding of DNA on Nanoparticles for High-Efficiency Molecular Transport in Cellular Imaging and Drug Delivery. *Angewandte Chemie International Edition*, *54*(8), pp.2431-2435.

[15] Lee, H., Lytton-Jean, A.K., Chen, Y., Love, K.T., Park, A.I., Karagiannis, E.D., Sehgal, A., Querbes, W., Zurenko, C.S., Jayaraman, M. and Peng, C.G., 2012. Molecularly self-assembled nucleic acid nanoparticles for targeted in vivo siRNA delivery. *Nature nanotechnology*, *7*(6), pp.389-393.

[16] Modi, S., Swetha, M.G., Goswami, D., Gupta, G.D., Mayor, S. and Krishnan, Y., 2009. A DNA nanomachine that maps spatial and temporal pH changes inside living cells. *Nature nanotechnology*, *4*(5), pp.325-330.

[17] Wang, J., 2013. *Nanomachines: fundamentals and applications*. John Wiley & Sons.

[18] Wang, W., Duan, W., Ahmed, S., Mallouk, T.E. and Sen, A., 2013. Small power: Autonomous nano-and micromotors propelled by self-generated gradients. *Nano Today*, *8*(5), pp.531-554.

[19] Wang, H. and Pumera, M., 2015. Fabrication of micro/nanoscale motors. *Chemical reviews*, *115*(16), pp.8704-8735.

[20] Sánchez, S., Soler, L. and Katuri, J., 2015. Chemically powered micro-and nanomotors. *Angewandte Chemie International Edition*, *54*(5), pp.1414-1444.

[21] Kim, K., Guo, J., Xu, X. and Fan, D.L., 2015. Recent Progress on Man-Made Inorganic Nanomachines. *Small*, *11*(33), pp.4037-4057.

[22] Cheng, R., Huang, W., Huang, L., Yang, B., Mao, L., Jin, K., ZhuGe, Q. and Zhao, Y., 2014. Acceleration of tissue plasminogen activator-mediated thrombolysis by magnetically powered nanomotors. *ACS nano*, *8*(8), pp.7746-7754.

[23] Gao, W., Dong, R., Thamphiwatana, S., Li, J., Gao, W., Zhang, L. and Wang, J., 2015. Artificial micromotors in the mouse's stomach: A step toward in vivo use of synthetic motors. *ACS nano*, *9*(1), pp.117-123.

[24] Peng, F., Tu, Y., van Hest, J.C. and Wilson, D.A., 2015. Self-Guided Supramolecular Cargo-Loaded Nanomotors with Chemotactic Behavior towards Cells. *Angewandte Chemie International Edition*, *54*(40), pp.11662-11665.

[25] Xuan, M., Shao, J., Lin, X., Dai, L. and He, Q., 2014. Self-propelled janus mesoporous silica nanomotors with sub-100 nm diameters for drug encapsulation and delivery. *ChemPhysChem*, *15*(11), pp.2255-2260.

[26] Gao, W. and Wang, J., 2014. Synthetic micro/nanomotors in drug delivery. *Nanoscale*, *6*(18), pp.10486-10494.

[27] Qiu, F., Fujita, S., Mhanna, R., Zhang, L., Simona, B.R. and Nelson, B.J., 2015. Magnetic helical microswimmers functionalized with lipoplexes for targeted gene delivery. *Advanced Functional Materials*, *25*(11), pp.1666-1671.

[28] Esteban-Fernández de Ávila, B., Martín, A., Soto, F., Lopez-Ramirez, M.A., Campuzano, S., Vasquez-Machado, G.M., Gao, W., Zhang, L. and Wang, J., 2015. Single cell real-time miRNAs sensing based on nanomotors. *ACS nano*, *9*(7), pp.6756-6764.

[29] Garcia-Gradilla, V., Orozco, J., Sattayasamitsathit, S., Soto, F., Kuralay, F., Pourazary, A., Katzenberg, A., Gao, W., Shen, Y. and Wang, J., 2013. Functionalized ultrasound-propelled magnetically guided nanomotors: Toward practical biomedical applications. *ACS nano*, *7*(10), pp.9232-9240.

[30] Garcia-Gradilla, V., Sattayasamitsathit, S., Soto, F., Kuralay, F., Yardımcı, C., Wiitala, D., Galarnyk, M. and Wang, J., 2014. Ultrasound-propelled nanoporous gold wire for efficient drug loading and release. *Small*, *10*(20), pp.4154-4159.

[31] Wu, Z., Li, T., Gao, W., Xu, T., Jurado-Sánchez, B., Li, J., Gao, W., He, Q., Zhang, L. and Wang, J., 2015. Cell-Membrane-Coated Synthetic Nanomotors for Effective Biodetoxification. *Advanced Functional Materials*, *25*(25), pp.3881-3887.

[32] Kiristi, M., Singh, V.V., Esteban-Fernández de Ávila, B., Uygun, M., Soto, F., Aktaş Uygun, D. and Wang, J., 2015. Lysozyme-based antibacterial nanomotors. *Acs Nano*, *9*(9), pp.9252-9259.

[33] Wang, W., Li, S., Mair, L., Ahmed, S., Huang, T.J. and Mallouk, T.E., 2014. Acoustic propulsion of nanorod motors inside living cells. *Angewandte Chemie International Edition*, *53*(12), pp.3201-3204.

[34] Guo, S., Huang, Y., Jiang, Q., Sun, Y., Deng, L., Liang, Z., Du, Q., Xing, J., Zhao, Y., Wang, P.C. and Dong, A., 2010. Enhanced gene delivery and siRNA silencing by gold nanoparticles coated with charge-reversal polyelectrolyte. *ACS nano*, *4*(9), pp.5505-5511.

[35] Lee, M.Y., Park, S.J., Park, K., Kim, K.S., Lee, H. and Hahn, S.K., 2011. Target-specific gene silencing of layer-by-layer assembled gold–cysteamine/siRNA/PEI/HA nanocomplex. *ACS nano*, *5*(8), pp.6138-6147.

[36] Miao, P., Wang, B., Meng, F., Yin, J. and Tang, Y., 2015. Ultrasensitive detection of microRNA through rolling circle amplification on a DNA tetrahedron decorated electrode. *Bioconjugate chemistry*, *26*(3), pp.602-607.

[37] Lin, C., Xie, M., Chen, J.J., Liu, Y. and Yan, H., 2006. Rolling-Circle Amplification of a DNA Nanojunction. *Angewandte Chemie International Edition*, *45*(45), pp.7537-7539.

[38] Yan, J., Hu, C., Wang, P., Zhao, B., Ouyang, X., Zhou, J., Liu, R., He, D., Fan, C. and Song, S., 2015. Growth and Origami Folding of DNA on Nanoparticles for High‐Efficiency Molecular Transport in Cellular Imaging and Drug Delivery. *Angewandte Chemie International Edition*, *54*(8), pp.2431-2435.

[39] Wang, W., Castro, L.A., Hoyos, M. and Mallouk, T.E., 2012. Autonomous motion of metallic microrods propelled by ultrasound. *ACS nano*, *6*(7), pp.6122-6132.

[40] Rao, K.J., Li, F., Meng, L., Zheng, H., Cai, F. and Wang, W., 2015. A force to be reckoned with: A review of synthetic microswimmers powered by ultrasound. *Small*, *11*(24), pp.2836-2846.

[41] Nadal, F. and Lauga, E., 2014. Asymmetric steady streaming as a mechanism for acoustic propulsion of rigid bodies. *Physics of Fluids*, *26*(8), p.082001.

[42] Thomas, P. and Smart, T.G., 2005. HEK293 cell line: a vehicle for the expression of recombinant proteins. *Journal of pharmacological and toxicological methods*, *51*(3), pp.187-200.

[43] Ahmed, S., Wang, W., Mair, L.O., Fraleigh, R.D., Li, S., Castro, L.A., Hoyos, M., Huang, T.J. and Mallouk, T.E., 2013. Steering acoustically propelled nanowire motors toward cells in a biologically compatible environment using magnetic fields. *Langmuir*, *29*(52), pp.16113-16118.

[44] Chng, E.L.K., Zhao, G. and Pumera, M., 2014. Towards biocompatible nano/microscale machines: self-propelled catalytic nanomotors not exhibiting acute toxicity. *Nanoscale*, *6*(4), pp.2119-2124.

[45] Gilleron, J., Querbes, W., Zeigerer, A., Borodovsky, A., Marsico, G., Schubert, U., Manygoats, K., Seifert, S., Andree, C., Stöter, M. and Epstein-Barash, H., 2013. Image-based analysis of lipid nanoparticle–mediated siRNA delivery, intracellular trafficking and endosomal escape. *Nature biotechnology*, *31*(7), p.638.

[46] Varkouhi, A.K., Scholte, M., Storm, G. and Haisma, H.J., 2011. Endosomal escape pathways for delivery of biologicals. *Journal of Controlled Release*, *151*(3), pp.220-228.

Chapter 4-An Investigation of RCA's Loading Capacity

Abstract:

Precision in drug delivery has been long sought to eliminate off target effects and maximize the efficacy of the therapeutic being delivered. We sought to address this issue by combining a macro gold nanomotor with that of a nano sized DNA machine to control both the steering and targeting of the combinatorial structure but also the release of the cargo in a specific micro environment. The DNA nanomachines were held in great density on the nanomotor through the use of the Rolling Circle Amplification product as described by our earlier work in utilizing the gold nanomotor/RCA hybrid to deliver siRNA to cells. The nanomachines are responsive to a decrease in pH in order to facilitate their release under acidic conditions such as tumors or late stage endosomes.

Introduction:

DNA nanomachines have been a large portion of the DNA nanotechnology field since its inception in the '80s [1]. Their ability to be responsive to a large variety of inputs such as pH, oligonucleotide strands, small molecules, and proteins allow them to be "coded" with instructions that essentially allow them to act autonomously, i.e. without an external addition of fuel [2-3]. This makes these structures especially attractive for uses in targeted drug delivery and small, cell level, diagnostics [4]. One could argue that DNA nanomachines have great future potential to cover both the highly specific and targeted delivery of a wide variety of therapeutics and also act as a diagnostic modality at the same time, allowing for real time monitoring of the therapeutic effect. [2]

An issue with delivering that DNA machines that can arise, however, is the fact of the negatively charged cellular membrane which can electrostatically repel the negatively charged DNA nanomachines [5]. This can be compensated for in a variety of methodology such as targeting ligands, PEGylation, attachment to a structure with a net positive charge, or encapsulation by a lipid membrane [6]. In this research, we utilized the electrostatic attachment of cystamine on a nanomotor surface, similar to that of our previous work with a Rolling Circle Amplification coated gold nanomotor for the delivery of siRNA. We also utilized the same methodology as our previous work (chapter 3), utilizing the gold nanomotors to drive the structures through the use of ultrasound. When the hybrid DNA and gold nanomachine structure was exposed to a certain environmental condition (a decrease in pH), the DNA nanomachine released their cargo as designed.

The DNA nanomachines were designed in two parts: the attachment structure to the RCA and the aptamer, or protein binding structure that holds the desired protein for delivery. Both structures utilize natural properties of DNA to allow them to react to outside environmental cues. The attachment sequence is rich in cytosine which allows it to form a DNA secondary structure known as an i-motif as pH decreases [7] and the aptamer sequence, which held the protein, acting as a protein capture mechanisms, that we used for the initial proof of concept, only forms its secondary structure when there is a cation and the protein itself, which encourages the guanine rich aptamer to form the structure known as a G-quadruplex [8]. Both these secondary structures are naturally found in DNA and allow these nanomachines to act autonomously as their properties are automatically ‘coded’ to work in response to these cues and produce a physical difference in the DNA structure and conformation. Other methodologies

that have been used for protein delivery include such structures as PLGA nanoparticles [9], liposomes [10], click hydrogels [11], and gold nanoparticles [12].

In this chapter, we will describe the design and functionality of this hybrid macromotor/nanomotor system and discuss how we utilized the intrinsic properties of the RCA to load two different proteins through manipulating its design, thrombin and lysozyme, onto the nanomotor for potential delivery and proof of its co-loading ability and potential for multiplexed delivery and diagnostic applications. Controlled co-loading of proteins and small molecular drugs, i.e. combinatorial therapy, is of great interest for cancer therapy and treatment of HIV/AIDS [9].

Results and Discussion:

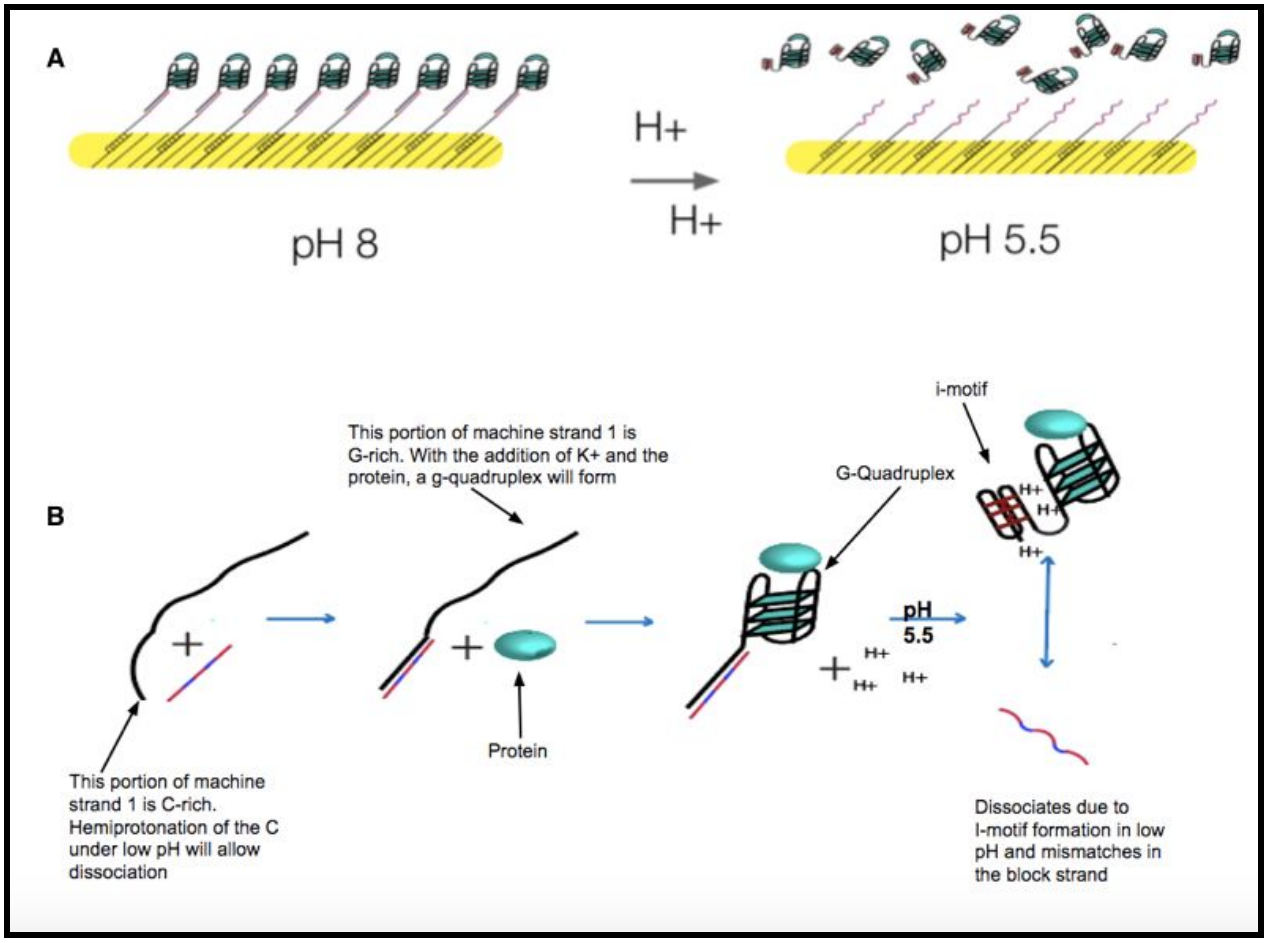

Figure 4.1 A) Cartoon representation of the protein being released through a decrease in pH B) Microscopic cartoon representation of the protein capture and pH release mechanism based on natural DNA properties.

A cartoon schematic of the combinatorial gold micromotors and DNA nanomotors is depicted in **Figure 4.1**, where part A shows the macroscopic view of the protein release, and part B shows the structural mechanism of protein capture and release based on pH and DNA mismatches within the base paired strands. Our design utilizes two of the natural structures that we discussed in chapter 2 of this thesis; the i-motif and the G-quadruplex.

The i-motif, incorporated into the “machine” strand, of our two strand design, binds to part of the strand that is duplexed to the RCA, the “block” strand, thusly ensuring that under an increase in protonation, the machine would dissociate from its connection to the RCA strand through the formation of the secondary structure. This is aided by the fact that there are mismatches between the bases of the block, or binding, strand, and the i-motif structure, thus weakening their bond. The use of the G-quadruplex in the machine strand, formed the aptamer that captured the thrombin protein when coming into contact with a monovalent cation and the protein itself.

We utilized a native (meaning in conditions where the binding is allowed to occur as normal) TAEMg 10% PAGE (Polyacrylamide) gel to visualize the binding of the machine strand and the block strand, and the capture of the protein as shown in **Figure 4.2 A**. Wells 1 and 2 contain the machine strand and the block strand respectively. Well 3 is the binding of the machine strand to the block strand, or the “complex”. We then tested the various strands with the thrombin protein in wells 5 through 6, which were the machine strand with thrombin, the block strand with thrombin, and the complex with thrombin respectively. As is visible from the gel, the machine strand and block strand bind together as a function complex, as does the machine strand with the thrombin and the complex with the thrombin. As expected, the block strand itself is unable to capture the protein as it shows no mobility shift.

We then utilized a native MES 10% PAGE gel to view the release of the protein and the machine strand from the block strand under pH 5.5. The wells are the same as the pH 8 gel, however the mobility difference between the different bands (the longer machine strand higher up in the gel and the shorter block strand, lower) successfully indicates the dissociation of the

complex strands under low pH and the protein release under low pH as indicated by **Figure 4.2 B**.

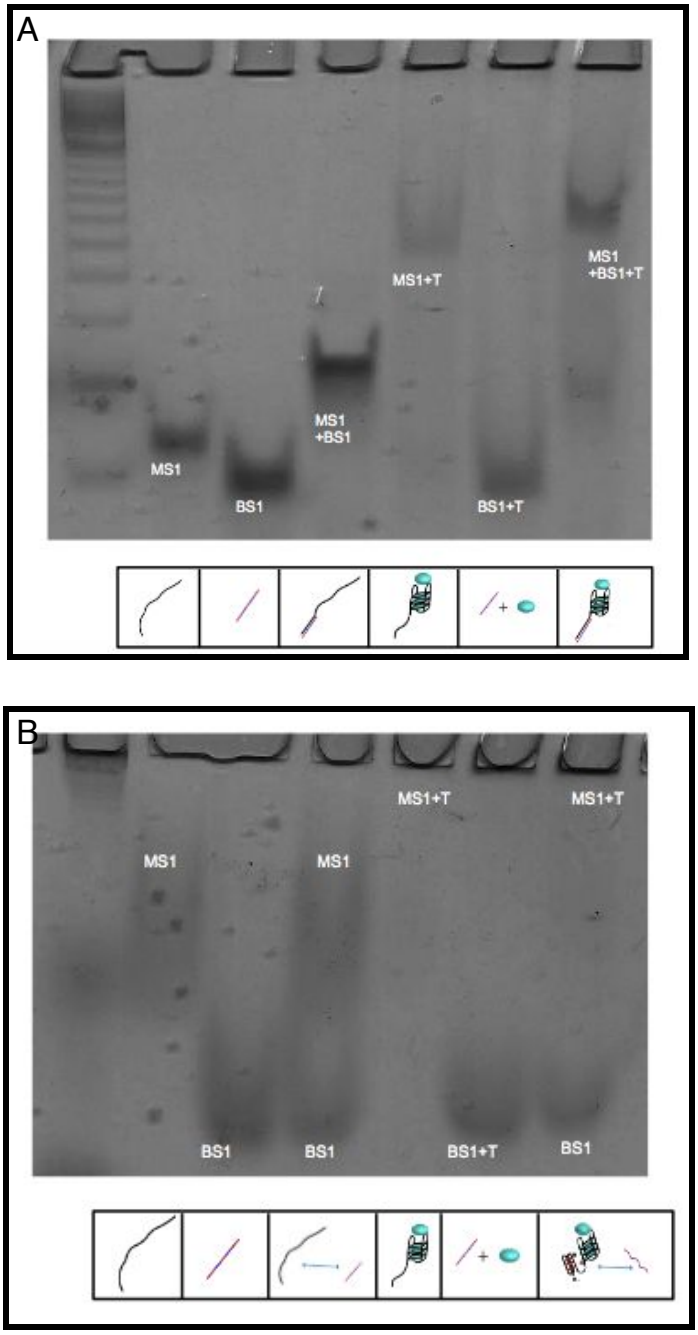

Figure 4.2 A) pH 8 10% PAGE showing structure formation and protein capture B) pH 5.5 10% PAGE showing the block strand dissociation and protein release

After ensuring that the DNA nanomachine captured the protein, we tested the release of the protein from the nanomachine over a range of pH, from pH 8 to pH 3, as seen in **Figure 4.3 A**. This was measured through the absorbance of the DNA in solution and then calculating

through percent change. The more the signal became quenched, the more the i-motif structure had formed, thus indicating the release. We took the absolute value of the curve to indicate the percent of secondary structure formation. The bottom graph is the derivative, or rate of formation along the same time period. We then affixed the DNA nanomachine to the RCA, which was electrostatically attached to the gold micromotor through cystamine in the same manner as it was in chapter 3 [13].

The protein was then incubated alongside the DNA/gold hybrid machine and then the release was tested using MES buffer to simulate the decrease in pH that the machine would face *in vivo*. We tested this to ensure that the release was a function of the increased hydrogen cations affecting and causing the subsequent i-motif formation and dissociation from the gold nanomotor.

In **Figure 4.3 B**, you can see a clear increase in the percentage of formation of the i-motif secondary structure in the top graph from 0 to 30 minutes and then it maintains until 90 minutes. In the bottom graph (the rate of formation), after 90 minutes, we see a spike in the rate release, but could also potentially attribute this to the pH disturbing the attachment of the cystamine rather than a release mechanism from the DNA control nanomachine as cystamine oxidizes under low pH [14].

We also tested the release of the protein after exposing it, and the motor that it was functionalized to, to ultrasound in the MES buffer, thus increasing the flow around the protein. We only saw a mild difference between the ultrasound driven release and the static motor, in **Figure 4.3 C**. This is potentially due to the increase in mixing between the motors and the

buffer, however this mostly shows that the release comes from the secondary structure, or i-motif, formation.

Figure 4.3. A) Measuring i-motif formation from pH 8 to pH 3 (Top is percentage of i-motif formation, bottom is rate of formation) B)Protein release under acidic conditions over a time period of 150 minutes (Top is percentage of i-motif formation, bottom is rate of formation) C) Static (black and purple) versus ultrasound (red and orange) release of the protein under acidic conditions over 90 minutes. (Top is percentage of i-motif formation, bottom is rate of formation)

A

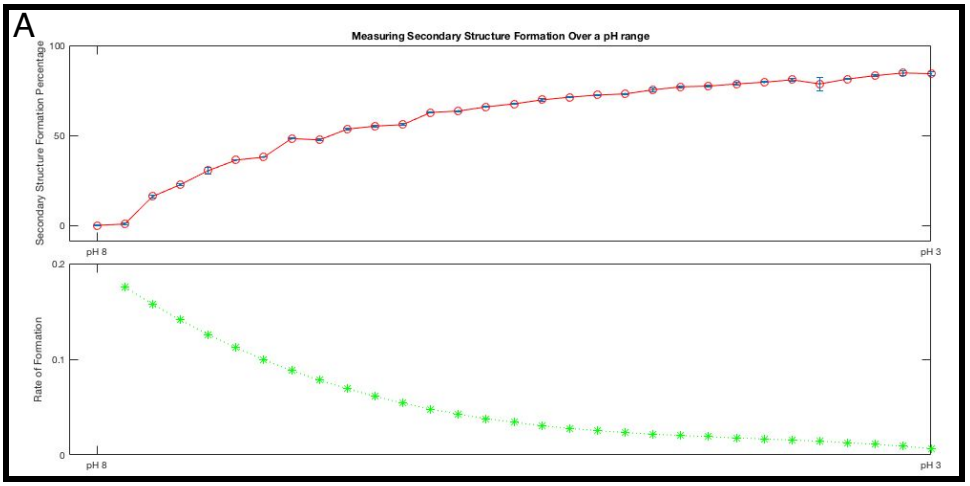
Measuring Secondary Structure Formation Over a pH range
Secondary Structure Formation Percentage
100
50
0
pH 8
pH 3
Rate of Formation
0.2
0.1
0
pH 8
pH 3

B

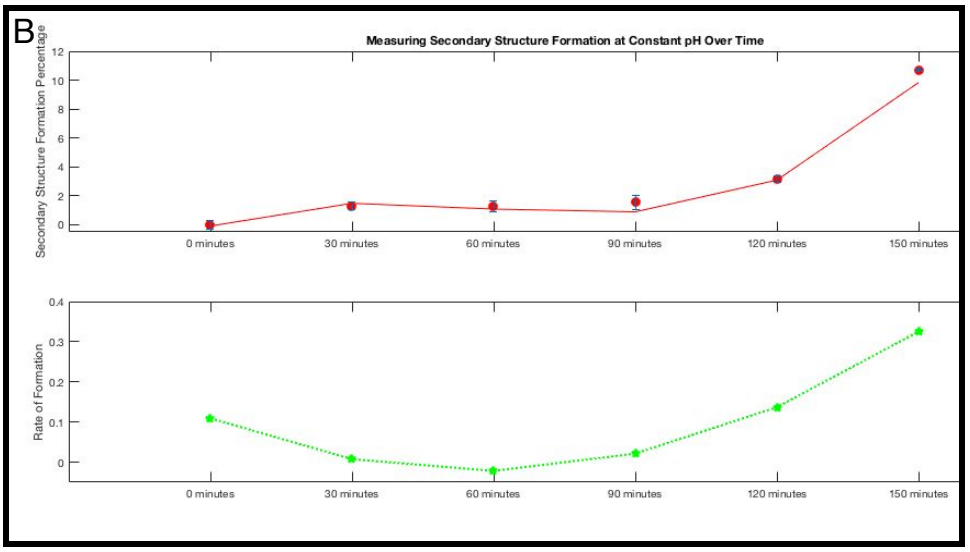
Measuring Secondary Structure Formation at Constant pH Over Time
Secondary Structure Formation Percentage
12
10
8
6
4
2
0
0 minutes
30 minutes
60 minutes
90 minutes
120 minutes
150 minutes
Rate of Formation
0.4
0.3
0.2
0.1
0
0 minutes
30 minutes
60 minutes
90 minutes
120 minutes
150 minutes

C

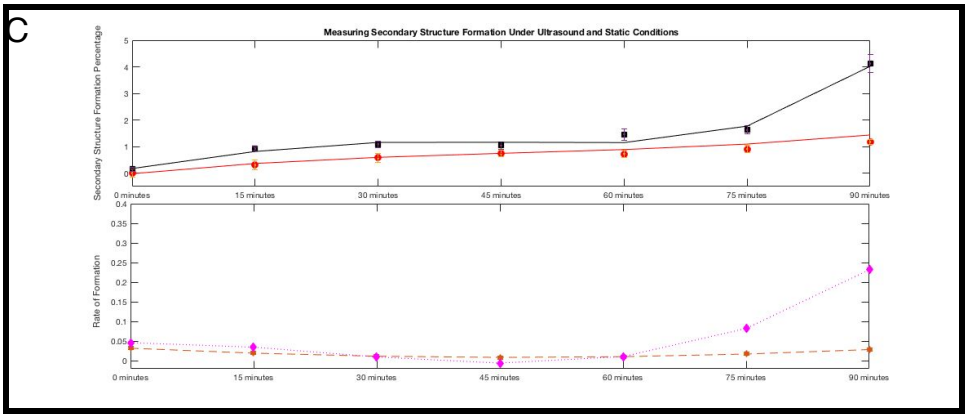
Measuring Secondary Structure Formation Under Ultrasound and Static Conditions
Secondary Structure Formation Percentage
5
4
3
2
1
0
0 minutes
15 minutes
30 minutes
45 minutes
60 minutes
75 minutes
90 minutes
Rate of Formation
0.4
0.35
0.3
0.25
0.2
0.15
0.1
0.05
0
0 minutes
15 minutes
30 minutes
45 minutes
60 minutes
75 minutes
90 minutes

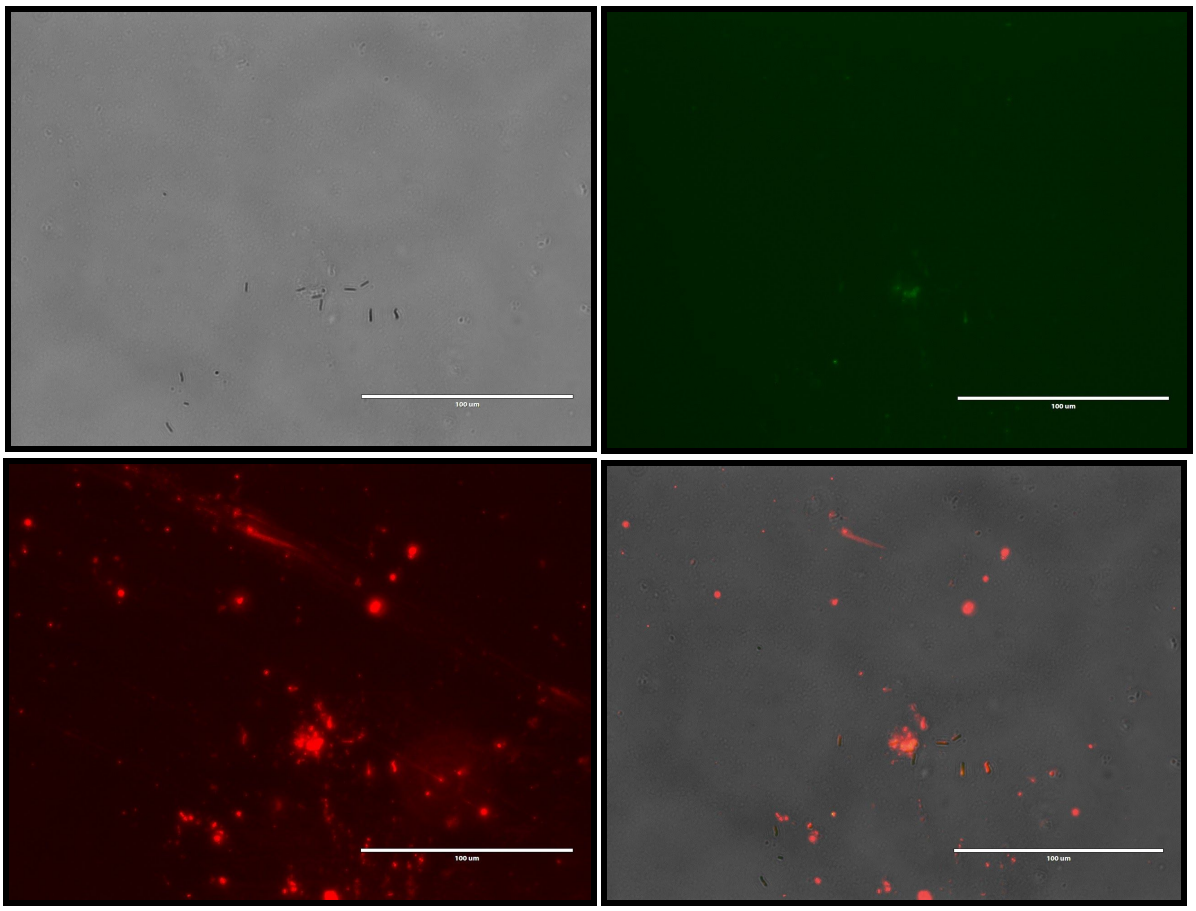

Figure 4.4 Colocalization of two protein signals on a single nanomotor. The top left corner is the brightfield image, the top right corner is the lysozyme labelled with FITC, the bottom left corner is the DYLIGHT labelled thrombin, and the bottom right corner is the overlay showing the signal colocalization on the nanomotor.

Our final function test for this concept was to see if we could load more than one protein onto the gold nanomotor using a slightly different RCA design with two different binding sections and one section to be left as a single strand to ensure wrapping flexibility. We tested thrombin and avidin, utilizing their respective aptamers to attach them, as our two proof of concept proteins. Both proteins were fluorescently labelled, the thrombin using the DYLIGHT kit, and the lysozyme functionalized with a FITC molecule. These motors were then viewed using an optical

microscope with fluorescent cubes. There is clear signal colocalization between the lysozyme (FITC signal), the thrombin (the red DYLIGHT signal), and the brightfield image that shows the motors themselves as seen in **Figure 4.4**. This test shows us that, using RCA and DNA nanotechnology, we can affix a variety of small molecules, drugs, and nanomachines to other vehicles for delivery and we can achieve multiplexed delivery through the tailoring of the RCA sequence to carry more than one type of cargo.

Materials and Methods:

Cysteamine hydrochloride was purchased from Sigma-Aldrich. All RCA products were purchased from Core Bio Services. Phosphate buffered saline (PBS) solution was purchased from Gibco, Invitrogen. All DNA strands were purchased from Integrated DNA Technologies.

Milli-Q water was used for the modification step of AuNWs with cysteamine. PBS solution pH 7.5, prepared with Milli-Q water, was used during the incubation of the cysteamine-modified AuNWs and siRNA samples, to perform the washing steps and during the US experiments.

All chemicals used were of analytical-grade reagents, and deionized water was obtained from a Millipore Milli-Q purification system (18.2 MΩ cm at 25 °C).

Nanomotors Fabrication. The gold nanowire (AuNWs) motors were prepared by a common template-directed electrodeposition protocol. A thin gold film was first sputtered on one side of the porous alumina membrane template containing 200 nm diameter cylindrical nanopores (Catalogue No. 6809-6022; Whatman, Maidstone, U.K.) to serve as a working electrode. The membrane was assembled in a Teflon plating cell with aluminum foil serving as an electrical contact for the subsequent electrodeposition. A sacrificial copper layer was

electrodeposited into the branched area of the membrane using a 1 M cupric sulfate pentahydrate solution (CuSO4·5H2O, Sigma-Aldrich, St. Louis, MO), using a charge of 8 C and a potential of −0.90 V (vs a Ag/ AgCl reference electrode, along with a Pt-wire as a counter electrode). The removal of this sacrificial layer helps to create the concave shape in one end of the gold wire motor. Subsequently, Au was plated using a commercial gold plating solution (Orotemp 24 RTU RACK; Technic, Inc., Anaheim, CA) at −1 V (vs Ag/AgCl), using a charge of -2 C. The resulting AuNWs had a length of around 4 μm. The sputtered gold layer and the copper sacrificial layer were simultaneously removed by mechanical polishing using cotton tip applicators soaked with 0.5 M CuCl2 solution in 20% HCl. The membrane was then dissolved in a 3 M NaOH solution for 30 min to completely release the nanowires. This was repeated a second time. The resulting nanomotors were separated from solution by centrifugation at 7000 rpm for 5 min and washed repeatedly (~10x) with ultrapure water (18.2 MΩ cm) until a neutral pH was achieved. Between washing steps, the nanomotors solution was mixed with ultrapure water and briefly sonicated (2−5 s) to ensure complete dispersion of nanomotors in the washing water. All AuNWs were stored in 1 mL of ultrapure water at room temperature.

Nanomotors Modification. The external gold surface of the AuNWs was modified by an overnight immersion in a 2 mM cysteamine hydrochloride solution prepared in water, to obtain an appropriate self-assembly monolayer (SAM). After a wash with ultrapure water (by centrifugation at 7000 rpm for 5 min), the cysteamine-modified AuNWs were incubated with the corresponding sample during 1 h under gentle shaking. After another washing step with ultrapure water, the GFP/RCA-modified ANWs were washed twice with PBS solution pH 7.5. All incubation steps were carried out at room temperature.

AuNWs were prepared using the same protocol to perform the corresponding control experiments.

RCA Preparation. All DNA sequences were purchased from Integrated DNA Technologies. The circle strand and the primer strand were ligated together in a 1:10 molar ratio using 148 μL of quick ligation buffer, 150 μL of DI water, and 15 μL of quick ligase for at least 16 h at 14 °C. Two picomoles of the ligated circle was combined with the nucleotides (12 μL, 120 nmol of dNTPS), water (up to 60 μL), the polymerase buffer (6 μL), bovine serum albumin (1.6 μL of 10 mg/mL), and the polymerase (3 μL, 30 units). This procedure comes from our earlier work. This was reacted for 2 hours at 37 °C and then the polymerase was inactivated at 70 °C for 10 min.

RCA Purification. The RCA was purified utilizing ethanol precipitation. The DNA was mixed with 4°C ethanol to form a 70% ethanol solution and incubated for 30 minutes. It was then spun at 13000 rcf for 30 minutes at 4 °C. The supernatant was removed and more 4°C 70% ethanol was added. This was then spun at 13000 rcf for 10 minutes and repeated for a total of three times. After the final wash, all supernatant was removed and the DNA was placed into a vacuum centrifuge and treated at 40 °C V-AQ for 40 minutes. The pellet was resuspended in water and shaken overnight on a vortex mixer.

DNA Aptamer Complex Preparation. We annealed 3 ug of the thrombin aptamer machine complex with the 2 hour RCA using the Native 30 program.

RCA Incubation with Nanomotors. The RCA with the aptamer complex was incubated for 1 hour, being shaken with the gold micromotors. It was then centrifuged at 7000 rpm for 5 min. After, it was washed with 200 μL TBE buffer (pH 8.3) and centrifugation at 7000 rpm for 3

min repeated 4 times. If we were attempting duo loading, we then incubated with equal molar value of the other aptamer strand.

BSA Incubation. We then incubated the motors with 200 µL of BSA solution (2 mg/mL in TBE) for 1h under shaking conditions to block the surface from non specific binding. Then, the motors were centrifuges at 7000 rpm for 5 min, washed with 200 µL TBE buffer (8.3) and again centrifuges at 7000 rpm for 3 min. This was repeated 4 times.

Thrombin Labelling. The thrombin was labelled with the DYLIGHT 650 ANTIBODY LABELING KIT according to its instructions. The motor/DNA complexes then underwent incubation with 14.39 µL fluo-thrombin (100 picomoles) for 1h under shaking conditions.

Centrifugation. The motors were again centrifuged at 7000 rpm for 5 min. We collected the supernatant, washed the motors with 200 µL 1x TBE buffer (8.3) and then centrifuged at 7000 rpm for 3 min. This washing repeated at least 4 times and the first wash supernatant was collected.

Release Characterization. We changed the pH to 5.5 using 0.2M MES buffer. We then viewed absorption over time points utilising the Nanodrop to view the release of the DNA from the motors by measuring the supernatant signal.

Fluorescence Characterization. We viewed the micromotors under brightfield and GFP and FITC filters. We then merged the images to view the dual loading colocalization in an overlay.

Conclusion:

This project showed that it is possible to combine motors on both a nano and micro scale. The flexibility of the RCA motif allows us to tailor what we wish to functionalize to a surface, whether that be DNA, RNA, small molecule drugs, or proteins. The combination of the RCA and the gold nanomotor allows us to further and enhance both their uses for potential applications in drug delivery. Secondly, the ability of the RCA to load more than one modality to a surface can mean that a patient could be treated by one dose of the structure, containing more than one therapy, rather than multiple therapies separately to get the synergistic effect. This effectively can lower the cost to patients who would not have to pay for separate medications. In fact, the medication could be tailored to their exact health needs by tailoring the number of RCA binding sites and attaching modalities as needed to the DNA structures through functionalization, click chemistry, or electrostatic interaction.

Consequently, the potential real world applications of RCA to load multiple types of cargo, from small molecule therapeutics, to DNA nanomachines, to DNA or RNA therapeutics are vast. As a result, RCA is an intensely powerful amplification process that can help limit the cost of delivery to patients through its ability for multiplexed delivery.

Chapter 4, in full is currently being prepared for submission for publication of the material. Angell, Chava; Marta J; Berta E; Doris R; Joseph W; Yi C. The dissertation author was the primary investigator and author of this material.

APPENDIX

Chapter 4 Sequences:

Sequence Name	Sequence
Machine Strand 1	5’- GGTTGGTGTGGTTGG TTTT CCA ACT TTT CCC TAA CCC TAA CCC TAA CCC-3’
Block Strand 1	5’- TTG TTA GGG TAA GTG TTA GTT TAA TTA ATG AA -3’
Circle-Protein	5’-/5Phos/ATA CAT ACA TAC ATA GCA GCA AAA AAA AAA AGC ATG GAA GCG TCG ATC TTG AAA AAA AAA AAG CAT GGA AGC GTC GAT CTT GAA AAA AAA AAA-3’
Primer-polyT	5′-TAT GTA TTT TTT TT -3′
APT-Thrombin 1T	5’-ATA CAT ACA TAC ATA GCA GCT GGT TGG TGT GGT TGG-3’
APT-Thrombin 2 ’	5’-GCA TGG AAG CGT CGA TCT TGG GTT GGT GTG GTT GG-3
APT-Avidin 1T	5’-ATA CAT ACA TAC ATA GCA GCT GGG AAC GCA CCG ATC GCA GGT TTC CC-3’
APT-Avidin 2T	5’-GCA TGG AAG CGT CGA TCT TGT GGG AAC GCA CCG ATC GCA GGT TTC CC-3’
APT-Lysozyme	5’-dTpdTpdTpdTpdTpdTpdApdTpdCpdApdGpdGpdGpdCpdTpdApdApdApdGpdApdGpdTpdGpdCpdApdGpdApdGpdTpdTpdApdCpdTpdTpdApdGp-3'

Chapter 4 BIBLIOGRAPHY

[1] Angell, C., Xie,S., Zhang, L. and Chen, Y., 2016. DNA nanotechnology for precise control over drug delivery and gene therapy. *Small*, *12*(9), pp.1117-1132.

[2] Angell, C., Kai, M., Xie, S., Dong, X. and Chen, Y., 2018. Bioderived DNA nanomachines for potential uses in biosensing, diagnostics, and therapeutic applications. *Advanced healthcare materials*, *7*(8), p.1701189.

[3] Bath, J. and Turberfield, A.J., 2007. DNA nanomachines. *Nature nanotechnology*, *2*(5), p.275.

[4] Linko, V., Ora, A. and Kostiainen, M.A., 2015. DNA nanostructures as smart drug-delivery vehicles and molecular devices. *Trends in biotechnology*, *33*(10), pp.586-594.

[5] Huo, S., Li, H., Boersma, A.J. and Herrmann, A., 2019. DNA Nanotechnology Enters Cell Membranes. *Advanced Science*, *6*(10), p.1900043.

[6] Zhang, R., Qin, X., Kong, F., Chen, P. and Pan, G., 2019. Improving cellular uptake of therapeutic entities through interaction with components of cell membrane. *Drug delivery*, *26*(1), pp.328-342.

[7] Abou Assi, H., Garavís, M., González, C. and Damha, M.J., 2018. i-Motif DNA: structural features and significance to cell biology. *Nucleic acids research*, *46*(16), pp.8038-8056.

[8] O Tucker, W., T Shum, K. and A Tanner, J., 2012. G-quadruplex DNA aptamers and their ligands: structure, function and application. *Current pharmaceutical design*, *18*(14), pp.2014-2026.

[9] Miao, L., Guo, S., Zhang, J., Kim, W.Y. and Huang, L., 2014. Nanoparticles with precise ratiometric co-loading and co-delivery of gemcitabine monophosphate and cisplatin for treatment of bladder cancer. *Advanced functional materials*, *24*(42), pp.6601-6611.

[10] Vyas, S.P., Rawat, M., Rawat, A., Mahor, S. and Gupta, P.N., 2006. Pegylated protein encapsulated multivesicular liposomes: A novel approach for sustained release of interferon α. *Drug development and industrial pharmacy*, *32*(6), pp.699-707.

[11] Jiang, Y., Chen, J., Deng, C., Suuronen, E.J. and Zhong, Z., 2014. Click hydrogels, microgels and nanogels: Emerging platforms for drug delivery and tissue engineering. Biomaterials, 35(18), pp.4969-4985.

[12] Ghosh, P., Han, G., De, M., Kim, C.K. and Rotello, V.M., 2008. Gold nanoparticles in delivery applications. *Advanced drug delivery reviews*, *60*(11), pp.1307-1315.

[13] Esteban-Fernández de Ávila, B., Angell, C., Soto, F., Lopez-Ramirez, M.A., Báez, D.F., Xie, S., Wang, J. and Chen, Y., 2016. Acoustically propelled nanomotors for intracellular siRNA delivery. *ACS nano*, *10*(5), pp.4997-5005.

[14] Shapiro, B. and Eldjarn, L., 1955. The mechanism for the degradation of cystamine by ionizing radiation. *Radiation research*, *3*(4), pp.393-399.

Chapter 5-pH Responsive RCA Nanoparticles for Theranostic Delivery

Abstract:

Drug delivery can often be limited by many factors. One such factor is that of endosomal escape in which the therapeutic reaches the inside of the cell but remains trapped in the endosomal pouch and cannot escape because the mature endosome merges with a lysosome. In this case, the therapeutic will be destroyed before it can have any effect. Endosomal escape techniques can vary, however, we approached this through the use of expanding DNA nanoballs that change their size and shape, by expanding, with respect to a negative change in pH. The protonation of the DNA nanostructure from the maturation of the endosome leads the structure to increase in size until such time that the structure disrupts the endosomal membrane and allows the therapeutic modality to reach its target inside the cells.

Introduction:

Since its inception in the early 1980's, DNA nanotechnology has been used to create a prolific profusion of structures and machines for uses including drug delivery [1], diagnostics, and therapeutics [2]. DNA nanotechnology is a branch of materials science that treats DNA not as a source of genetic material, but as a building material [2]. Utilizing the inherent properties and constraints that are known from Watson-Crick complementary binding, a wide variety of structures can be built with multiple levels of functionality and creativity. Structures such as large arrays, walking nanomotors, DNA based logic gates, and nanorobots used for smart delivery have all been created by this burgeoning science[3]. This field is incredibly flexible due to the ability to design with DNA complementarity in mind. It is relatively common knowledge that Adenine binds with Thymine and Guanine binds with Cytosine and as such, structures can be built with extraordinary levels of creativity in multiple dimensions [4]. Typical construction

methods include those such as oligonucleotide synthesis, which is comprised of multiple small strands being hybridized together to form a two or three dimensional structure, and DNA origami, which is comprised of folding a large, circular bacteriophage DNA with the help of many, many staple strands. [3]

It is also possible to include natural modalities, that have existing responsiveness to small molecules or environmental changes, into the DNA structures to give them functionality and responsivity to environmental factors, thusly creating machines with a wide variety of usages. These “smart” machines have the ability to walk along tracks, recognize certain populations of cells for cellular targeting, respond to receptor populations, recognize and react to changes in pH, and control the delivery of therapeutic modalities. [5] These DNA nanomachines allow us to target specific issues within drug delivery including that such as off-site delivery effects, burst delivery, and problems with endosomal escape. [6]

Endosomal escape is a particularly tricky obstacle in drug delivery to overcome. If the therapeutic modality of interest remains trapped in the endosome after being endocytosed (brought into the cell through the process of encapsulation with a bilayer capsule of membrane), there is a chance that it will be destroyed once the matured endosome fuses with a lysosome (another membrane bilayer structure that contains enzymes capable of breaking down a variety of biomolecules, in a sense, acting as a cellular “janitor”). [7]

The challenge is in creating some mechanism for the therapeutic modality to “escape” before it is degraded in order to ensure that it reaches its desired target and has its intended effect [8]. There are many approaches that researchers have undergone in order to facilitate this escape. This includes disruption of the membrane through pore formation (bacteria), materials that swell in response to a decrease in pH (protonation), membrane destabilization through the fusion of certain peptides, photochemical disruption, the incorporation of natural agents used by

bacteria and viruses for endosomal escape,[7] or mechanically as demonstrated by our earlier work utilizing the ultrasound powered nanomotors to avoid endosomal encapsulation completely [9].

We approached the issue of endosomal escape by designing DNA nanoballs that undergo a 7x increase in size under the protonation of the maturing endosomes in order to disrupt the lipid bilayer. These nanoballs require far fewer strands than other DNA nanomachines as the core of their structure is formed through a process known as Rolling Circle Amplification, or RCA. The other advantage to our structures is that only one single staple strand is required for particle formation, as opposed to multiple staple strands that are utilized in oligonucleotide structures and DNA origami structures [10].

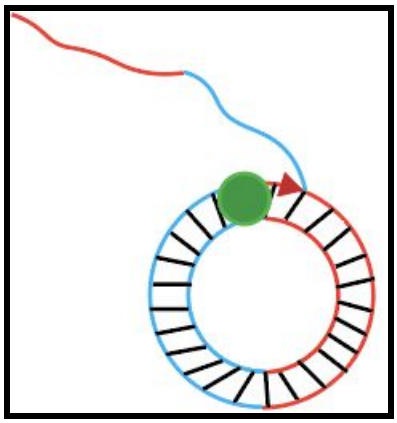

Figure 5.1. Rolling Circle Amplification Process. The green dot represents the polymerase advancing along the circular strand of DNA and adding the complementary base pairs to produce the RCA product

RCA is an isothermal amplification process, unlike that of PCR (Polymerase Chain Reaction) [11] that amplifies a circular piece of DNA (made circular through DNA ligation) through the use of bacterial polymerase, buffer, and single nucleotides (dNTPs) [12] as shown in **Figure 5.1**. This process creates long, repeating DNA strands whose total lengths are

predicated on the length of the reaction and the concentration of base materials, including the nucleotides, that are included at the start.

Our structures take advantage of inherent DNA properties by utilizing a cytosine-rich, duplex to triplex transition [13] (created in part by the staple strand sequence and partially by the RCA sequence itself) as the pH decreases inside the maturing endosome [14]. This design can be seen in **Figure 5.2**. This transition ensures that the structure transitions from a tightly coiled ball, to an expansion of rod-like structures that disrupt the cellular membrane and allow the nanoballs' cargo to be delivered to the cytosol as shown in **Figure 5.3**.

The structures also contain equally spaced binding regions, as utilized in our previous work [9], that is included onto the single staple, to allow for easy and diverse functionalization with dyes, proteins, therapeutics, and targeting ligands [15] and could be adapted to contain diagnostic functionality by the inclusion of DNA nanomachines [16] that serve a separate function.

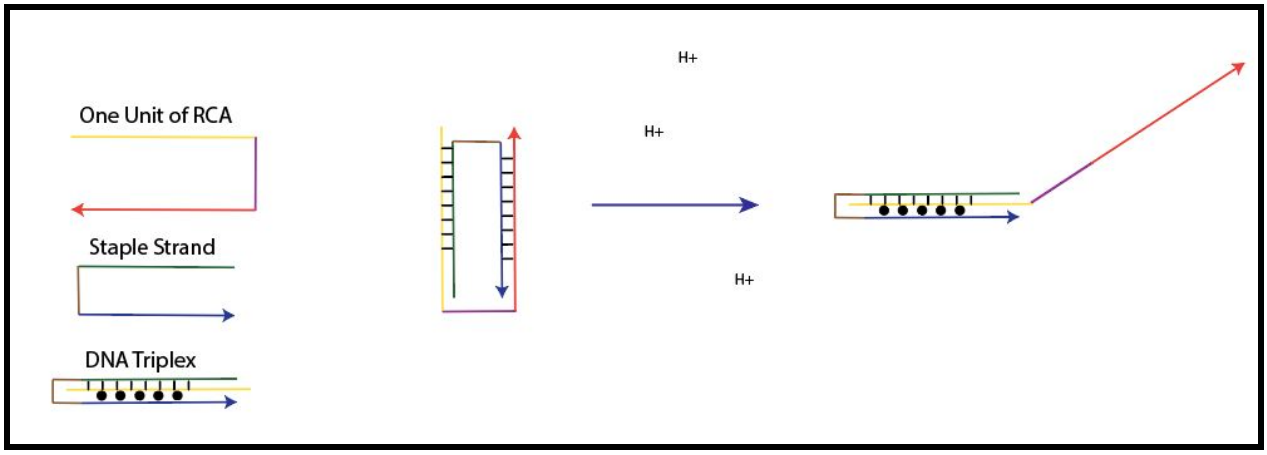

Figure 5.2. Cartoon view of a single unit of RCA binding to a staple and then expanding when exposed to a decrease in pH.

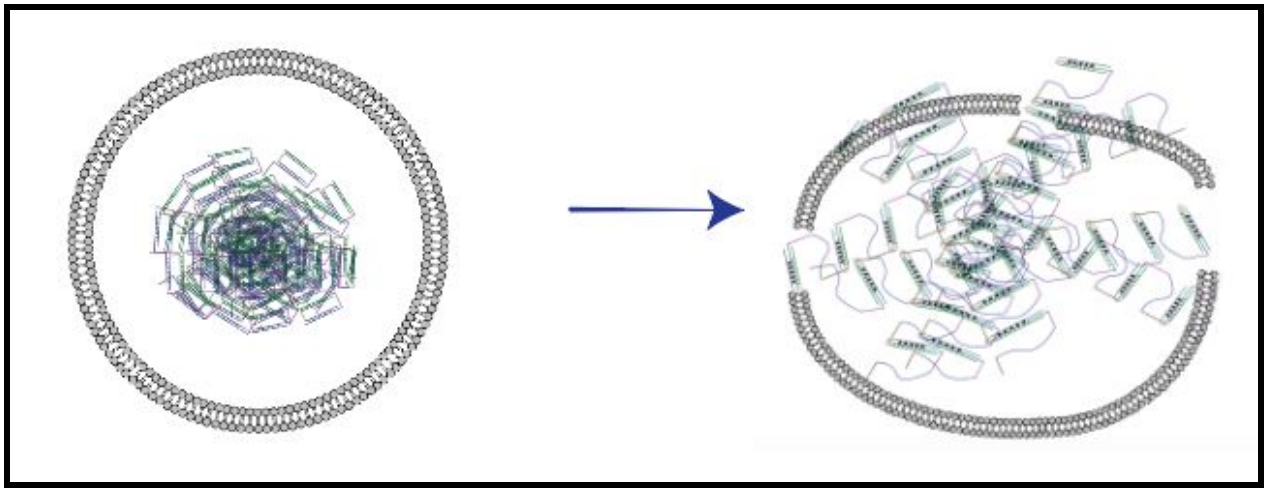

Figure 5.3. Cartoon view of an RCA particle encapsulated in an endosome or liposome in neutral pH, cartoon view of the expanded particle in the broken endosome under acidic pH.

Discussion and Results:

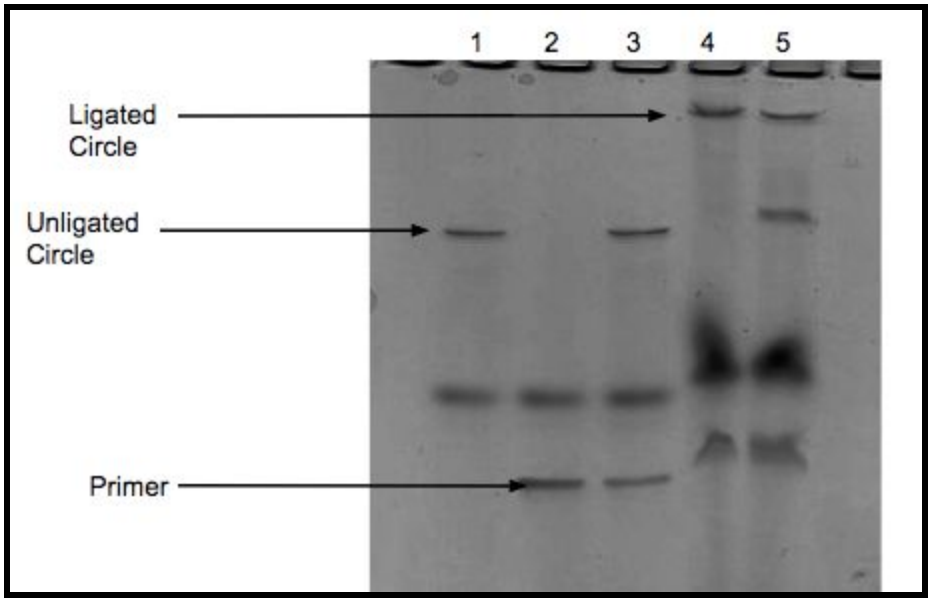

Figure 5.4. 20% denaturing PAGE showing the successful ligation of the circle. Lane one contains the circle strand, lane two contains the primer strand, lane three contains the circle strand and the primer strand in the same well, lane four contains the ligated circle, and lane five contains the ligated circle with additional circle strand added for comparison.

Successful ligation of the circle template, using a 1:10 molar ratio of circle to the connecting primer strand, was visualized through the use of a 20% denaturing PAGE (polyacrylamide gel electrophoresis). As can be seen above in **Figure 5.4**, there was almost 100% success in ligating the linear sequence of DNA into a circle as shown in lanes four and five. There is no visible unligated circle in lane four, which contained just the ligated product. This can easily be visualized by looking at lane five and viewing the placement of the additional unligated circle that was added into the well for comparison.

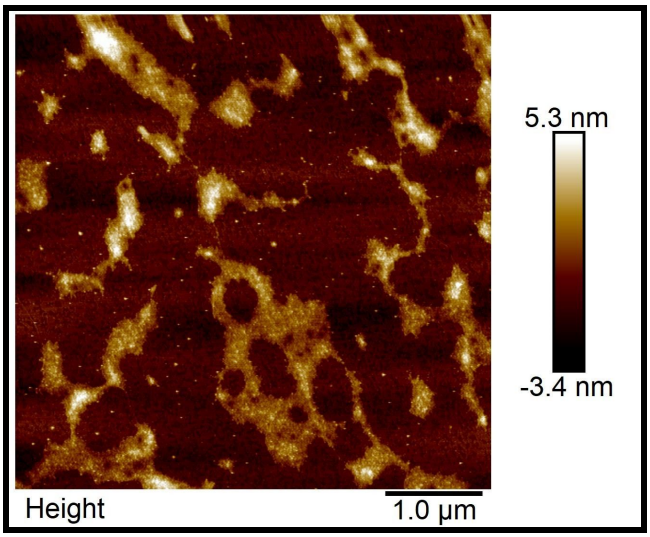

Figure 5.5. AFM confirmation of pure RCA synthesis in pH 8 (using TAEMg buffer), lacking staple strands

The RCA material synthesis itself was successfully characterized through both the use of Atomic Force Microscopy (**Figure 5.5**) or AFM. The figure shows the amorphous product created by the RCA under a one hour condition with no real shape or structure to it. It was also marked visually by observing known changes in the rheology of the RCA containing fluid. As the concentration of RCA strands intensify, the solution becomes increasingly viscous and harder to manipulate with a pipette. Appropriate staple to RCA product concentration was determined

through trial and error with approximate calculations utilized to estimate the amount of binding regions that would be available for the length of RCA reaction that was used for these particles. We tested binding site to staple ratios from 120:1 to 1:1 (120:1 through 70:1 are in **Supplementary Figure 1**) to tune the size of the particles and their expanding abilities and found that the most successful particle in both its pH 8 morphology and in its ability to expand was the 1:1 particle. Binding site to staple ratios 60:1 through 1:1 are found in **Figure 5.6.**

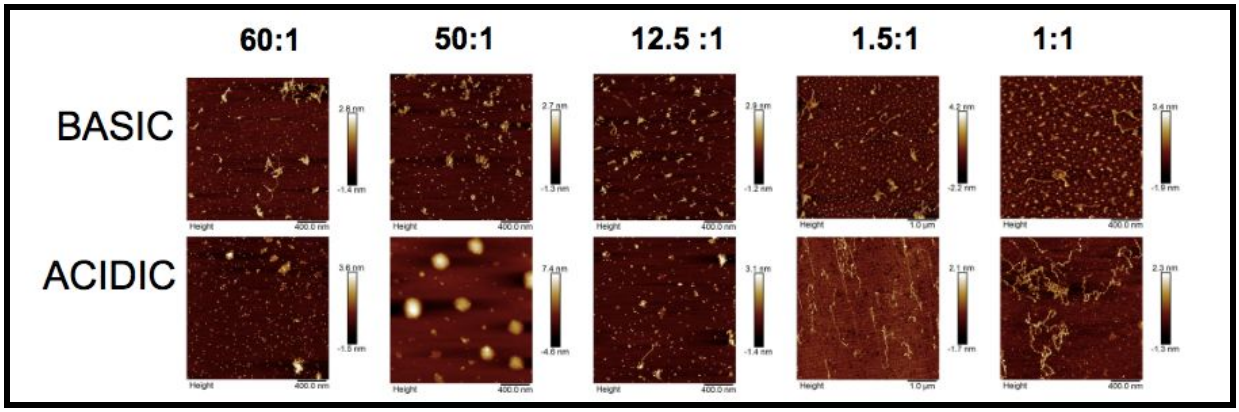

Figure 5.6. Tuning particle binding site to staple ratio to achieve the desired transition from a small sphere to a liner spear.

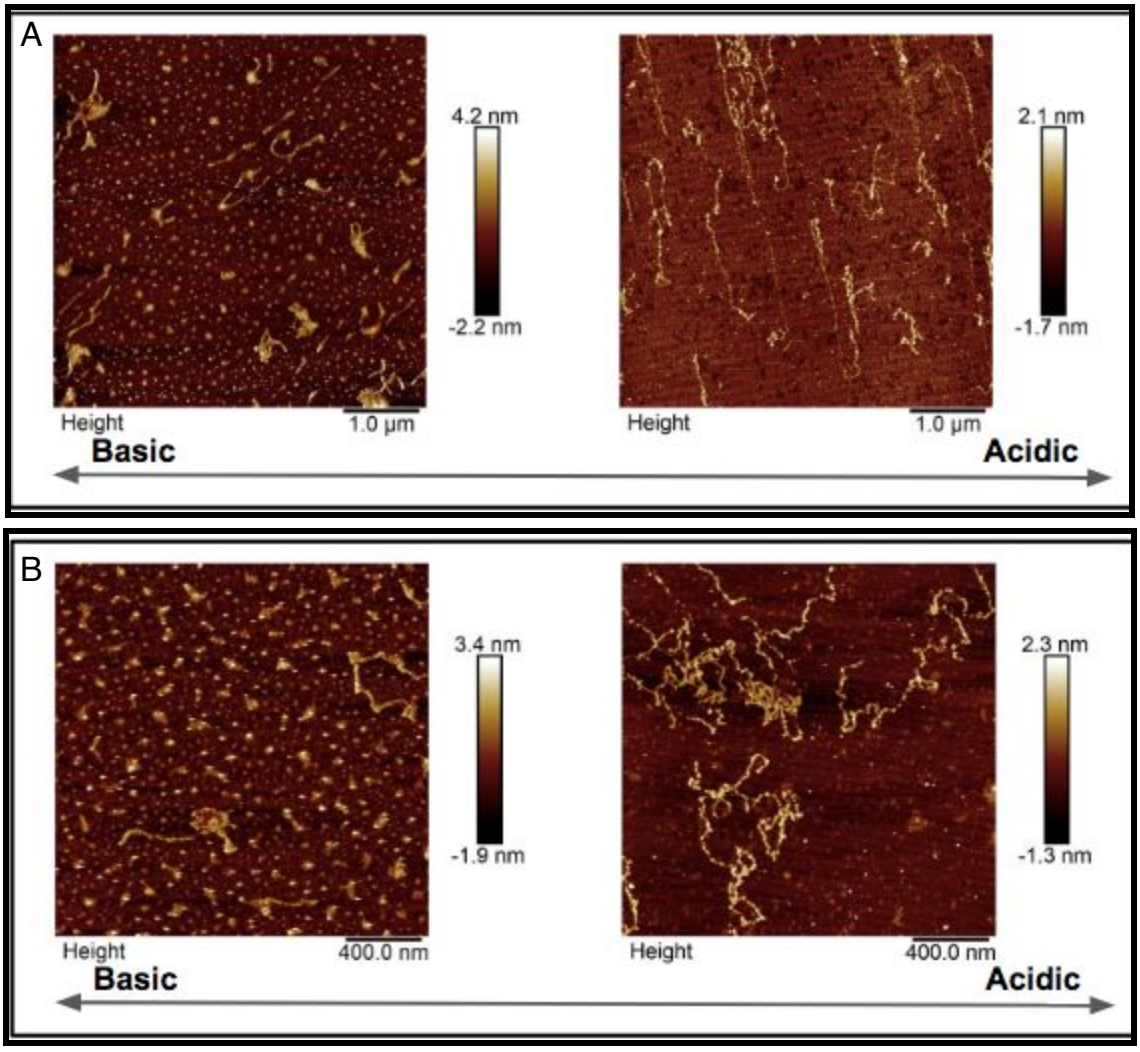

Figure 5.7. A) AFM confirmation of particle synthesis and expansion. The left image shows the particles under pH 8 in TAEMg buffer, the right image shows the particles under pH 5.5 after being treated with MES buffer. This figure was used for ImageJ64 analysis and a clear 7x increase in size is seen. This is the 1.5:1 binding site to staple ratio particle. B) 1:1 Binding site to staple ratio particle. The left image shows the particles under pH 8 in TAEMg buffer, the right image shows the particles under pH 5.5 after being treated with MES buffer.

Particle formation was also characterized using AFM as can be seen in **Figure 5.7**. In the **Figure 5.5** discussed above, we see the unformed RCA particles lacking the necessary staples to help them become the particles they were always meant to be. Once the staples have been added (as shown in **Figure 5.7 A left**), the RCA strands condense down into dense, amorphous particles with a more regular average size of ~100nm in diameter. When the surrounding environment of the particles is lowered to a pH of ~5.5 using MES buffer, the

particles expand in a linear fashion, with a dimensional change of up to 7x the previous diameter (**Figure 5.6 A right**) as measured by ImageJ64. We can see the 1:1 binding site to staple ratio in (**Figure 5.7 B**). The non-expanding particle control is shown in **Supplementary Figure 2.**

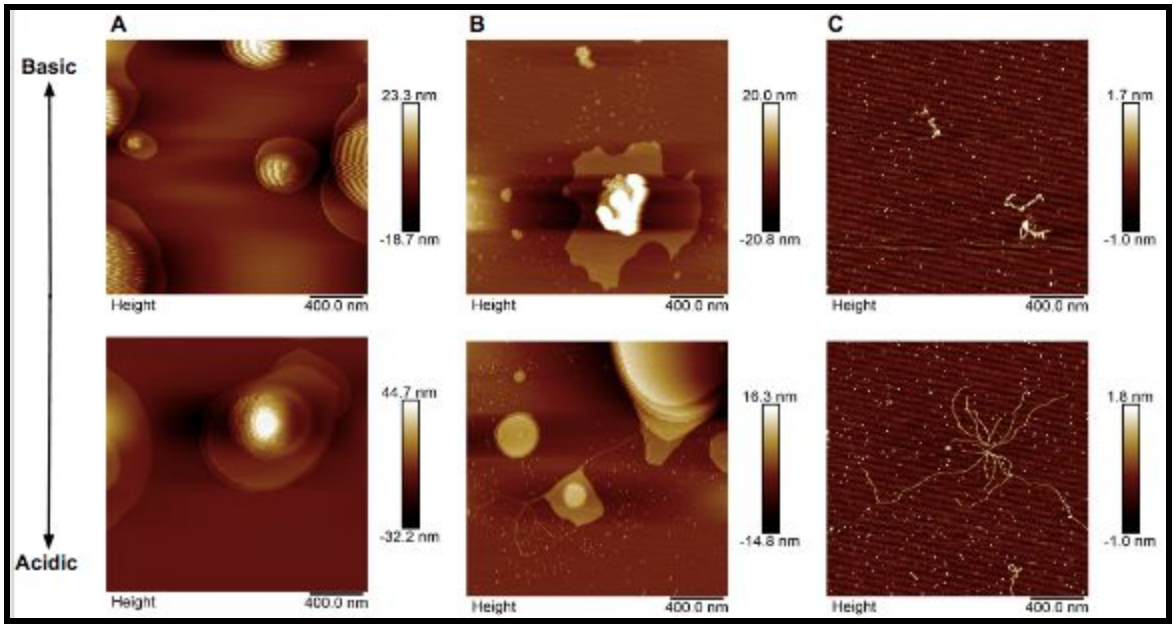

Figure 5.8. AFM comparison of the pure liposome (Picture A), the RCA Nanoparticle encapsulated in the liposome (picture B), and the pure particle (picture C), before treated with an acidic buffer (top) and after (bottom).

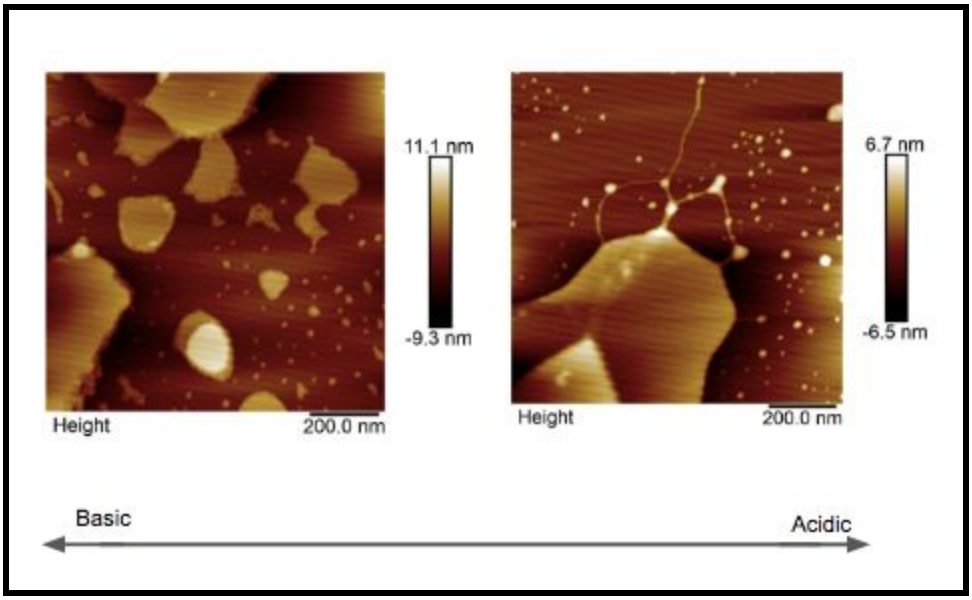

Figure 5.9. AFM image of the particles encapsulated under basic pH(left) and under acidic pH(right). The tendrils extending from the liposome are those of the DNA particle.

This process was further characterized by encapsulating the particles within liposomes and then exposing the liposomes to a more acidic pH (again using the MES buffer). As can be seen in **Figure 5.8** , there are clear tendrils of DNA (measuring blank in height) extending out from the liposomal membrane under acidic conditions (further images of this example can be seen in the supplementary material). This disruption is clearly perpetrated by the DNA machine as liposomes lacking the nanoballs do not show the same membranal disturbance under acidic conditions. As endsomes are composed of lipid bilayer, this is an accurate approximation for what occurs when these particles are taken up by cells. A closer image of this process is shown in **Figure 5.9**.

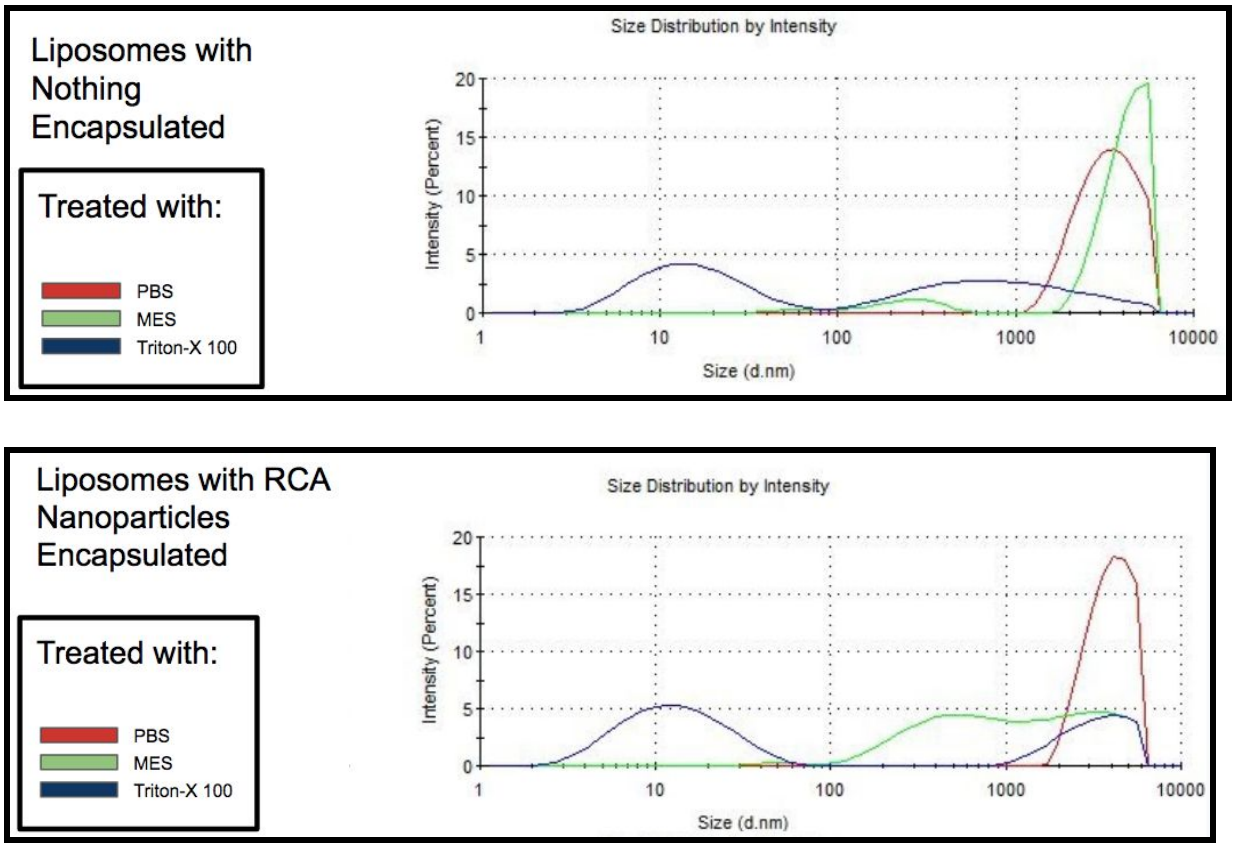

Figure 5.10. Dynamic Light Scattering Comparison of Liposomes encapsulating RCA-Nanoparticle versus a control liposome with nothing contained. The top graph contains the liposomes with no DNA encapsulated, the bottom graph has the RCA nanoparticles encapsulated. The red line, in both graphs, stands for the samples that are treated with Phosphate Buffered Saline, the green line strands for those treated with the acidic MES buffer, and the blue line stands for those treated with a lysing agent, Triton-X 100.

Other experiments with the liposome encapsulated DNA nanoballs were performed utilizing a Dynamic Light Scattering technique. This measured the size distribution before and after certain agents were added to the solution surrounding the liposomes. We compared the addition of a control PBS solution (Phosphate Buffered Saline), acidic MES buffer meant to trigger the DNA transformation, and TritonX-100, which is a lysing detergent meant to disrupt the liposomal membrane. There is a clear divergence between the DNA filled liposomes and the unfilled liposomes when treated with the MES buffer, indicating a disruption of the liposomal

membrane under acidic conditions of pH 5.5 when the particles were present as shown in **Figure 5.10**. We then emulated how the nanoparticles would aid in release of a therapeutic modality inside the late stage endosome by loading doxorubicin, an intercalating anti-cancer therapeutic with a strong fluorescence signal, into a liposome with the RCA expanding nanoparticles . After being treated with the acidic MES buffer to approximate the conditions inside the endosome, there was an increase in the fluorescence signal of the doxorubicin (Excitation:470 nm, Emission: 590 nm), indicating release through the puncture of the liposome. We compared our liposome encapsulated RCA nanoparticles (with doxorubicin) to that of a liposome with no particle inside (with doxorubicin) in **Figure 5.11** to calculate the percent of liposomal breakdown. We saw about 30% of all liposomes broken down with a $p<0.001$ with the control group using a student t-test.

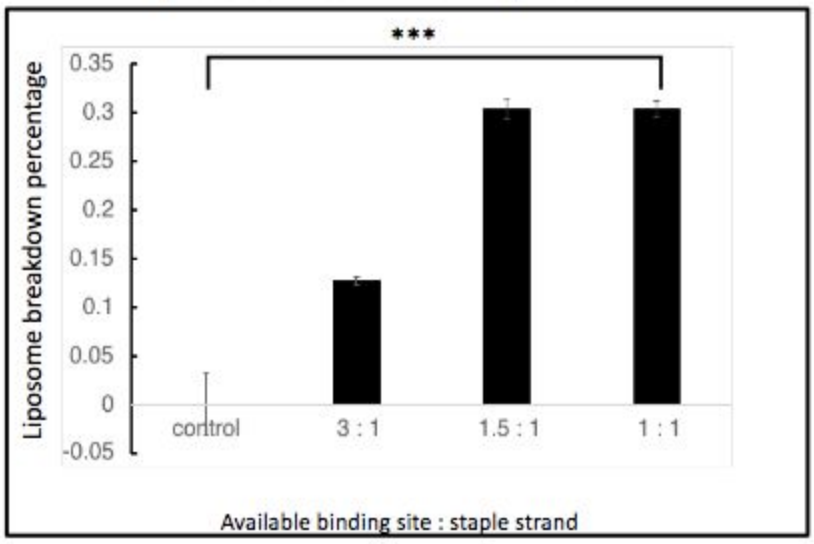

Figure 5.11. A) Percent liposomes broken by the RCA nanoparticle using Doxorubicin fluorescence to characterize (normalized by control liposome with doxorubicin encapsulated but no nanoparticle. *p<0.05, **p<0.01, ***p<0.001 versus control group with the Student t test.)

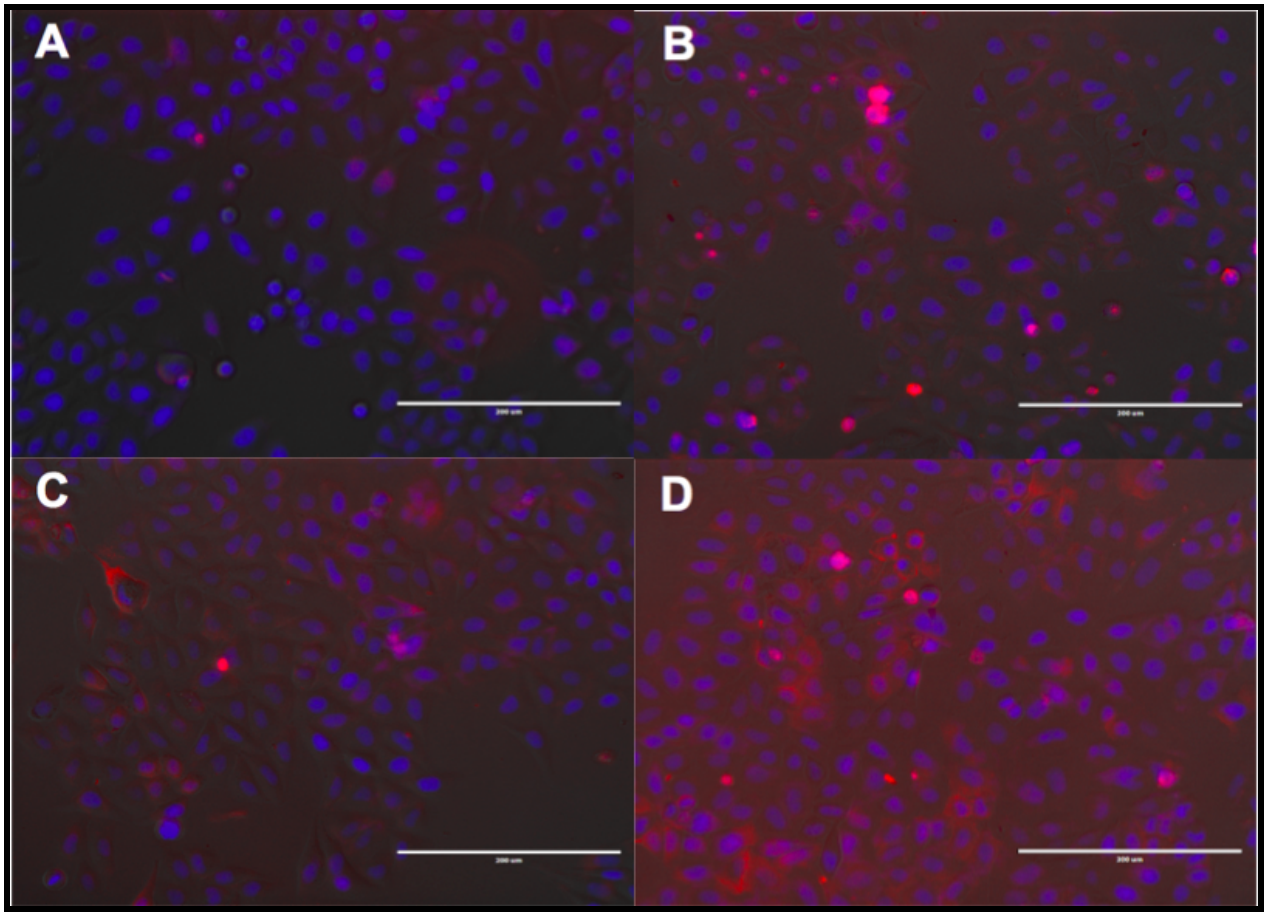

Figure 5.12. Cellular internalization data using particles labelled with Alexa-647 and using Folic Acid to target. A reflects 10 minutes of treatment, B reflects 30 minutes of treatment, C reflects 1 hour of treatment, and D reflects 1.5 hours of treatment. All nuclei were stained with Hoechst staining. The scale bar is 200 um.

Using the empty binding spaces on the particles found on the staple strands, we functionalized them using targeting folate ligands with a 20T tail on them and fluorescent dye. Using this fluorescent dye and Hoescht, we visualized the internalization of the DNA nanoballs over a 1.5 hour time period as shown in **Figure 5.12**. The binding of the folate targeting ligands to the cell membrane and the uptake was clearly visualized as more signal surrounded and entered the cells within that time period. We can claim this is endosomal escape as the fluorescence goes from being punctate in the beginning of the time points, to diffuse and intense

at an hour and a half. This indicates successful escape as described in the 2018 review paper from Samuel Smith *et al*. [17]

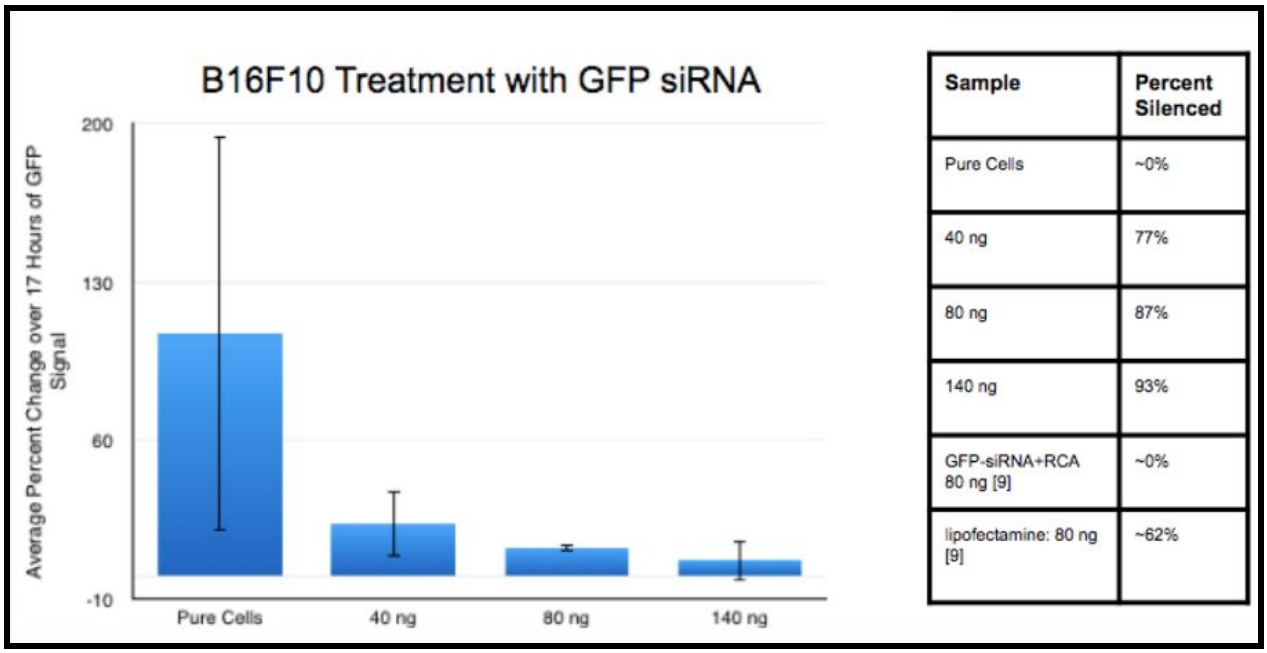

Sample	Percent Silenced
Pure Cells	~0%
40 ng	77%
80 ng	87%
140 ng	93%
GFP-siRNA+RCA 80 ng [9]	~0%
lipofectamine: 80 ng [9]	~62%

Figure 5.13. Cellular dosage response of B16F10 cells dosed with increasing dosages (in nanograms) of anti-GFP siRNA. Control comes from previous work [9]

With a similar method, we treated 6000 per well GFP fluorescent B16F10 cells with increasing dosages of anti-GFP siRNA (from 40 ng to 140 ng) and viewed the fluorescence over a period of 17 hours (**Figure 5.12**).There is a clear trend of silencing compared to the non treated B16F10 cells that were imaged, as their fluorescence signal continued to grow, while those of the treated cells mostly plateaued. From this data, we gleaned that the cells were approximately 90% silenced with an siRNA dosage of 140 ng.

Materials and Methods:

All RCA products were purchased from Core Bio Services. Phosphate buffered saline (PBS) solution was purchased from Gibco, Invitrogen. All DNA strands were purchased from Integrated DNA Technologies.

B16F10-GFP cells were obtained from the University of California, San Diego (UCSD), Nanomaterials & Nanomedicine Laboratory. The cell lines were grown in Corning cellular DMEM media with 4.5 g/L glucose, L-glutamine, and sodium pyruvate purchased from Fisher Scientific; 10% HyClone Bovine Growth Serum (FBS) purchased from VWR International; 100ug/ml of hygromycin-B received from the University of California, San Diego (UCSD), Nanomaterials & Nanomedicine Laboratory, and 1% penicillin streptomycin purchased from Core Bio Services, and the cells were used immediately for the experiments. To prepare the cells suspension, after removing the cell culture media, cells were detached from the flask by treating them with 2 mL of Trypsin-EDTA (0.25%), obtained from Core Bio Services, for 2 min. The trypsin was then inactivated using the supplemented media, centrifuged for 5 min at 0.7 RCF, and resuspended to the correct concentration in media using a hemocytometer.

All chemicals used were of analytical-grade reagents, and deionized water was obtained from a Millipore Milli-Q purification system (18.2 MΩ cm at 25 °C).

Ligation. To create the ligated circle, a 1:10 molar ratio of circle to primer was used. This translated to a volume of 1.08 uL of circle and 13.84 uL of primer, both at 100 uM. 150 uL of millipore water was added along with 140 uL of ligation buffer, and 3 uL of T4 DNA ligase. This was incubated at 14C overnight and the ligation was tested using a 20% denaturing PAGE gel.

RCA Synthesis. The RCA was created utilizing 6.34 uL of the ligated circle, 12 uL of dNTPS, 6 uL of Phi Buffer, .6 uL of BSA, 31.2 uL of millipore water, and 3 uL of Phi29 DNA Polymerase (which translates to 30 units). This was then annealed at 37C for 1 hour, and then heated at 75C for 15 minutes to denature the enzyme. If more volume was required, multiple tubes were annealed at the same time. These tubes were then combined into the same microcentrifuge tube to undergo the process of ethanol precipitation. The reason for the precipitation is twofold; one, to remove excess salts, and two, to allow us to create a more concentrated form of the RCA scaffold. 100% ethanol was added to the tube at -20C, in order to make the ethanol concentration 70%. This was then incubated, until the entire tube was -20C, and then spun down in a temperature controlled centrifuge at 4C at 13000 RCF for 30 minutes. The supernatant was removed, and then replaced with more chilled 70% ethanol. This process was repeated 3 more times, however, at 10 minutes as opposed to 30. After the final purification, all supernatant was removed and the vial went into the vacuum centrifuge for 40 minutes at 45C to remove any lingering ethanol. The pellet was resuspended in millipore water, at a ratio of 15uL per original tube of RCA and then shaken overnight at room temperature.

Particle Synthesis. We mixed 28.6 uL of the purified 1 hour RCA, with 29.97 uL of the staple strand with the 20T binding region on it. We also included 50.05 uL of 10x TAEMg, and 391.82 uL of millipore water. We then annealed it with our “Native 30” program (hold for 5 min at 90 °C, ramp down to 65 °C, hold for 30 min, ramp down to 50 °C, hold for 30 min, ramp down to 37 °C, hold for 30 min, and then ramp down to 22 °C and hold). This synthesized the particles.

AFM Characterization. The morphology of the RCA strand with and without the staple strand was analyzed by AFM (Credit Sibai Xie). AFM imaging was performed under room temperature in dry conditions. Three μL of sample DNA solution was dropped onto freshly cleaved mica surface, and incubated at room temperature for 1−2 min for surface adsorption. The drop was washed off by 30 μL of 2 mM Mg(Ac)2 solution, and was dried by compressed air. Scanasyst- Air tip (Bruker, Camarillo, CA) with a spring constant of 0.4 N/m was used on a Multimode AFM (Vecco Metrology, Santa Barbara, CA). Amplitude setpoint was controlled at the lowest possible value to avoid scratching on the structure.

Liposome Synthesis and Nanoparticle Encapsulation. Using a 10mg/mL stock solution of cholesterol in chloroform, we measured out 2.5 uL and mixed with 56.25 uL of 2.25mg/mL phospholipid in chloroform solution. We then added an additional 441.25 uL of chloroform to ensure full miscibility. The chloroform was then removed by using nitrogen to purge the solvent, leaving only a lipid film layer. The lipid film was then either hydrated with 500 uL of PBS solution or 500 uL of the DNA nanoball solution for one hour at room temperature. After hydration, both vials were vortexed thoroughly, probe sonicated for a minute, and then extruded through a 400 nm membrane. Aliquots were equally treated with either equal volumes of PBS or 0.2M MES, resulting in pH 8 or pH 5.5. These samples were then imaged through AFM.

For the doxorubicin samples, 10 ul of 10mg/ml doxorubicin hydrochloride in DMSO was added to each vial and then the signal was read before and after treatment with the acidic buffer using the plate reading with the excitation being 470 nm and the emission being 595 nm.

Cell Treatment. Approximately 6000 B16F10 GFP fluorescent cells were seeded into a 96-well plate. 24 hours later, these cells were treated with the particles that had been equally

functionalized with both folic acid for cellular targeting and anti-GFP siRNA to demonstrate the ability of the particles to act inside the cell and deliver their cargo. Three wells were utilized per sample dosage, which was given by increasing the volume of sample per well and included these dosages: 40 ng, 80ng, and 140 ng of siRNA. The wells were then read for fluorescent readout for GFP at 0 hours, 1 hours, 2 hours, and then again at 17 hours.

Conclusion:

Throughout this paper, we have clearly demonstrated the creation and utilization of our expanding DNA nanoballs. These nanoballs are incredibly easy to synthesize, have a wide variety of functionalization capability, and have proven their ability to puncture and disrupt a bilayer membrane. These particles could be easily modified to have different triggers for expansion, allowing them to function for different cellular environments, or could be modified to contain a plethora of DNA nanomachines themselves on the surface. Therefore, there is a huge potential for the particles to be used in a theranostic capability, both “smartly” delivering the drugs and monitoring the actual effects during the therapy, thus ensuring our ability to monitor the internal conditions of whatever we are delivering and optimizing the delivery in the future.

These particles also have the benefit of being assembled in an isothermal environment, which is far gentler on proteins and small molecules, unlike PCR, and require far fewer strands than many DNA nanomachines. This allows us to decrease the cost of this therapy by mass producing the framework RCA strand. In the future, the staple strand itself could also be mass produced by creating an RCA template with a nicking region on it, allowing us to synthesize vast quantities, and then digest it into the individual staple strand as needed, thus drastically decreasing the cost further. The possibilities of these particles far outweigh the inability to completely control the size due to the amorphous nature of the staples binding into the strands.

To overcome the amorphous nature, we could potentially use a similar base modification such as Lee *et al* [18] did in 2016 to control the morphology of their RCA particles.

Chapter 5 in full has been submitted for publication of the material. Angell, Chava; Sibai X; Yi C. The dissertation author was the primary investigator and author of this material.

APPENDIX

Chapter 5 Sequences:

Sequence Name	Sequence
Primer-RCA-pH	5’-AGG GAG TTT TTT TTT T-3’
Circle-RCA-pH	5’-/5Phos/ACC TCC CTT CTC CTA AAA AAA AAA AAA AAA AAA AAT ACA TAC ATA CAT AGC AGC-3’
pH-linker-20T	5’-TCC TCT TCC CTC ATC TCC CTT CTC CTT TTT TTT TTT TTT TTT TTT T-3’
RCA-Linker-N	5’-TGT GTA TGT ATA AGC TGC TAT G-3’
RCA-pH-linker-20A	5’-TCC TCT TCC CTC ATC TCC CTT CTC CTA AAA AAA AAA AAA AAA AAA A-3’
sense-GFP-20A	5’-rArCrArUrGrArArGrCrArGrCrArCrGrArCrUrUTT AAA AAA AAA AAA AAA AAA AA-3’
antisense-GFP	5’-rArArGrUrCrGrUrGrCrUrGrCrUrUrCrArUrGrUTT-3’

Supplementary Figures for Chapter Five:

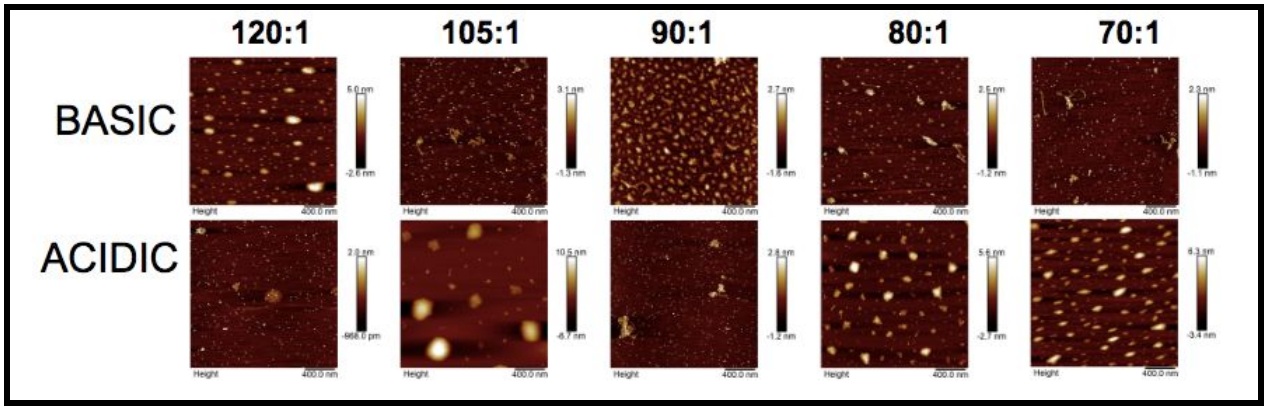

Supplementary Figure 1. Tuning binding site to staple ratios 120:1 through 70:1.

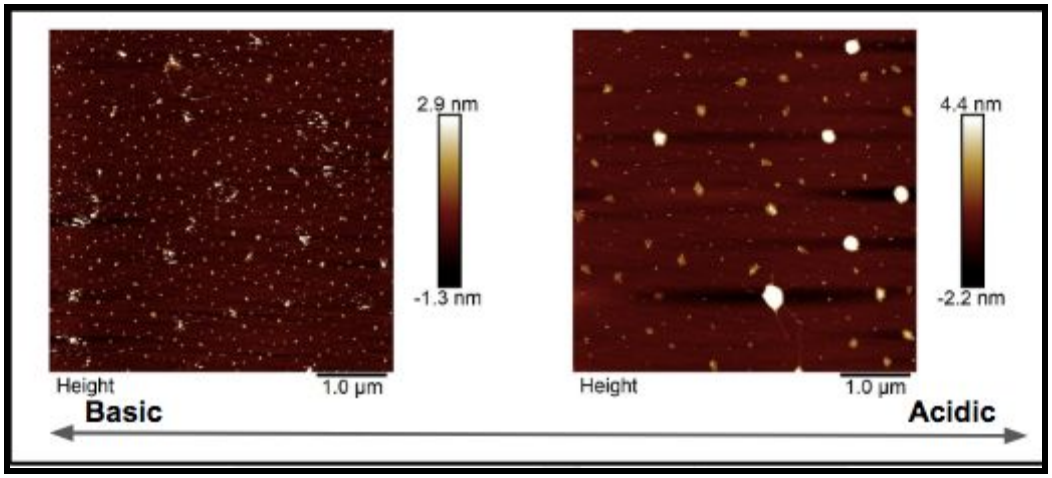

Supplementary Figure 2. Non-expanding particle control.

Chapter 5 BIBLIOGRAPHY

[1] Chen, T., Ren, L., Liu, X., Zhou, M., Li, L., Xu, J. and Zhu, X., 2018. DNA nanotechnology for cancer diagnosis and therapy. *International journal of molecular sciences*, *19*(6), p.1671.

[2] Seeman, N.C. and Sleiman, H.F., 2018. DNA nanotechnology. *Nature Reviews Materials*, *3*(1), p.17068.

[3] Angell, C., Xie, S., Zhang, L. and Chen, Y., 2016. DNA nanotechnology for precise control over drug delivery and gene therapy. *Small*, *12*(9), pp.1117-1132.

[4] Zadegan, R.M. and Norton, M.L., 2012. Structural DNA nanotechnology: from design to applications. *International journal of molecular sciences*, *13*(6), pp.7149-7162.

[5] Angell, C., Kai, M., Xie, S., Dong, X. and Chen, Y., 2018. Bioderived DNA nanomachines for potential uses in biosensing, diagnostics, and therapeutic applications. *Advanced healthcare materials*, *7*(8).

[6] Douglas, S.M., Bachelet, I. and Church, G.M., 2012. A logic-gated nanorobot for targeted transport of molecular payloads. *Science*, *335*(6070), pp.831-834.

[7] Varkouhi, A.K., Scholte, M., Storm, G. and Haisma, H.J., 2011. Endosomal escape pathways for delivery of biologicals. *Journal of Controlled Release*, *151*(3), pp.220-228.

[8] LeCher, J.C., Nowak, S.J. and McMurry, J.L., 2017. Breaking in and busting out: cell-penetrating peptides and the endosomal escape problem. *Biomolecular concepts*, *8*(3-4), pp.131-141.

[9] Esteban-Fernández de Ávila, B., Angell, C., Soto, F., Lopez-Ramirez, M.A., Báez, D.F., Xie, S., Wang, J. and Chen, Y., 2016. Acoustically propelled nanomotors for intracellular siRNA delivery. *ACS nano*, *10*(5), pp.4997-5005.

[10] Tadakuma, H., Masubuchi, T. and Ueda, T., 2016. RNA Study Using DNA Nanotechnology. In *Progress in molecular biology and translational science* (Vol. 139, pp. 121-163). Academic Press.

[11] Ali, M.M., Li, F., Zhang, Z., Zhang, K., Kang, D.K., Ankrum, J.A., Le, X.C. and Zhao, W., 2014. Rolling circle amplification: a versatile tool for chemical biology, materials science and medicine. Chemical Society Reviews, 43(10), pp.3324-3341.

[12] Zhang, Y. and Tanner, N.A., 2017. Isothermal amplification of long, discrete DNA fragments facilitated by single-stranded binding protein. *Scientific reports*, *7*(1), p.8497.

[13] Frank-Kamenetskii, M.D. and Mirkin, S.M., 1995. Triplex DNA structures. *Annual review of biochemistry*, *64*(1), pp.65-95.

[14] Hu, Y.B., Dammer, E.B., Ren, R.J. and Wang, G., 2015. The endosomal-lysosomal system: from acidification and cargo sorting to neurodegeneration. *Translational neurodegeneration*, *4*(1), p.18.

[15] Bujold, K.E., Lacroix, A. and Sleiman, H.F., 2018. DNA nanostructures at the interface with biology. *Chem*, *4*(3), pp.495-521.

[16] Chandrasekaran, A.R., Punnoose, J.A., Zhou, L., Dey, P., Dey, B.K. and Halvorsen, K., 2019. DNA nanotechnology approaches for microRNA detection and diagnosis. *Nucleic acids research*, *47*(20), pp.10489-10505.

[17] Smith, S.A., Selby, L.I., Johnston, A.P. and Such, G.K., 2018. The endosomal escape of nanoparticles: Toward more efficient cellular delivery. *Bioconjugate chemistry*, *30*(2), pp.263-272.

[18] Lee, S.Y., Kim, K.R., Bang, D., Bae, S.W., Kim, H.J. and Ahn, D.R., 2016. Biophysical and chemical handles to control the size of DNA nanoparticles produced by rolling circle amplification. *Biomaterials science*, *4*(9), pp.1314-1317.

Chapter 6-Conclusion

Throughout the course of my research, we have shown that through the use of the Rolling Circle Amplification Process, it is possible to create DNA structures and machines that have the ability to facilitate the efficiency of drug, and small molecule, delivery and therapeutic diagnostics at a lower cost. This is due to the fact that RCA creates a greater volume of product and requires far fewer strands to create a comprehensive nanostructure.

This is cost advantageous as DNA nanostructures such as origami requires hundreds of staple strands which can greatly increase the cost of production, considering the cost of constructing a new DNA origami structure is approximately $700 [1]. The cost per base is approximately $0.10, thus, our structure is vastly cheaper, only requiring the small circle strand, ligation strand, staple strand, and enzymatic amplification materials. The total cost of all these materials is approximately $290 dollars, however, these materials allow us to produce many many doses of the RCA nanoparticles as approximately 46 rounds of RCA can be completed off of one batch of ligated circle, still leaving many raw materials to create more ligated circles, and only requiring a small amount of polymerase, nucleotides, and buffer to complete a single round of RCA.

Table 6.1. Cost of creating RCA and the RCA particles

Cost of Ligation	***Cost of RCA Reaction***	***Total Cost of 1 round of RCA***	***Per Volume of Particle***
T4 Ligase-$50.78 ~6 cents per round of RCA DNA ~$1.50 per primer ~1 cent per round ~$6.70 per circle ~47 cents per round of RCA	Polymerase-$177.76 ~$4.33 per round of RCA DNTPs-$48.41 ~73 cents per round of RCA	1 round of RCA=$5.60	Staple~42 cents per 1 round of particles **$11.62 per volume of 500.44 ul of particles** Dosages Between 34 and 192 dosages of siRNA (not included in this calculation: **Between 6 cents for lower dosages and 34 cents for higher dosages**

The approximate cost per cellular dose is between 6 cents for lower dosages and 34 cents for higher dosages as calculated by summing the costs per round of RCA and dosage of RCA nanoparticle. Similarly as mentioned, our structures utilize a natural amplification process thus making it far easier to create a high volume of product with fewer resources, and, consequently, cheaper DNA nanostructures. RCA also allows us to amplify isothermally, making it a process more friendly to other biologically processes, thusly making it optimal to create structures for in vivo processes.

We have also shown that RCA structures afford the ability to load a wide variety of DNA devices, targeting ligands, and small molecules through our work with both the siRNA loading (chapter 3) and the nanomachine loading (chapter 4). These works show that loading has the potential to be tailored to the specific therapeutic needs, whether it need be a genetic therapy

such as siRNA, mRNA, or CRISPR, or a small molecule or protein therapy linked to the DNA structure through aptamers or by taking advantage of natural DNA properties such as the G-quadruplex, I-motif, or other responsive sequences. This indicates that, not only can the structures be used for delivery of DNA or RNA, it can also be used to hold DNA machines to be used for diagnostic purposes for pH or small molecules, or can even be used as a multi-purpose device, encompassing both delivery and diagnostics to provide a more full picture of the treatment microenvironment during treatment.

We have also shown that it is possible to load a high density of cargo using our RCA motifs, thus requiring a lower volume per “dosage” of our structures. This is due to the fact that the RCA nanostructures have many repeating areas for binding cargo, and as such, the binding limitation is based on how long the RCA reaction goes on, for this affects the number of binding sites produced. The high volume of binding sites allows the RCA created nanostructures to be highly versatile in both desired usage and dosage control.

A drawback of this process is the amorphousness of the structures that are created which leads to a variation in size if they are further folded in structures as we did with the pH responsive DNA nanoballs. The particles ranged in size from 100 nanometers to 600 nanometers. No attempts were made to filter the particles in an attempt to standardize the size, however I believe that with a liposomal extruder, with increasingly smaller membrane pore sizes, or another size filtration system such as dialysis, we could create a more standardized pool of particles to work with.

Another downside to RCA is the inability to create more complicated shapes or structures due to the overarching scheme of repeating sequences. This limits the RCA to very generalized shapes, such as the particles we created. However, it may be possible to build

structures out of multiple stretches or arrays of varying RCA designs, either using RCA as staples, or binding the RCA structures together in an additive fashion. This was an avenue we briefly considered following, and may be a path our lab takes into the future.

I have high hopes for the advantages of RCA-based DNA nanostructures and believe that overcoming the disadvantages will potentially be a function of filtration and of the addition of more RCA strands into the overarching system. This project itself could be furthered through *in vitro* cellular exploration of the small molecule delivery functions of the RCA nanoparticles.

Chapter 6 BIBLIOGRAPHY

[1] Pinheiro, A.V., Han, D., Shih, W.M. and Yan, H., 2011. Challenges and opportunities for structural DNA nanotechnology. *Nature nanotechnology*, *6*(12), p.763.